It is through science that we prove, but through intuition that we discover.

Jules Henri Poincaré

University of Alberta

Microstructure Development in Viscoelastic Fluid Systems

by

Huaping Li

A thesis submitted to the Faculty of Graduate Studies and Research
in partial fulfillment of the requirements for the degree of

Doctor of Philosophy
in
Chemical Engineering

Department of Chemical and Materials Engineering

©Huaping Li
Fall 2009
Edmonton, Alberta

Permission is hereby granted to the University of Alberta Libraries to reproduce single copies of this thesis and to lend or sell such copies for private, scholarly or scientific research purposes only. Where the thesis is converted to, or otherwise made available in digital form, the University of Alberta will advise potential users of the thesis of these terms.

The author reserves all other publication and other rights in association with the copyright in the thesis and, except as herein before provided, neither the thesis nor any substantial portion thereof may be printed or otherwise reproduced in any material form whatsoever without the author's prior written permission.

Library and
Archives Canada

Published Heritage
Branch

395 Wellington Street
Ottawa ON K1A 0N4
Canada

Bibliothèque et
Archives Canada

Direction du
Patrimoine de l'édition

395, rue Wellington
Ottawa ON K1A 0N4
Canada

Your file Votre référence
ISBN: 978-0-494-51245-6
Our file Notre référence

NOTICE:
The author has granted a non-exclusive license allowing Library and Archives Canada to reproduce, publish, archive, preserve, conserve, communicate to the public by telecommunication or on the Internet, loan, distribute and sell theses worldwide, for commercial or non-commercial purposes, in microform, paper, electronic and/or any other formats.

The author retains copyright ownership and moral rights in this thesis. Neither the thesis nor substantial extracts from it may be printed or otherwise reproduced without the author's permission.

AVIS:
L'auteur a accordé une licence non exclusive permettant à la Bibliothèque et Archives Canada de reproduire, publier, archiver, sauvegarder, conserver, transmettre au public par télécommunication ou par l'Internet, prêter, distribuer et vendre des thèses partout dans le monde, à des fins commerciales ou autres, sur support microforme, papier, électronique et/ou autres formats.

L'auteur conserve la propriété du droit d'auteur et des droits moraux qui protège cette thèse. Ni la thèse ni des extraits substantiels de celle-ci ne doivent être imprimés ou autrement reproduits sans son autorisation.

In compliance with the Canadian Privacy Act some supporting forms may have been removed from this thesis.

While these forms may be included in the document page count, their removal does not represent any loss of content from the thesis.

Conformément à la loi canadienne sur la protection de la vie privée, quelques formulaires secondaires ont été enlevés de cette thèse.

Bien que ces formulaires aient inclus dans la pagination, il n'y aura aucun contenu manquant.

Canada

Examining Committee

Uttandaraman Sundararaj (*Supervisor*), Chemical and Materials Engineering

Suzanne Kresta, Chemical and Materials Engineering

Anthony Yeung, Chemical and Materials Engineering

Subir Bhattacharjee, Mechanical Engineering

Pierre Carreau, Chemical Engineering, École Polytechnique Montréal

To the memory of my father, Rengui Li

ABSTRACT

This thesis deals with the mechanisms of microstructure development in polymer blends. Much work has been performed on the breakup process of immiscible systems where the dispersed phase is suspended inside another matrix. The fluids used were polymer melts or model viscoelastic fluids, and the processing flows were model shear flow or processing flows seen in industry.

It is found that in industrial extruders or batch mixers, the morphology of the dispersed polymer evolves from pellets to films, and subsequently to fibers and particles. In this thesis, it is demonstrated based on force analysis that the in-situ graft reactive compatibilization facilitates breakup of the dispersed phase by suppressing slip at the interface of the dispersed phase and matrix phase.

The morphology development of polymer blends in industrial mixers was simulated by performing experiments of model viscoelastic drop deformation and breakup under shear flow. Two distinct modes of drop deformation and breakup were observed. Namely, viscoelastic drops can elongate and breakup either in (1) the flow direction or (2) the vorticity direction. The first normal stress difference N_1 plays a decisive role in the conditions and modes of drop breakup. Drop size is an important factor which determines to a great extent the mode of drop breakup and the critical point when the drop breakup mechanism changes. Small drops break along the vorticity direction, whereas large drops break in the flow direction.

A dramatic change in the critical shear rate was found when going from one breakup mode to another.

Polymer melts processed under shear flow present different morphology development mechanisms: films, fibers, vorticity elongation and surface instability. The mechanisms depend greatly on the rheological properties of both the dispersed and matrix phases, namely the viscosity ratio and elasticity ratio. High viscosity ratio and high elasticity ratio result elongation of the dispersed phase in the vorticity direction. Medium viscosity ratio and low elasticity ratio result in fiber morphology. Low viscosity ratio and high elasticity ratio result in film morphology. The surface instability is caused by the shear-thinning effect of the dispersed polymer.

ACKNOWLEDGEMENTS

I would like to express my deepest gratitude to my supervisor, Professor Uttandaraman Sundararaj, for all the guidance, encouragement and patience he has offered me throughout my thesis research. I have learned a lot from him, within research and beyond it.

I wish to thank my supervisory committee, Professors Suzanne Kresta and Anthony Yeung, for their valuable suggestion and guidance. Their research and insights have been a great source of inspiration for me over the years.

My gratitude is due to all the past and present fellow members of the Sundararaj group who have been a great source of knowledge, expertise and support. In particular, I would like to thank Dr. Bin Lin who has provided suggestion and support in all aspects of my research. I wish to acknowledge the assistance from the technical staff at the University of Alberta, Mr. Bob Smith, Mr. Boddez and Mr. Richard Cooper who helped in construction of Couette device, and Mr. George Braybrook who assisted in SEM characterization.

The Natural Sciences and Engineering Research Coucil of Canada (NSERC) is acknowledged for financial support of this research. Queen Elizabeth II Graduate Scholarship, Captain Thomas Farrell Greenhalgh Graduate Memorial Scholarship, Mary Louis Graduate Student Award and the GSA Professional

Development Grants are also highly acknowledged.

During my study at the University of Alberta, I have been receiving help and encouragement from many friends. They have given me springlike warmth during long winters in Edmonton. In particular, I highly appreciate the brotherly friendship from Shu Pan, and Professor Chengyou Kan at Tsinghua University.

My family has been a source of unfailing support. I thank my parents for their love and hard work to support me throughout my life. Their unwavering belief in education has always encouraged me. I thank my brother and sisters who have always given me support and encouragement. I thank my mother-in-law for taking care of my daughter, and my brother-in-law Yonghui Wang for all his support and understanding. I thank my daughter Jonelle for being a wonderful source of joy and hope. My final and greatest thanks go to my wife Jing Wang for her love, understanding, encouragement, and hard work.

TABLE OF CONTENTS

Chapter 1 Introduction **1**
- 1.1 Morphology Development of Polymer Blends 1
- 1.2 Drop Deformation and Breakup 5
  - 1.2.1 Newtonian systems 6
  - 1.2.2 Viscoelastic systems 10
- 1.3 Survey of the Thesis 13
- 1.4 References 14

Chapter 2 Morphology Development of Polymer Blends **23**
- 2.1 Introduction 23
- 2.2 Experimental Section 27
  - 2.2.1 Materials 27
  - 2.2.2 Blending Experiments 31
  - 2.2.3 Microscopic Characterization 33
- 2.3 Results and Discussion 34
  - 2.3.1 Morphology development and flow fields 34
  - 2.3.2 Effect of compatibilization 38
  - 2.3.3 Mechanism of the effect of compatibilization on the initial morphology development 45
  - 2.3.4 Effect of rotation rate 54
- 2.4 Conclusion 56
- 2.5 References 58

Chapter 3 Viscoelastic Drop Deformation in Newtonian Matrix at High Capillary Number under Simple Shear Flow **65**
- 3.1 Introduction 65
- 3.2 Experimental Section 69
  - 3.2.1 Materials 69
  - 3.2.2 Apparatus 72
  - 3.2.3 Procedure 74
- 3.3 Results and Discussion 74
  - 3.3.1 Observations of drop deformation 74
  - 3.3.2 Effect of viscolasticity 83
  - 3.3.3 Effect of drop size 89
  - 3.3.4 Effect of viscosity ratio 92
  - 3.3.5 Short remarks on breakup 94
- 3.4 Conclusion 94

3.5 References 95

Chapter 4 Visualization of Viscoelastic Drop Breakup in Shear Flow.... 101
4.1 Introduction 101
4.2 Experimental Section.. 107
4.2.1 Materials 107
4.2.2 Setup 110
4.2.3 Procedure 112
4.3 Results and Discussion 113
4.3.1 Breakup modes.. 113
4.3.2 Effect of drop size 116
4.3.3 Effect of viscoelasticity 128
4.4 Conclusion 131
4.5 References 132

Chapter 5 Polymer Blends under Shear Flow 136
5.1 Introduction 136
5.2 Experimental Section.. 140
5.2.1 Materials 140
5.2.2 Experimental Setup 142
5.2.3 Procedure 143
5.3 Results 145
5.3.1 PE/PS system under different shear rates 145
5.3.2 PC140/PS and PE/PC1050 systems 151
5.4 Discussion.. 154
5.4.1 Surface instability 154
5.4.2 Film, fiber and vorticity elongation 157
5.4.3 Morphology development during blending 160
5.5 Conclusion 162
5.6 References 163

Chapter 6 Conclusions and Future Work 168
6.1 General Discussion and Conclusions 168
6.1.1 Polymer melts in industrial mixers 168
6.1.2 Model viscoelastic fluids under simple shear flow.. 171
6.1.3 Polymer blends under shear flow.. 174
6.2 Recommendations for future work 176
6.2.1 Critical drop size for drop breakup 176
6.2.2 Compatibilization during polymer blending 177
6.2.3 Polymer blends under shear flow 177
6.3 References 180

Appendix

Appendix I Flow in Couette Device 181
Appendix II Magnification from the Side View of Couette Device 183

List of Tables:

Table 2-1 Glass transition temperature of polymers..29

Table 2-2 Polymer blend systems in extrusion..31

Table 2-3 Polymer blend systems in batch mixer..33

Table 2-4 Drop size and distribution* 41

Table 2-5 Magnitude of stresses and stress ratio 51

Table 3-1 Compositions of materials used in this study..70

Table 3-2 Experimental systems and their viscosity ratios 70

Table 4-1 Viscosity and formulations of material used in the study 108

Table 4-2 Relaxation time of Boger fluids 110

Table 4-3 The effect of drop size on breakup mode and condition 118

Table 4-4 Critical capillary number and viscosity ratio. 130

Table 5-1 Polymer systems used for parallel plate blending experiments 145

Table 5-2 Polymer systems and morphology 158

List of Figures:

Figure 1-1 Polymer blend morphologies and their characteristic properties. 2

Figure 1-2 Schematic of morphology development during blending. 3

Figure 1-3 Deformation and breakup process of a corn syrup drop in PDMS under shear flow in a Couette device, η_r=0.55...7

Figure 1-4 Schematic of drop deformation in a shear flow..................................8

Figure 1-5 Correlation of critical capillary number and viscosity ratio for Newtonian drop breakup...9

Figure 1-6 A Boger fluid drop is sheared in Newtonian PDMS in a Couette device. η_r=6.4. 11

Figure 2-1 Polymer blend morphologies and their characteristic properties.. 24

Figure 2-2 Coupling reaction between aPA and PSMA. 29

Figure 2-3 Rheological properties of polymers at 220°C....................................30

Figure 2-4 Schematic of sampling locations along Berstorff ZE25A UTX Ultraglide co-rotating twin screw extruder. 32

Figure 2-5 Morphology development of PS143/aPA (20 wt% aPA) at 220°C, rotation rate of 400 rpm and a feed rate of 25 kg/hr in Berstorff twin screw extruder.. 37

Figure 2-6 The flow fields in extruder and the evolution of the dispersed phase down the length of the extruder. 38

Figure 2-7 Morphology development of PSMA/aPA (20 wt% aPA) at 220°C, rotation rate of 400 rpm and a feed rate of 25 kg/hr in Berstorff twin screw extruder.. 42

Figure 2-8 Morphology development of PS143/aPA (20 wt% aPA) at 220°C, rotation rate of 1000 rpm and a feed rate of 62.5 kg/hr in Berstorff twin screw extruder. 43

Figure 2-9 Morphology development of PSMA/aPA (20 wt% aPA) at 220°C, rotation rate of 1000 rpm and a feed rate of 62.5 kg/hr in Berstorff twin screw extruder. 44

Figure 2-10 Viscosities of polymer blends obtained from location P of the extruder. 46

Figure 2-11 Optical photomicrographs of PS1200/aPA and PSMA/aPA obtained from internal batch mixer at 220°C and 100 rpm after mixing for 10 seconds and 20 seconds. 49

Figure 2-12 Optical photomicrographs of PMMA/aPA and PSMA/aPA obtained from internal batch mixer at 220°C and 20 rpm after mixing for 20 seconds and 40 seconds. 50

Figure 2-13 Compatibilization reduces slip at the interface of polymer blends. 54

Figure 3-1 Rheological properties of Boger fluids. 71

Figure 3-2 A schematic of the Couette apparatus. 73

Figure 3-3 A schematic of a drop subjected to simple shear flow 75

Figure 3-4 Flow direction deformation of system M3/D3, η_r=2.6, D_0=1.16mm.. 76

Figure 3-5 Reduced radii of M3/D3, η_r=2.6, D_0=1.16mm.. 77

Figure 3-6 Vorticity direction deformation of system M3/D4, $\eta_r = 3.2$, D_0=0.88mm. 79

Figure 3-7 Reduced radii of M3/D4, $\eta_r = 3.2$, D_0=0.88 mm. 80

Figure 3-8 Vorticity direction deformation of system M1/D4, $\eta_r = 32$, D_0=1.6mm. 82

Figure 3-9 Reduced radii of M1/D4, $\eta_r = 32$, D_0=1.6mm....83

Figure 3-10 Development of stresses and deformations with increasing capillary number of M3/D3....85

Figure 3-11 Development of stresses and deformations with increasing capillary number of M3/D4....87

Figure 3-12 Development of stresses and deformations with increasing capillary number of M3/D5....89

Figure 3-13 The effect of drop size on deformation of M3/D4....91

Figure 3-14 Drop deformation of D4 sheared in different PDMS....93

Figure 4-1 Critical capillary number versus viscosity ratio for Newtonian drop breakup....103

Figure 4-2 Deformation and breakup process of a corn syrup drop in PDMS under shear flow in a Couette device. η_r=1.1....104

Figure 4-3 Steady rheology properties of Boger fluids....109

Figure 4-4 Couette apparatus diagram....112

Figure 4-5 Drop deformation and breakup modes....114

Figure 4-6 Disturbance causes instability of vorticity-elongated drop....116

Figure 4-7 Breakup modes of M3/D3, η_r=2.6, for different drop sizes....119

Figure 4-8 The critical shear rate jumps when the breakup mechanism changes....120

Figure 4-9 Dependence of stress ratio on shear rate for different drop sizes for system M3/D3....123

Figure 4-10 Drop size effect on the stresses at breakup, M3/D3....125

Figure 4-11 The relationship between Ca_c and η_r for viscoelastic drop breakup..129

Figure 5-1 Complex viscosity (η^*) versus frequency (ω) for polymers at 220°C..141

Figure 5-2 Elastic modulus (G') versus frequency (ω) for polymers at 220°C..141

Figure 5-3 Schematics of the parallel-plate device. The black dot denotes a pellet of the dispersed phase. 143

Figure 5-4 PS sphere sheared in PE matrix at a rotation rate of 1rpm of the master rotor. 147

Figure 5-5 PE/PS sheared at a rotation rate of 5rpm of the master rotor. 148

Figure 5-6 PE/PS sheared at a rotation rate of 10 to 50 rpm of the master rotor. 150

Figure 5-7 PS drops are sheared in PE matrix while the rotation rate is increased stepwise by 1 rpm/min. 151

Figure 5-8 PS drops are deformed into films in PC140 matrix at 1 rpm.. 152

Figure 5-9 PC1050 drops are sheared in PE matrix at different shear rates. 154

Figure 5-10 Surface instability of polymer drop during shearing. 155

Figure 5-11 The effect of viscoelastic properties on morphology. 159

Figure 5-12 Morphology development mechanism during blending. 161

Figure 6-1 Basic design of cone-plate (top) and Couette device for simple shear flow. 179

Figure II-1 Cross section of the Couette device. The shaded areas denote the inner cylinder and the outer cylinder respectively.. 185

List of Symbols

B	Minor axis length
C	Constant
Ca	Capillary number
d	Gap of parallel plates
D	Diameter, mm
Df	Deformation
Df_1	Side Deformation
Df_2	Bottom Deformation
D_n	Number average diameter, μm
De	Deborah number
G'	Elastic modulus, Pa
k'	ratio of the relaxation time
L	Major axis length, pellet length
M	Molecular weight, power law coefficient
M_n	Number average molecular weight
M_w	Weight average molecular weight
n	Power law index, number
N	Rotation rate
N_1	First normal stress difference
N_2	Second normal stress difference
Q	Feed rate
R	Radius

R_0	Original drop radius
R_1	Half length in flow direction
R_2	Half length in velocity gradient direction
R_3	Half length in vorticity direction
S_r	Stress ratio
t	Time
T	Temperature
T_g	Glass transition temp[illegible]ure
U	Velocity
X	Radial position
$\hat{\mathrm{X}}$	Characteristic deformation
x	Flow direction
y	Velocity gradient direction
z	Vorticity direction
$\dot{\gamma}$	Shear rate
Γ	Interfacial tension, mN/m
η	Viscosity
η^*	Complex viscosity
η_r	Viscosity ratio
λ	Relaxation time
τ	Shear stress
Φ	Diameter of pellet
ψ_{01}	First normal stress difference coefficient at 0 shear rate

ψ_1	First normal stress difference coefficient
ω	Frequency
Ω	Rotation speed

Subscripts

c	Critical
d	Drop phase, dispersed phase
i	Inner cylinder, *ith* particle
m	Matrix phase or major phase
o	Outer cylinder
p	Polymer
s	Solvent
0	Initially or zero time

Abbreviations for Chemicals

EP	Poly(ethylene-co-propylene)
Ker	Kerosene
aPA	Amorphous Nylon
PA	Polyamide, Nylon
PA6,6	Nylon 6,6
PB	Polybutene
PC	Polycarbonate
PDMS	Polydimethylsiloxane
PE	Polyethylene
PIB	Polyisobutylene
PMMA	Poly(methyl methacrylate)
PS	Polystyrene
PSMA	Polystyrene-maleic anhydride

Chapter 1
Introduction

1.1 Morphology Development of Polymer Blends

Polymer blends represent a large fraction of all plastic resins produced today [1]. Blending two or more polymers has been of technological importance since it provides an economical way to tailor the properties of polymers without the high investment costs of synthesizing new polymers [2, 3]. Most polymer blends are immiscible, and if properly formulated they can possess enhanced properties over either of their components [3]. For example, adding 10% to 25% rubber to Nylon can improve its ductility over the pure polymer [4].

It is widely known that the properties of polymer blends are closely correlated to their morphologies [3, 5, 6]. Different morphologies offer different properties to meet different requirements. For example, the lamellar morphology of PE/PA 6,6 blend presents excellent diffusion barriers for fuel tank application [7], and a double emulsion morphology of PA 6,6/ EP leads to improvement of toughness [8]. Figure 1-1 shows some useful types of morphology with their key properties.

Polymer blends are mostly produced in batch mixers or extruders. The components of polymer blends are usually added to the mixers in pellet form and the blending process results in different morphologies depending on the properties of polymers and processing conditions. Therefore, it is crucial to understand how the morphologies are developed in the mixers and how to control the mixing conditions to obtain a proper morphology as shown in Figure 1-1.

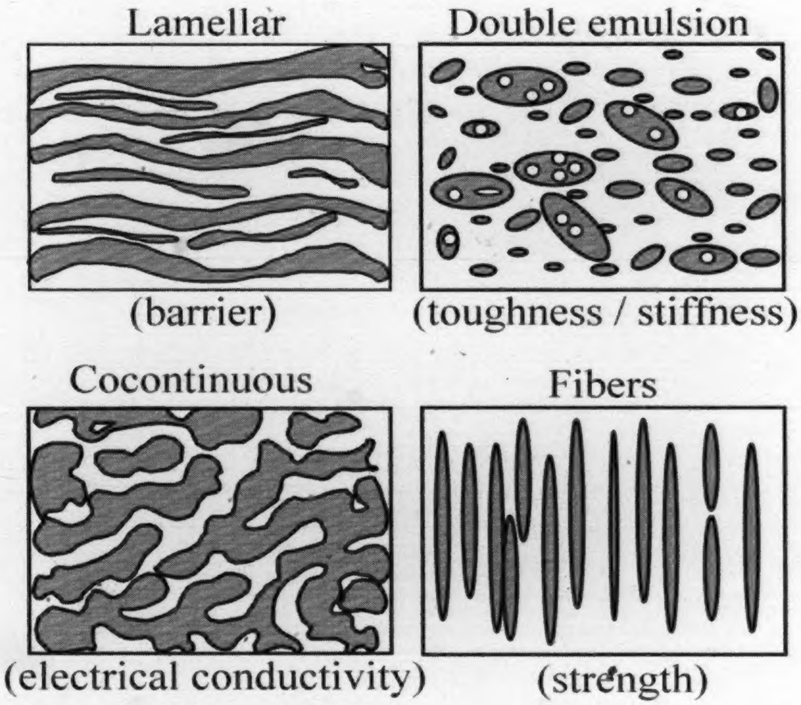

Figure 1-1 Polymer blend morphologies and their characteristic properties. Adapted from [3, 9].

The polymer blending process is a complex time-dependent process which involves flow-induced breakup and coalescence of viscoelastic polymer melts [10-12]. Early studies used microscopy to investigate the morphology development during blending. Microscopic samples were taken at different locations of extruders or after different mixing time in batch mixers. It has been demonstrated that the major changes in the morphology of polymer blends occur in the initial mixing stage [13-17]. During blending, pellets of the dispersed phase are stretched into sheets, and then the sheets break up into fibers, and subsequently, the fibers break up into particles [3, 13, 15, 16, 18]. The morphology development of polymer blends is shown schematically in Figure 1-2. Different morphologies, such as lamellar, fiber/matrix and particle/matrix, could be obtained if the blending process is stopped at different stages [3]. A lot of work has been done on the effects of different influential factors on the morphology development of polymer blends. These factors include polymer blend composition, viscosity ratio, processing time, temperature and shear rate [11, 19-22].

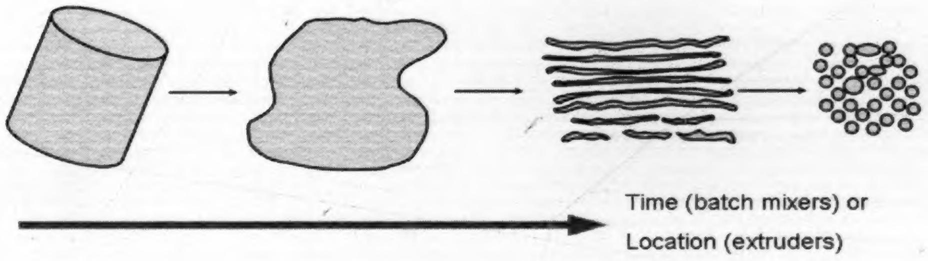

Figure 1-2 Schematic of morphology development during blending.

An important approach to improve the mixing of polymer blends and stabilize the morphology is using compatibilization. Compatibilization can be achieved by adding block copolymer or conducting in-situ graft or crosslinking reaction [23, 24] during polymer blending. Block copolymers at the interface between the phases can reduce interfacial tension. However, studies on the final particle size of dispersed phase show that the main effect of compatibilization in reducing particle size is resistance to droplet coalescence while the decrease in interfacial tension has only a minor effect [11, 25, 26]. Studies on the effect of compatibilization during the initial stage where the major morphological change occurs are rare [25, 27-30]. Cartier and Hu reported that the morphology of compatibilized blends developed faster than uncompatibilized blends [31]. This implies that compatibilization plays an important role in the initial breakup process which determines the final morphology of polymer blends to a great extent.

The microscopic method gives a relatively good understanding of morphology development during polymer blending in real mixers. However, morphological change may occur during sampling, and accurate correlation between the flow field parameters and the morphology is missing. The fundamental problem underlying the topic of morphology development during blending is how the flow field in mixers along with the polymer properties determines the polymer blend morphology. Due to the complexity of the rheological properties of polymer melts and the complexity of the flow field inside industrial mixers, one may apply model fluids and/or model flow fields to the investigation of this problem. Typical model fluids are Newtonian fluids, Boger fluids, polymer solutions etc., and typical model flow fields are simple shear flow, 1-D extensional flow etc.

1.2 Drop Deformation and Breakup

The study of morphology development during polymer blending aims to describe how one fluid is deformed and broken up in another immiscible fluid. The dispersion of immiscible liquids has been investigated as drop deformation and breakup in well-defined flow fields. It has been extensively investigated since Taylor's work in the 1930s [32, 33]. To date, most research work has been focused on an isolated Newtonian drop immersed in another Newtonian fluid. Negligible buoyancy force and low Reynolds number have typically been employed to further simplify the research. It was found that the correlation of two dimensionless groups, capillary number which is the ratio of shear stress and interfacial stress, and viscosity ratio of the two phases can be used to describe drop deformation and breakup. The effects of viscosity ratio, type of flow field, flow history and surfactant were studied extensively [34-36]. Studies on Newtonian systems have provided a reasonably clear understanding on the physical mechanism [32-39].

Early studies in morphology development of polymer blends used theories of drop deformation and breakup in Newtonian systems. However, these theories are not valid for polymer blending since polymers are viscoelastic fluids. Drop deformation and breakup for viscoelastic fluids is more complex than that for Newtonian fluids due to the complexity of rheological properties and the modification of stresses and flows by viscoelasticity [40-52]. To date, there is no universally-applicable theory for drop deformation and breakup for viscoelastic systems and the research is still in its infancy. Moreover, most research with viscoelastic fluids were confined to model fluids such as polymer solutions or Boger fluids. Studies on drop deformation and breakup of polymer melts at high temperature are rare [17, 42, 53-62].

1.2.1 Newtonian systems

When a drop of Newtonian fluid is suspended in a second Newtonian fluid which is undergoing shear flow, the drop will deform and may break up under critical conditions. Figure 1-3 shows a typical drop deformation and breakup process of Newtonian systems under shear flow.

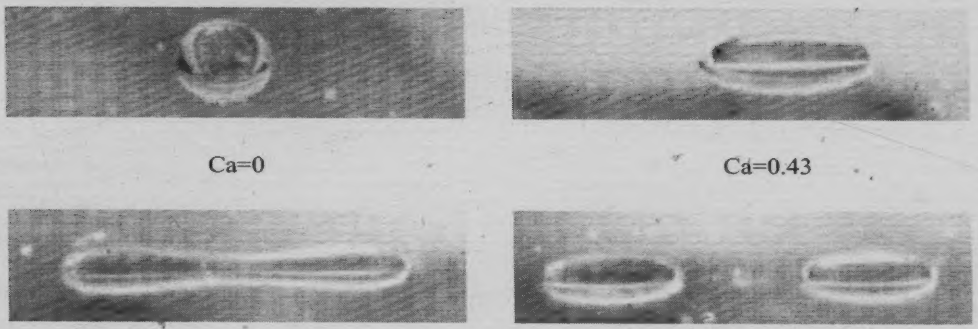

Ca=0 Ca=0.43

Ca=0.47 Ca=0.47

Figure 1-3 Deformation and breakup process of a corn syrup drop in polydimethylsiloxane (PDMS) under shear flow in a Couette device, $\eta_r=0.55$. The original drop diameter is 1.2mm.

Figure 1-4 gives a schematic of drop deformation and breakup. Here we denote the viscosities of the drop and the matrix as η_d and η_m, respectively. The matrix and drop have the same density. The interfacial tension coefficient between the phases is Γ and the radius of the undeformed drop is R. $\dot{\gamma}$ is the shear rate. Two dimensionless groups, capillary number ($Ca = \frac{\eta_m \dot{\gamma} R}{\Gamma}$) and viscosity ratio ($\eta_r = \frac{\eta_d}{\eta_m}$), are found to govern drop deformation and breakup. Deformation (Df) of the drop was defined by Taylor [33] as

$$Df = \frac{L - B}{L + B} \tag{1.1}$$

where L and B are the major axis length and minor axis length. Df is a function of Ca and η_r. Review articles by Rallison [63] and Stone [64] summarize theoretical and experimental studies on drop deformation.

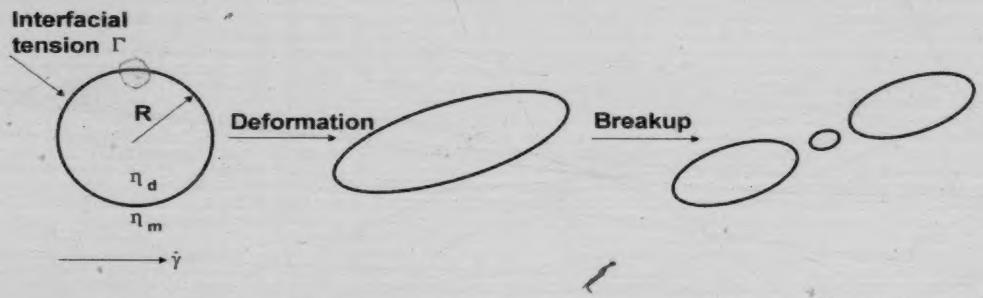

Figure 1-4 Schematic of drop deformation in a shear flow.

When interfacial force cannot balance shear force, the drop will break up in the shear direction into two or more daughter drops (Figure 1-4). The critical conditions of drop breakup have been of great interest because of the significance of dispersion in many industrial processes. The critical capillary number (Ca_c) is found to be a function of viscosity ratio. Grace's monumental work [34] gives a quantitative correlation of the critical capillary number and viscosity ratio for drop breakup in both simple shear and extensional flows. The results are summarized in Figure 1-5. Grace's results indicate that it is impossible to break a drop in simple shear flow when the viscosity ratio is higher than 4.

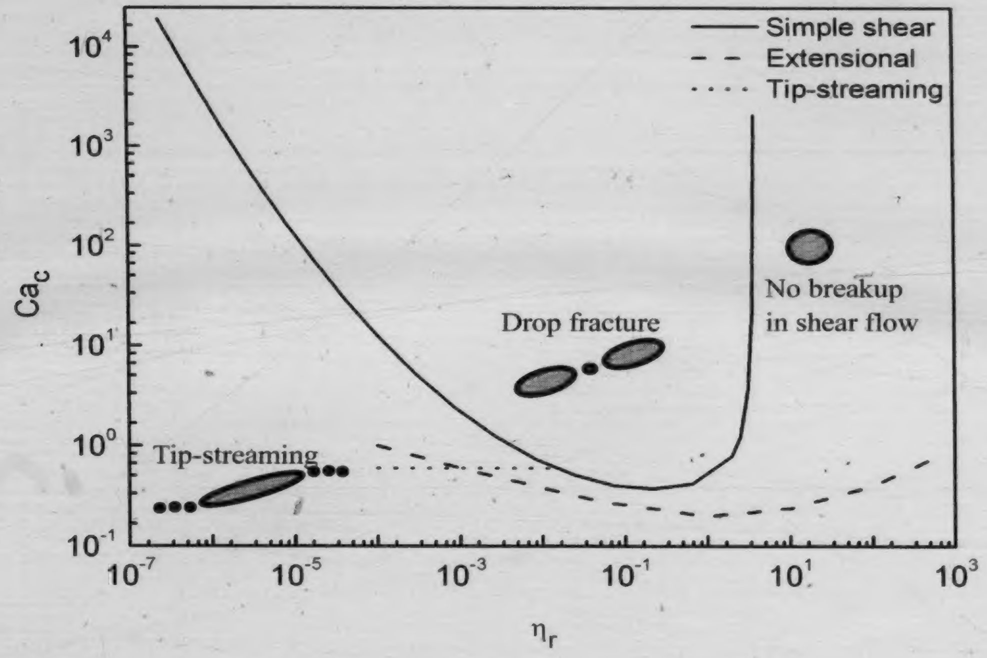

Figure 1-5 Correlation of critical capillary number and viscosity ratio for Newtonian drop breakup. Adapted from [34].

Besides the regular breakup mode shown in Figure 1-4, a special breakup phenomenon, tip-streaming, is also found in Newtonian systems under simple shear flow. In this phenomenon, small droplets continuously break from the tips of the mother drop. The critical capillary number for tip-streaming is lower than that for regular breakup as shown in Figure 1-4. De Bruijn [65] demonstrated that tip-streaming is caused by non-uniform distribution of surfactant at the interface. The surfactant is swept toward the ends of the drop and viscous stresses tear the narrow end regions away.

1.2.2 Viscoelastic systems

1.2.2.1 Model viscoelastic fluids

Most research on drop deformation and breakup of viscoelastic systems involves polymeric solutions or Boger fluids at room temperature [45, 47, 66-70]. Besides capillary number and viscosity ratio, elasticity of both phases is another factor affecting the drop deformation and breakup in viscoelastic systems. The elasticity of the drop has been reported to inhibit deformation [41, 54, 71]. The critical capillary number for viscoelastic drop breakup is found to be higher than its Newtonian counterpart [36, 41, 52, 61]. Normal stresses are found to play an important role in the viscoelastic drop deformation [42, 45, 54, 71]. Simple models of force balance among shear stress, interfacial stress and normal stresses by De Bruijn [36] and Aggarwal & Sarkar [52] can be used to explain the effect of drop elasticity on drop deformation.

While the influence of drop elasticity on drop deformation is straightforward and can be easily understood, the effect of matrix elasticity on drop deformation is quite complex. Experimental results reported in literature are not consistent. Mighri *et al.* [41] found that matrix viscoelasticity increases drop deformation, while Flumerfelt [72], Guido *et al.* [47] and Verhulst and Moldenaers [73] found that matrix viscoelasticity hinders drop deformation and breakup. Yue *et al.*

clarified this non-monotonic behaviour by investigating the modification of stresses and flow field by viscoelasticity [50].

A new mechanism of drop deformation in viscoelastic systems was reported by Migler [74]. He indicated that at high capillary numbers, a Boger fluid drop sheared in Newtonian PDMS matrix can align along vorticity direction. Figure 1-6 shows results from our work on the vorticity alignment of a viscoelastic drop which is sheared in a Newtonian matrix. Mighri and Huneault found the elongation along vorticity direction were related to normal stress and drops can break up in vorticity direction [45].

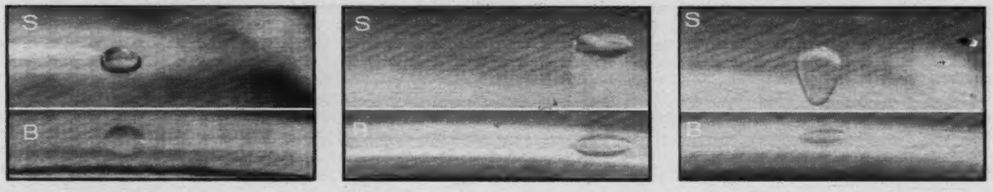

$\dot{\gamma} = 0\,\mathrm{s}^{-1}$ $\dot{\gamma} = 3.26\,\mathrm{s}^{-1}$ $\dot{\gamma} = 8.6\,\mathrm{s}^{-1}$

Figure 1-6 A Boger fluid drop (consists of 0.6% polyisobutylene, 8.5% kerosene and 90.9% polybutene) is sheared in Newtonian polydimethylsiloxane (viscosity is 4.9 Pa.s) fluid in a Couette device. η_r=6.4. The initial drop diameter is 1.06mm. At high shear rate, the drop aligns in the vorticity direction. S and B denote the side view and bottom view of the Couette device, respectively. The horizontal direction of each picture is flow direction; the vertical direction in S is the vorticity direction and in B is the velocity gradient direction.

1.2.2.2 Polymer melts

There are not many studies on drop deformation and breakup for polymer melts. Sundararaj *et al.* [17] investigated drop deformation in polymer melt systems under shear flow. Polymer drops are found to deform into films or fibers depending on the stress ratio and relaxation time. Elasticity of the systems were included in the stress ratio and the relaxation time [75, 76]. Levitt and Macosko observed drop widening effect in shear flow and related this effect to the second normal stress difference [54]. These experiments were done under relatively low shear rate, which means the elasticity exerts relatively weak influence on drop deformation. Migler *et al.* [77] visualized the morphology of polystyrene (PS) drops in a polyethylene (PE) matrix under flow in a transparent slit die installed at the end of a twin-screw extruder. A variety of droplet shapes were observed as a function of shear rate and viscosity ratio. In the limit of strong shear, PS droplets were observed to elongate along vorticity direction. This elongation along vorticity direction is related to the normal stress difference between drop and matrix [42].

Lerdwijitjarud *et al.* found for different viscosity ratios critical capillary number increases in the ratio of the first normal stress difference between the drop and matrix phases [56]. More recently, Sundararaj and coworkers [57-60, 78] reported four types of polymer drop breakup modes: erosion, parallel breakup, vorticity breakup and tip-streaming. Stress ratio ($S_R = \frac{\eta_m \dot{\gamma} + 2G_m'}{\Gamma / R + 2G_d'}$) *vs.* Deborah number (De) was used to characterize breakup criterion for each mode. S_R decreases with increasing De. These results show that the drop breakup in polymer melt systems is very complex. The four mechanisms reported by Sundararaj and coworkers can coexist for the same system.

1.3 Survey of the Thesis

The main objective of this thesis is to understand the fundamentals underlying morphology development during polymer blending. Experimental systems include polymer melts processed in industrial mixer, model viscoelastic fluids processed in shear flow and polymer melts processed in shear flow.

Different topics are discussed in Chapters 2-5. The chapters have been written so that each can be read separately. These topics are related to polymer morphology development but with different emphasis. Chapter 2 deals with morphology development of polymer blends in industrial mixers. The morphology development is investigated using microscopy. Effects of compatibilization and rotation rate on the morphology development are discussed. Chapter 3 and Chapter 4 investigate the deformation and breakup of a Boger fluid drop sheared in a Newtonian matrix by visualization method. Emphasis is given on the effects of rheological properties and drop size on the drop deformation and breakup. Chapter 5 presents the drop deformation and breakup of polymer melts under shear flow. Efforts were made to more closely simulate real polymer blending process. Different systems and shear rates are employed to understand the morphology development. Chapter 6 summarizes this thesis work and provides recommendations for future work.

1.4 References

[1] L. A. Utracki, "Polymer blends handbook", Kluwer Academic Publishers, Boston, (2002).

[2] L. A. Utracki, "Polymer alloys and blends -- thermodynamics and rheology", Hanser Publishers, New York, (1989).

[3] C. W. Macosko, "Morphology development and control in immiscible polymer blends," Macromol. Symp. **149**, 171 (2000).

[4] S. H. Wu, "Phase-structure and adhesion in polymer blends - a criterion for rubber toughening," Polymer **26**, 1855 (1985).

[5] M. Evstatiev, S. Fakirov, G. Bechtold and K. Friedrich, "Structure-property relationships of injection- and compression- molded microfibrillar-reinforced PET/PA-6 composites," Adv. Polym. Technol. **19**, 249 (2000).

[6] A. Gonzalezmontiel, H. Keskkula and D. R. Paul, "Impact-modified nylon-6 polypropylene blends. 1. Morphology-property relationships," Polymer **36**, 4587 (1995).

[7] P. M. Submaranian, "Permeability barriers by controlled morphology of polymer blends," Polym. Eng. Sci. **27**, 663 (1987).

[8] B. N. Epstein, "Tough thermoplastic nylon compositions," U. S. Patent 4174358 (1979).

[9] U. Sundararaj, C. K. Shih and C. W. Macosko, "Evidence for inversion of phase continuity during morphology development in polymer blending," Polym. Eng. Sci. **36**, 1769 (1996).

[10] L. A. Utracki and H. Shi, "Development of polymer blend morphology during compounding in a twin-screw extruder. Part I: Droplet dispersion and coalescence-a review," Polym. Eng. Sci. **32**, 1824 (1992).

[11] U. Sundararaj and C. W. Macosko, "Drop breakup and coalescence in polymer blends - the effects of concentration and compatibilization," Macromolecules **28**, 2647 (1995).

[12] C. L. Tucker and P. Moldenaers, "Microstructural evolution in polymer blends," Annu. Rev. Fluid Mech. **34**, 177 (2002).

[13] C. E. Scott and C. W. Macosko, "Model experiments concerning morphology development during the initial stages of polymer blending," Polymer Bulletin **26**, 341 (1991).

[14] J. T. Lindt and A. K. Ghosh, "Fluid mechanics of the formation of polymer blends. Part I: Formation of lamellar structures," Polym. Eng. Sci. **32**, 1802 (1992).

[15] U. Sundararaj, C. W. Macosko, R. J. Rolando and H. T. Chan, "Morphology development in polymer blends," Polym. Eng. Sci. **32**, 1814 (1992).

[16] C. E. Scott and C. W. Macosko, "Morphology development during the initial stages of polymer-polymer blending," Polymer **36**, 461 (1995).

[17] U. Sundararaj, Y. Dori and C. W. Macosko, "Sheet formation in immiscible polymer blends: Model experiments on initial blend morphology," Polymer **36**, 1957 (1995).

[18] R. C. Willemse, E. J. J. Ramaker, J. Van Dam and A. Posthuma De Boer, "Morphology development in immiscible polymer blends: Initial blend morphology and phase dimensions," Polymer **40**, 6651 (1999).

[19] H. E. Burch and C. E. Scott, "Effect of viscosity ratio on structure evolution in miscible polymer blends," Polymer **42**, 7313 (2001).

[20] J. K. Lee and C. D. Han, "Evolution of polymer blend morphology during compounding in a twin-screw extruder," Polymer **41**, 1799 (2000).

[21] S. Joseph and S. Thomas, "Morphology development and mechanical properties of polystyrene/polybutadiene blends," Eur. Polym. J. **39**, 115 (2003).

[22] C. Harratsa, T. Omonova, G. Groeninckxa and P. Moldenaers, "Phase morphology development and stabilization in polycyclohexylmethacrylate/ polypropylene blends: Uncompatibilized and reactively compatibilized blends using two reactive precursors," Polymer **45**, 8115 (2004).

[23] M. Xanthos and S. S. Dagli, "Compatibilitation of polymer blends by reactive processing," Polym. Eng. Sci. **31**, 929 (1991).

[24] A. Ajji and L. A. Utracki, "Interphase and compatibilization of polymer blends," Polym. Eng. Sci. **36**, 1574 (1996).

[25] H. Li and G.-H. Hu, "The early stage of the morphology development of immiscible polymer blends during melt blending: Compatibilized vs. Uncompatibilized blends," J. Polym. Sci., Part B: Polym. Phys. **39**, 601 (2001).

[26] S. T. Milner and H. W. Xi, "How copolymers promote mixing of immiscible homopolymers," J. Rheol. **40**, 663 (1996).

5

[27] L. Y. Yang, T. G. Smith and D. Bigio, "Melt blending of linear low-density polyethylene and polystyrene in a haake internal mixer. 1. Compatibilization and morphology development," J. Appl. Polym. Sci. **58**, 117 (1995).

[28] A. K. Bhowmick, T. Chiba and T. Inoue, "Reactive processing of rubber-plastic blends - role of chemical compatibilizer," J. Appl. Polym. Sci. **50**, 2055 (1993).

[29] H. K. Jeon and J. K. Kim, "Morphological development with time for immiscible polymer blends with an in situ compatibilizer under controlled shear conditions," Polymer **39**, 6227 (1998).

[30] Y. Li, S. Hu and J. Sheng, "Evolution of phase dimensions and interfacial morphology of polypropylene/polystyrene compatibilized blends during mixing," Eur. Polym. J. **43**, 561 (2007).

[31] H. Cartier and G.-H. Hu, "Morphology development of in sifu compatibilized semicrystalline polymer blends in a co-rotating twin-screw extruder," Polym. Eng. Sci. **39**, 996 (1999).

[32] G. I. Taylor, "The viscosity of a fluid containing small drops of another fluid," Proc. R. Soc. London Ser. A **138**, 41 (1932).

[33] G. I. Taylor, "The formation of emulsions in definable fields of flow," Proc. R. Soc. London Ser. A **146**, 501 (1934).

[34] H. P. Grace, "Dispersion phenomena in high-viscosity immiscible fluid systems and application of static mixers as dispersion devices in such systems," Chem. Eng. Commun. **14**, 225 (1982).

[35] B. J. Bentley and L. G. Leal, "An experimental investigation of drop deformation and breakup in steady, two-dimensional linear flows," J. Fluid Mech. **167**, 241 (1986).

[36] R. A. De Bruijn, PhD Thesis, "Deformation and breakup of drops in

simple shear flows," Eindhoven University of Technology, Eindhoven (1989).

[37] R. G. Cox, "Deformation of a drop in a general time-dependent fluid flow," J. Fluid Mech. **37**, 601 (1969).

[38] E. J. Hinch and A. Acrivos, "Long slender drops in a simple shear-flow," J. Fluid Mech. **98**, 305 (1980).

[39] P. L. Maffettone and M. Minale, "Equation of change for ellipsoidal drops in viscous flow," J. Non-Newtonian Fluid Mech. **78**, 227 (1998).

[40] F. Mighri, A. Ajji and P. J. Carreau, "Influence of elastic properties on drop deformation in elongational flow," J. Rheol. **41**, 1183 (1997).

[41] F. Mighri, P. J. Carreau and A. Ajji, "Influence of elastic properties on drop deformation and breakup in shear flow," J. Rheol. **42**, 1477 (1998).

[42] E. K. Hobbie and K. B. Migler, "Vorticity elongation in polymeric emulsions," Phys. Rev. Lett. **82**, 5393 (1999).

[43] S. Ramaswamy and L. G. Leal, "The deformation of a viscoelastic drop subjected to steady uniaxial extensional flow of a Newtonian fluid," J. Non-Newtonian Fluid Mech. **85**, 127 (1999).

[44] S. Ramaswamy and L. G. Leal, "The deformation of a Newtonian drop in the uniaxial extensional flow of a viscoelastic liquid," J. Non-Newtonian Fluid Mech. **88**, 149 (1999).

[45] F. Mighri and M. A. Huneault, "Dispersion visualization of model fluids in a transparent couette flow cell," J. Rheol. **45**, 783 (2001).

[46] S. B. Pillapakkam and P. Singh, "A level-set method for computing solutions to viscoelastic two-phase flow," J. Comput. Phys. **174**, 552 (2001).

[47] S. Guido, M. Simeone and F. Greco, "Deformation of a Newtonian drop in a viscoelastic matrix under steady shear flow - experimental validation of slow flow theory," J. Non-Newtonian Fluid Mech. **114**, 65 (2003).

[48] J. Beaucourt, T. Biben and C. Verdier, "Elongation and burst of axisymmetric viscoelastic droplets: A numerical study," Phys. Rev. E **71**, 066309-1 (2005).

[49] V. Sibillo, S. Guido, F. Greco and P. L. Maffettone, "Single drop dynamics under shearing flow in systems with a viscoelastic phase," Macromol. Symp. **228**, 31 (2005).

[50] P. T. Yue, J. J. Feng, C. Liu and J. Shen, "Viscoelastic effects on drop deformation in steady shear," J. Fluid Mech. **540**, 427 (2005).

[51] D. Khismatullin, Y. Renardy and M. Renardy, "Development and implementation of vof-prost for 3D viscoelastic liquid-liquid simulations," J. Non-Newtonian Fluid Mech. **140**, 120 (2006).

[52] N. Aggarwal and K. Sarkar, "Deformation and breakup of a viscoelastic drop in a Newtonian matrix under steady shear," J. Fluid Mech. **584**, 1 (2007).

[53] U. Sundararaj, Y. Dori and C. W. Macosko. "Visualization of morphology development in polymer blends," in ANTEC 1994, San Francisco, CA, USA.

[54] L. Levitt, C. W. Macosko and S. D. Pearson, "Influence of normal stress difference on polymer drop deformation," Polym. Eng. Sci. **36**, 1647 (1996).

[55] L. Levitt and C. W. Macosko, "Shearing of polymer drops with interface modification," Macromolecules **32**, 6270 (1999).

[56] W. Lerdwijitjarud, A. Sirivat and R. G. Larson, "Influence of elasticity on dispersed-phase droplet size in immiscible polymer blends in simple

shearing flow," Polym. Eng. Sci. **42**, 798 (2002).

[57] B. Lin, F. Mighri, M. A. Huneault and U. Sundararaj, "Parallel breakup of polymer drops under simple shear," Macromol. Rapid Commun. **24**, 783 (2003).

[58] B. Lin, U. Sundararaj, F. Mighri and M. A. Huneault, "Erosion and breakup of polymer drops under simple shear in high viscosity ratio systems," Polym. Eng. Sci. **43**, 891 (2003).

[59] B. Lin and U. Sundararaj, "Sheet formation during drop deformation and breakup in polyethylene/polycarbonate systems sheared between parallel plates," Polymer **45**, 7605 (2004).

[60] B. Lin, F. Mighri, M. A. Huneault and U. Sundararaj, "Effect of premade compatibilizer and reactive polymers on polystyrene drop deformation and breakup in simple shear," Macromolecules **38**, 5609 (2005).

[61] T. Cherdhirankorn, W. Lerdwijitjarud, A. Sirivat and R. G. Larson, "Dynamics of vorticity stretching and breakup of isolated viscoelastic droplets in an immiscible viscoelastic matrix," Rheol. Acta **43**, 246 (2004).

[62] F. Mighri and M. A. Huneault, "In situ visualization of drop deformation, erosion, and breakup in high viscosity ratio polymeric systems under high shearing stress conditions," J. Appl. Polym. Sci. **100**, 2582 (2006).

[63] J. M. Rallison, "The deformation of small viscous drops and bubbles in shear flows," Annu. Rev. Fluid Mech. **16**, 45 (1984).

[64] H. A. Stone, "Dynamics of drop deformation and breakup in viscous fluids," Annu. Rev. Fluid Mech. **26**, 65 (1994).

[65] R. A. De Bruijn, "Tipstreaming of drops in simple shear flows," Chem. Eng. Sci. **48**, 277 (1993).

[66] W. J. Milliken and L. G. Leal, "Deformation and breakup of viscoelastic

drops in planar extensional flows " J. Non-Newtonian Fluid Mech. **40**, 355 (1991).

[67] P. P. Varanasi, M. E. Ryan and P. Stroeve, "Experimental-study on the breakup of model viscoelastic drops in uniform shear-flow," Ind. Eng. Chem. Res. **33**, 1858 (1994).

[68] W. Lerdwijitjarud, A. Sirivat and R. G. Larson, "Influence of dispersed-phase elasticity on steady-state deformation and breakup of droplets in simple shearing flow of immiscible polymer blends," J. Rheol. **48**, 843 (2004).

[69] H. Li and U. Sundararaj, "Does drop size affect the mechanism of viscoelastic drop breakup? " Phys. Fluids **20**, 053101-1 (2008).

[70] H. Li and U. Sundararaj, "Experimental investigation of viscoelastic drop deformation in Newtonian matrix at high capillary number under simple shear flow," J. Non-Newtonian Fluid Mech. (submitted).

[71] H. Vanoene, "Modes of dispersion of viscoelastic fluids in flow," J. Colloid Interface Sci. **40**, 448 (1972).

[72] R. W. Flumerfelt, "Drop breakup in simple shear fields of viscoelastic fluids," Ind. Eng. Chem. Fund. **11**, 312 (1972).

[73] K. Verhulst and P. Moldenaers, "Drop shape dynamics of a Newtonian drop in a non-Newtonian matrix during transient and steady shear flow," J. Rheol. **51**, 261 (2007).

[74] K. B. Migler, "Droplet vorticity alignment in model polymer blends," J. Rheol. **44**, 277 (2000).

[75] U. Sundararaj, PhD Thesis, "Morphology development during polymer blending," University of Minnesota, Minneapolis (1994).

[76] P. G. Ghodgaonkar and U. Sundararaj, "Prediction of dispersed phase drop

diameter in polymer blends: The effect of elasticity," Polym. Eng. Sci. **36**, 1656 (1996).

[77] K. B. Migler, E. K. Hobbie and F. Qiao, "In line study of droplet deformation in polymer blends in channel flow," Polym. Eng. Sci. **39**, 2282 (1999).

[78] B. Lin, PhD Thesis, "Visualization of polymer blending and drop breakup," University of Alberta, Edmonton (2005).

Chapter 2

Morphology Development of Polymer Blends*

2.1 Introduction

Blending immiscible polymers is of technological importance since it provides an economical way to achieve a variety of desirable properties which cannot be obtained from a single polymer [1-3]. It has attracted scientists working in polymers, rheology and fluid mechanics to uncover the dispersion mechanisms in polymer blends [4-25]. The blending process is a complex time-dependent process which involves flow-induced breakup and coalescence of viscoelastic fluids [16, 19, 26-28]. It results in a certain morphology of polymer blends which can be partly characterized by the size, shape and orientation of the phases [15]. It is widely known that the performance and properties of polymer blends are directly related to the morphology of the blends [2, 29, 30]. Different morphologies offer different properties to meet different requirements. For example, double emulsion morphology of the blends of PA 6,6 and EP leads to improvement in toughness, and lamellar morphology of the blends of PE and PA 6,6 presents excellent diffusion barriers [2]. Figure 2-1 shows some useful types of morphology with their key properties.

---

[*] Portions of this chapter are published in Macromol. Chem. Phys. (2009).

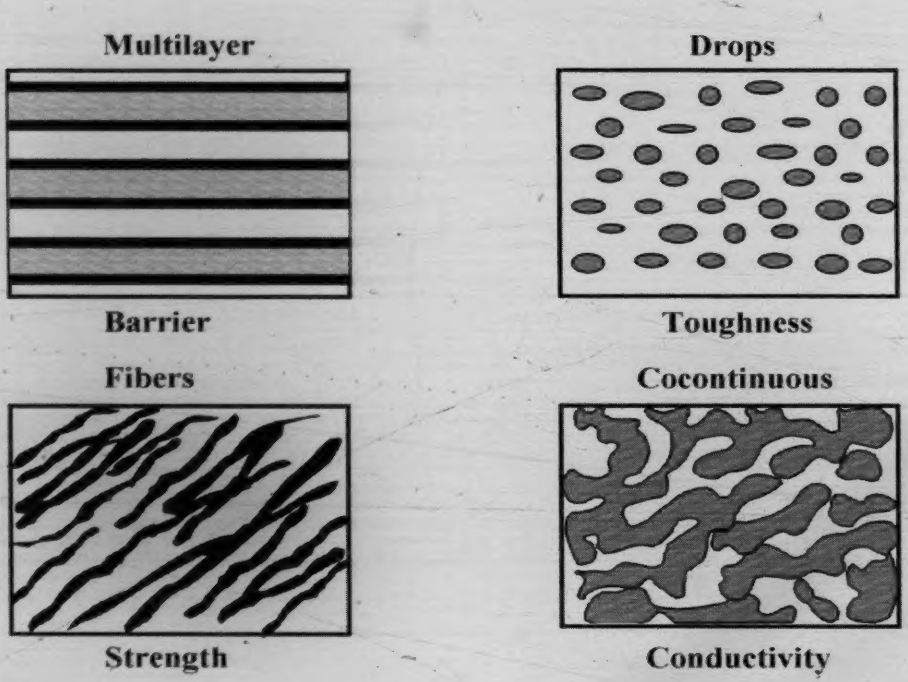

Figure 2-1 Polymer blend morphologies and their characteristic properties. Adapted from [2, 31].

Blending in most mixing equipment involves melting, breaking and coalescence processes. A good understanding of the mechanism of morphology development of polymer blends over the time scale (batch mixers) or over the length scale (extruders) would be helpful to control the final morphology and in the design of processing equipment [32]. Early studies revealed that major changes in the morphology of polymer blends occur in the initial mixing stage [26, 32-35]. During blending, pellets of the dispersed phase are stretched into sheets, and then the sheets break up into fibers, and subsequently, the fibers break into particles [2, 32, 33, 35, 36]. If the blending process is stopped at different stages, different morphologies, such as lamellar, fiber/matrix and particle/matrix, could be obtained [2]. It is believed that the early mixing stage is controlled by breakup and the final stage is dominated by the balance between drop breakup and coalescence [27, 37-40]. Besides this general observation, the effects of polymer composition, viscosity ratio, processing time or temperature, and shear rate on morphology evolution of polymer blends have also been investigated [27, 41-44].

Compatibilization is a common method used to improve the mixing of polymer blends and control the morphology. It is achieved by adding block copolymer or conducting in-situ reaction [45, 46] during polymer blending. The main effect of compatibilization is resistance to droplet coalescence while the decrease in interfacial tension has only a minor effect on the final particle size [27, 47, 48]. In-situ reaction results in better compatibilization effect than block copolymer [27]. However, the effect of compatibilization during the whole polymer blending process, especially the initial stage and intermediate stage where major morphological changes occur, has rarely been examined [47, 49, 50]. Cartier and Hu indicated that the morphology of compatibilized blends developed faster than uncompatibilized blends [51]. This implies that compatibilization also has an important effect on the initial breakup process which determines the final morphology of polymer blends to a great extent.

A fundamental problem in the study of morphology development of polymer blends is how the processing conditions and polymer properties affect the morphology. This is essentially a problem of viscoelastic drop deformation, breakup and coalescence. However, many studies on the polymer blending process applied results of drop breakup in Newtonian fluid systems, such as Taylor's small deformation theory or Grace's breakup curve [52, 53]. Not surprisingly, the theories of Newtonian fluids were found inapplicable for polymer blending [6, 14, 27]. The reasons for the discrepancies are twofold: 1) polymers are non-Newtonian fluids; and 2) the flow field in polymer blending equipment is much more complex than most flows studied. Early research efforts on this problem employed model viscoelastic fluid (for example, polymer solutions or Boger fluids) and/or model flow fields (for example, simple shear flow or extensional flow). Several researchers investigated polymer solution/Boger fluid drop breakup in shear flow [4, 9, 24, 54]. Other researchers studied drop breakup of polymer solution/Boger fluid under elongational flow [8, 10]. Sundararaj *et al.* [26] and Levitt *et al.* [7] investigated sheet formation under shear in molten polymers. Lin *et al.* studied polymer drop breakup under shear in molten polymers [16, 17, 22]. These progresses in fluid mechanics research inspired a revisit of morphology development in polymer blends.

In this work, we found morphology developed faster in compatibilized system of amorphous Nylon (aPA)/polystyrene-maleic anhydride copolymer (PSMA) than in uncompatibilized system of amorphous Nylon (aPA)/polystyrene

(PS). To separate the effect of compatibilization from that of rheological properties, model experiments of poly(methyl methacrylate) (PMMA)/aPA blends, PS/aPA blends, and PSMA/aPA blends were performed. The morphology development of polymer blends was investigated from the perspective of fluid mechanics. The role of compatibilization during the initial/intermediate blending stage was determined by applying recent developed theories of viscoelastic fluids. The dispersion mechanism due to compatibilization was further reinforced by investigating the effect of rotation rate on morphology development.

2.2 Experimental Section

2.2.1 Materials

All materials are commercial polymers obtained in pellet form. Amorphous nylon (aPA, Selar 3452 from DuPont), was used as dispersed phase in this study. Poly(styrene-maleic anhydride) (PSMA), poly (methyl methacrylate) (PMMA) and two kinds of polystyrene (PS) were used as the matrix phases. In all experiments, the ratio of the matrix phase to the dispersed phase is 80:20 on mass basis. PS143 (Styrol 143, BASF) and PSMA (Dylark 332, Nova Chemicals) were used in extrusion. PSMA is a copolymer of styrene and maleic anhydride, in which the content of maleic anhydride is 14%. In experiments conducted in a batch mixer, PS1200 (Nova Chemicals), PMMA (PMMA V920, Altuglas) and PSMA were used as matrix phases. Reaction between amine and anhydride groups provides in situ compatibilization between PSMA and aPA. The reaction is shown in Figure 2-2 [55].

The interfacial tension between PS and aPA is 19 mN/m [56]. Levitt and Macosko reported that there was no evidence to indicate that the interfacial tension was reduced by the graft polymerization between PSMA and aPA [57]. Therefore, the interfacial tension of PSMA and aPA should be close to 19 mN/m. The interfacial tension between PMMA and aPA is 3.4mN/m measured in our laboratory using the drop retraction method [58, 59]. The glass transition temperature (Tg) of the samples obtained from a differential scanning calorimeter (DSC2910, TA Instruments) are listed in Table 2-1.

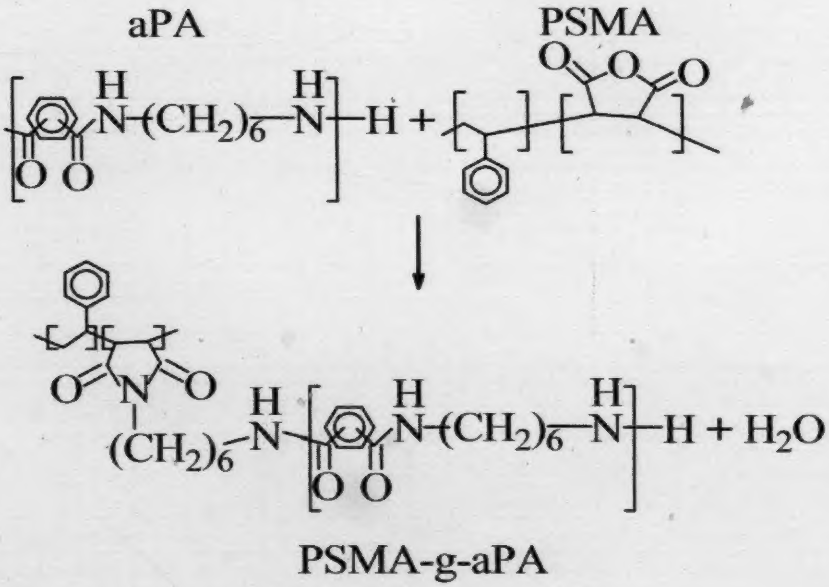

Figure 2-2 Coupling reaction between aPA and PSMA.

Dynamic rheological properties of the polymers were obtained with a Rheometrics RMS800 rheometer using parallel plate geometry at 10% strain at 220°C. Figure 2-3 shows the complex viscosity and elastic modulus of the polymers.

Table 2-1 Glass transition temperature of polymers

Polymer	PS143	PSMA	aPA	PS1200	PMMA
Tg, °C	88	130	130	107	107

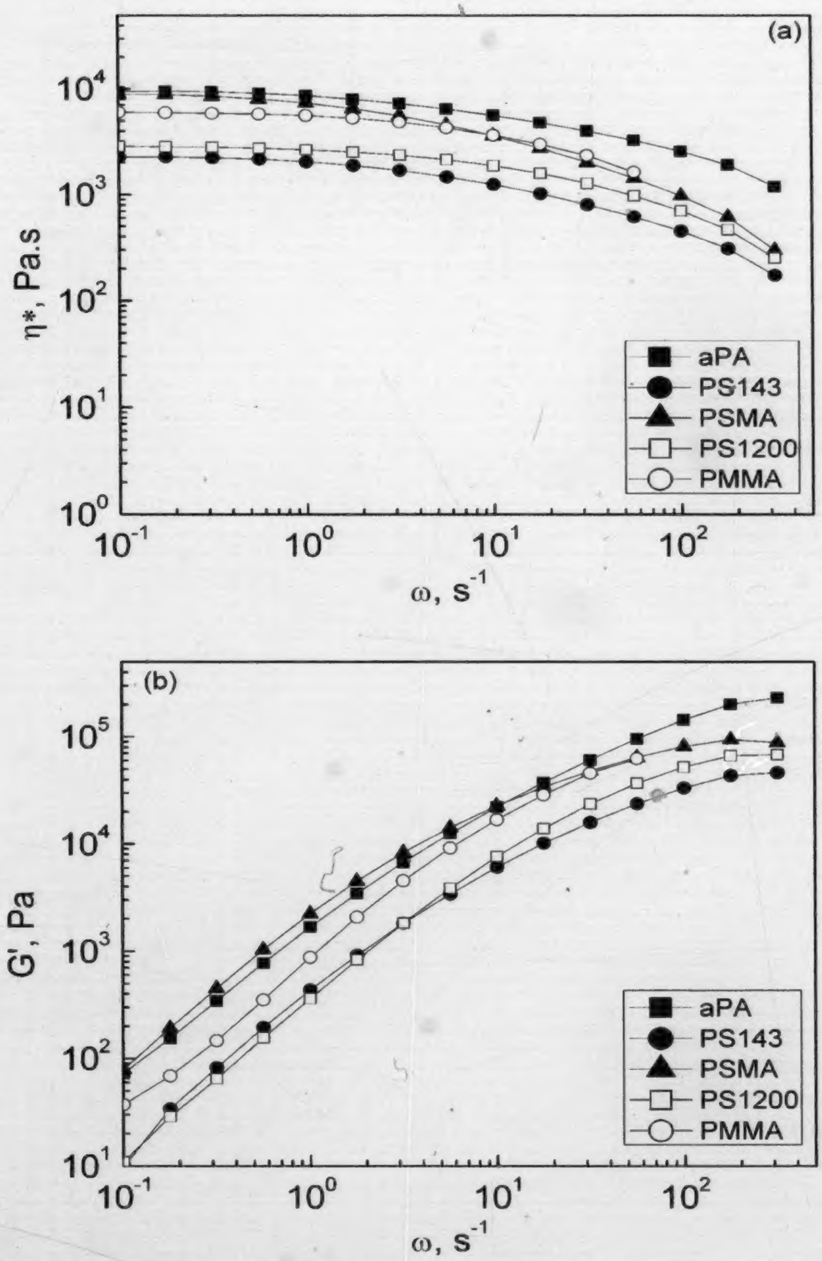

Figure 2-3 Rheological properties of polymers at 220°C. (a) Complex viscosity; (b) Elastic modulus.

2.2.2 Blending Experiments

2.2.2.1 Blending in extruder

Polymer blends were prepared using a co-rotating twin screw extruder (Berstorff ZE25A UTX Ultra-glide Extruder). The blend samples were PS143/aPA (80:20) and PSMA/aPA (80:20). Four runs of blending experiments were performed. The details of the experimental conditions are shown in Table 2-2. In all cases the ratio of feed rate (Q) to rotation rate (N) was kept constant at Q/N=1/16.

Table 2-2 Polymer blend systems in extrusion

Run	Blend	Type	Feed Rate (kg/hr)	Rotation rate (rpm)	Temperature (°C)
1	PS143/aPA	Uncompatibilized	25	400	220
2	PSMA/aPA	Compatibilized	25	400	220
3	PS143/aPA	Uncompatibilized	62.5	1000	220
4	PSMA/aPA	Compatibilized	62.5	1000	220

After each run, the screws were pulled out and samples were taken from different locations along the extruder, as shown in Figure 2-4. The samples were cooled in liquid nitrogen immediately after being taken from the screws. Sample 1-3 were from the first kneading section where the melting occurred. Sample A was between the first kneading section and the second kneading section. Sample 4-6 were from the second kneading section, which is used for mixing. Sample P was the product at the end of the extruder.

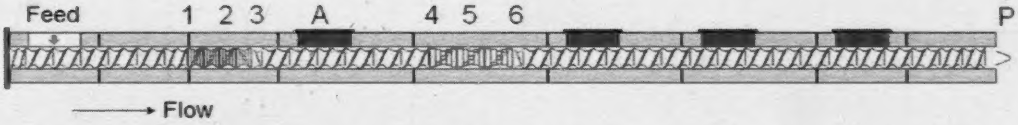

Figure 2-4 Schematic of sampling locations along Berstorff ZE25A UTX Ultraglide co-rotating twin screw extruder.

2.2.2.2 Model blending experiments in batch mixer

Model polymer blending experiments were done using a Haake Rheomix 600 internal batch mixer with a Haake System 90 drive (Thermo Scientific). The major phases were PS1200, PMMA and PSMA. The minor phase was aPA. The ratio of the major phase to the minor phase was 80:20 on mass basis. The temperature of the internal batch mixer was first increased to 220°C. Polymer pellets were then fed to the mixer and melted without rotation of the rotors for 10 minutes until the melt reached a steady temperature of 220 °C. This time is also long enough for reaction to occur at the interface between PSMA and aPA [60, 61]. Polymers occupied 70% of the free volume of the batch mixer. The rotors were started after the 10 minutes heating. Rotation speeds of 100 rpm and 20 rpm were used for PS1200/aPA and PMMA/aPA, respectively, in order to have a close match in rheological properties between PS1200 and PSMA, and between PMMA and PSMA. Details of the experiments are shown in Table 2-3.

After mixing for a specified time, the motor was stopped. The front plate and the middle barrel were removed. Polymer blend samples were taken from the mixing roller blades and were quenched immediately in liquid nitrogen.

Table 2-3 Polymer blend systems in batch mixer

Controlled group	Blend	Type	Rotation rate (rpm)	Temperature (°C)
1	PS1200/aPA	Uncompatibilized	100	220
	PSMA/aPA	Compatibilized	100	220
2	PMMA/aPA	Uncompatibilized	20	220
	PSMA/aPA	Compatibilized	20	220

2.2.3 Microscopic Characterization

Blend samples from the extruder were examined using scanning electron microscopy. To determine the morphology of both the major phase and the minor phase of polymer blends, samples were extracted using selective solvents and then viewed under JEOL 6301F field emission scanning electron microscope (SEM) at 5.0kV acceleration voltage. The solvents used were: 1) methylene chloride to dissolve PS, PMMA and PSMA, and 2) formic acid to dissolve aPA. Samples were sputter-coated with gold before being imaged under SEM.

Samples obtained from internal batch mixer were microtomed into slices 2 to 5μm thick, and then viewed under MacroFire LM CCD Digital Camera (Optronics).

2.3 Results and Discussion

2.3.1 Morphology development and flow fields

Figure 2-5 shows typical morphology development of polymer blends along the Berstorff twin-screw extruder. The system shown in Figure 2-5 is PS143/aPA (80:20) processed at temperature of 220°C, rotation rate of 400 rpm and feed rate of 25 kg/hr. In the first kneading zone, the dispersed polymer pellets deform into thin sheets within the matrix phase and the sheets break up via instabilities. In the second kneading zone, the dispersed phase evolves from sheets to mainly fibers. The fibers continue to break up into droplets after the second kneading zone. This observation agrees with previous studies by other researchers [32, 33, 35, 36]. One might notice that the shape of the holes in the matrix left by dissolving the dispersed phase does not exactly match the morphology obtained from the dispersed phase. For example, at location 5, the matrix shows elongated drops but the dispersed phase shows cylinders and ribbons as the dominant shapes. This type of discrepancy is normal since the dispersed phase could have different orientations within the matrix phase. A fractured surface may only contain part of the morphological information of the dispersed phase. The morphology obtained by dissolving the matrix phase gives a clearer picture of the dispersed phase. However, it gives only dispersion information. Information about spatial distribution can only be obtained from the matrix. Thus, it is important to obtain morphologies from both phases. The morphology of other polymer blends processed in Berstorff extruder evolves in the same way, which will be shown in the following sections of this article.

From the hopper of the extruder to the first kneading zone, the temperature of polymer pellets increases from room temperature to a temperature close to the set temperature as a result of heat transfer from the barrel and heat transfer due to viscous dissipation. Polymers start to melt and soften in this stage. The shear stress applied by the rotating screws starts to stretch the polymer pellets in the flow direction. The minor dimensions of the dispersed phase (the radius of cylinders or the thickness of ribbons) decrease. In the first kneading zone, the polymers experience intensive mixing. The shear rate in this region is very high and consequently, so is the shear stress. The dispersed phase is stretched biaxially into thinner films. Due to instability, film breakup occurs in this stage. The breakup may be due to holes forming in the films. It is envisaged that the holes increase in size until they impinge on each other forming fibers [26, 32, 33, 35, 56]. Other instabilities may also break the films into cylinders. Small particles of the dispersed phase may also be expected in the early stage of mixing due to erosion and tip-streaming [17, 21, 22].

Between the kneading zones, the shear rate and shear stress are lower than those in the kneading zones. In this region of the extruder, the polymer melt relaxes and the relaxation process helps to further break the films of the dispersed phase into fibers. When the polymers enter the second kneading zone, they experience a high shear stress again. The fibers are stretched longer and thinner. These fibers can break up into droplets via fiber instabilities. Further breakup occurs during the relaxation process in the conveying section immediately after the second kneading zone. Droplet coalescence could also be expected in this stage [27].

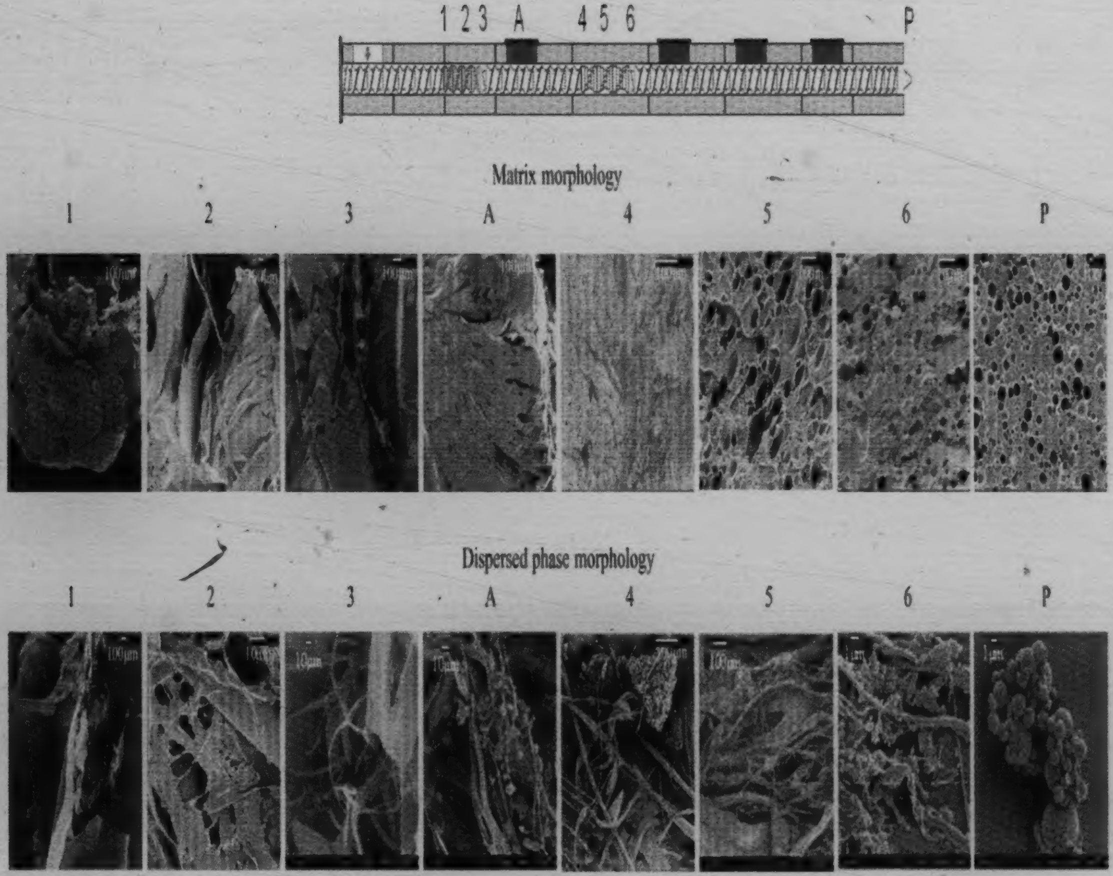

Figure 2-5 Morphology development of uncompatibilized system PS143/aPA (20 wt% aPA) at 220°C, rotation rate of 400 rpm and a feed rate of 25 kg/hr in Berstorff twin screw extruder. (Note different scale bars).

The dispersion process, i.e. the deformation and breakup process of the dispersed phase under changing flows, along the length of the extruder is summarized in Figure 2-6.

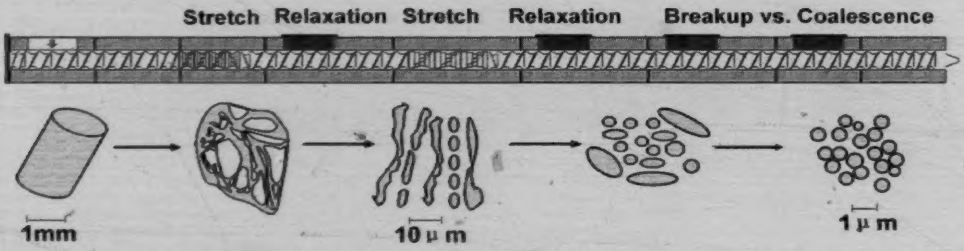

Figure 2-6 The flow fields in extruder and the evolution of the dispersed phase down the length of the extruder.

2.3.2 Effect of compatibilization

Figure 2-7 shows the morphology development of polymer blends PSMA/aPA (80:20) at 220°C, rotation rate of 400 rpm, and a feed rate of 25 kg/hr. The difference between Figure 2-5 and Figure 2-7 is that the system shown in Figure 2-7 has in-situ reactive compatibilization. The reaction between PSMA and aPA is very fast at 220°C [60, 61]. In Figure 2-7, the dispersed phase in the compatibilized system evolves from pellets to films, then films to fibers and finally fibers to particles, which is the same as that of the uncompatibilized system. Compatibilization does not influence the development of polymer blend morphology qualitatively, as observed by Scott and Macosko [32].

However, a closer observation of the morphologies at different locations shows that morphology change in the compatibilized system is faster than that in the uncompatibilized system. Comparing the morphologies obtained from locations 1 and 2 in Figure 2-5 and Figure 2-7, one can see that the films of the dispersed phase are thinner in the compatibilized system and the breaking of the films in compatibilized system is more extensive. Note the different scale bars when comparing micrographs for different locations for the same system and when comparing Figure 2-5 and Figure 2-7. At locations 3 and A, the compatibilized system has more and thinner fibers than the uncompatibilized system. From the morphologies obtained from location 1 to location A, it can be seen that morphology developed faster in the compatibilized system. At locations 4, 5 and 6, the fibers formed initially continue to become thinner and eventually break up. In these locations, the decrease in dimensions of the fibers in the compatibilized system is faster than that in the uncompatibilized system. At location 5, the dispersed polymer exists as fibers and particles in the compatibilized system, while big sheets can still be found in the uncompatibilized system. At location 6, the morphology consists of a combination of particles and long fibers in the uncompatibilized system, while in the compatibilized system, no long fibers are observed.

Figure 2-8 and Figure 2-9 show the morphology development of polymer blends PS143/aPA (80:20) and PSMA/aPA (80:20) processed at 220°C, rotation rate of 1000 rpm and feed rate of 62.5 kg/hr, respectively. The films in the initial stages are thinner in the compatibilized system than those in the uncompatibilized system. Thin films break more quickly into fibers and the eventual fiber breakup results in more uniform and smaller particles in the compatibilized system. At location P, a number of long fibers are seen in the uncompatibilized system while only spherical particles are observed in the compatibilized system. Again, the morphology development in these two systems demonstrates that compatibilization enhances dispersion in polymer blends.

At the outlet of the extruder, location P, spherical particles are found in both compatibilized and uncompatibilized systems (except Figure 2-8). These particles result from the breaking of the fibers present in the upstream locations. Table 2-4 gives the final particle diameters and final particle size distribution of different systems. The number average drop diameter and the volume average drop diameter are defined as:

$$D_n = \sum n_i D_i / \sum n_i \tag{2.1}$$

$$D_v = \sum n_i D_i^4 / \sum n_i D_i^3 \tag{2.2}$$

where n_i and D_i are the number and the apparent diameter of the ith domain. A comparison of the particle size distribution shows that particles of the dispersed phase in the compatibilized systems is both smaller and more uniform in size than those in the uncompatibilized systems. Sundararaj and Macosko [27] demonstrated that the smaller size and uniform particles in the compatibilized system can be attributed to the reduction in drop coalescence due to compatibilization.

From the morphology development of the compatibilized and uncompatibilized systems, it has been shown that in the initial stages of blending, the morphological change is mainly due to the breakup of the dispersed phase; and in the later stages of blending, the morphological change is determined by a balance between drop breakup and coalescence. Compatibilization facilitates the breakup process in the initial stages and allows the dispersed phase to resist drop coalescence in the later stages.

Table 2-4 Drop size and distribution*

Blends	PS143/aPA	PSMA/aPA	PS143/aPA **	PSMA/aPA
Type	Uncompatibilized	Compatibilized	Uncompatibilized	Compatibilized
Rotation rate, rpm	400	400	1000	1000
D_n, μm	0.71	0.32	2.9	0.32
D_v, μm	2.2	0.50	10	0.45
D_v/D_n	3.0	1.6	3.4	1.4

* All drop sizes were measured using the matrix SEM picture of the sample at location P (product).

** Uncompatibilized system PS143/aPA (1000 rpm) has fibers in sample P. The drop size measured here was based on the matrix SEM picture, so the actual particle size may be higher than reported.

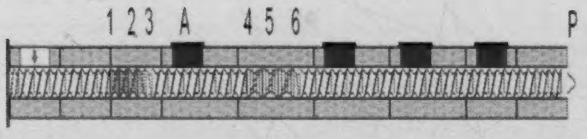

Matrix morphology

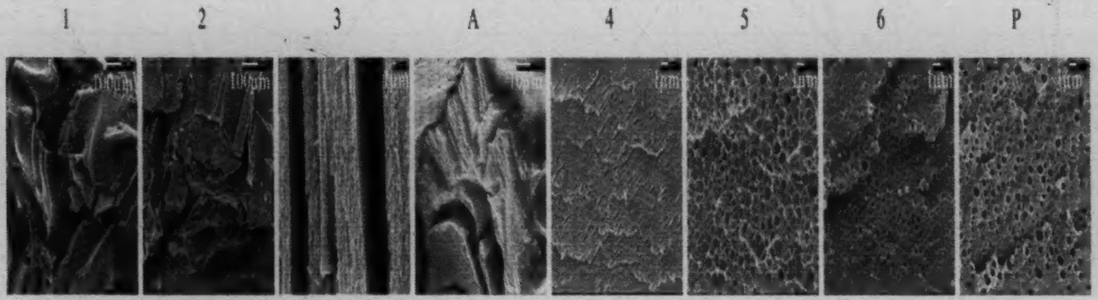

Dispersed phase morphology

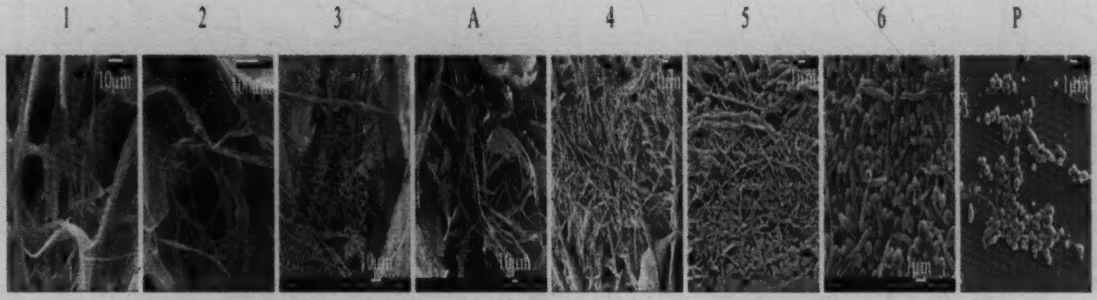

Figure 2-7 Morphology development of compatibilized system PSMA/aPA (20 wt% aPA) at 220°C, rotation rate of 400 rpm and a feed rate of 25 kg/hr in Berstorff twin screw extruder. (Note different scale bars).

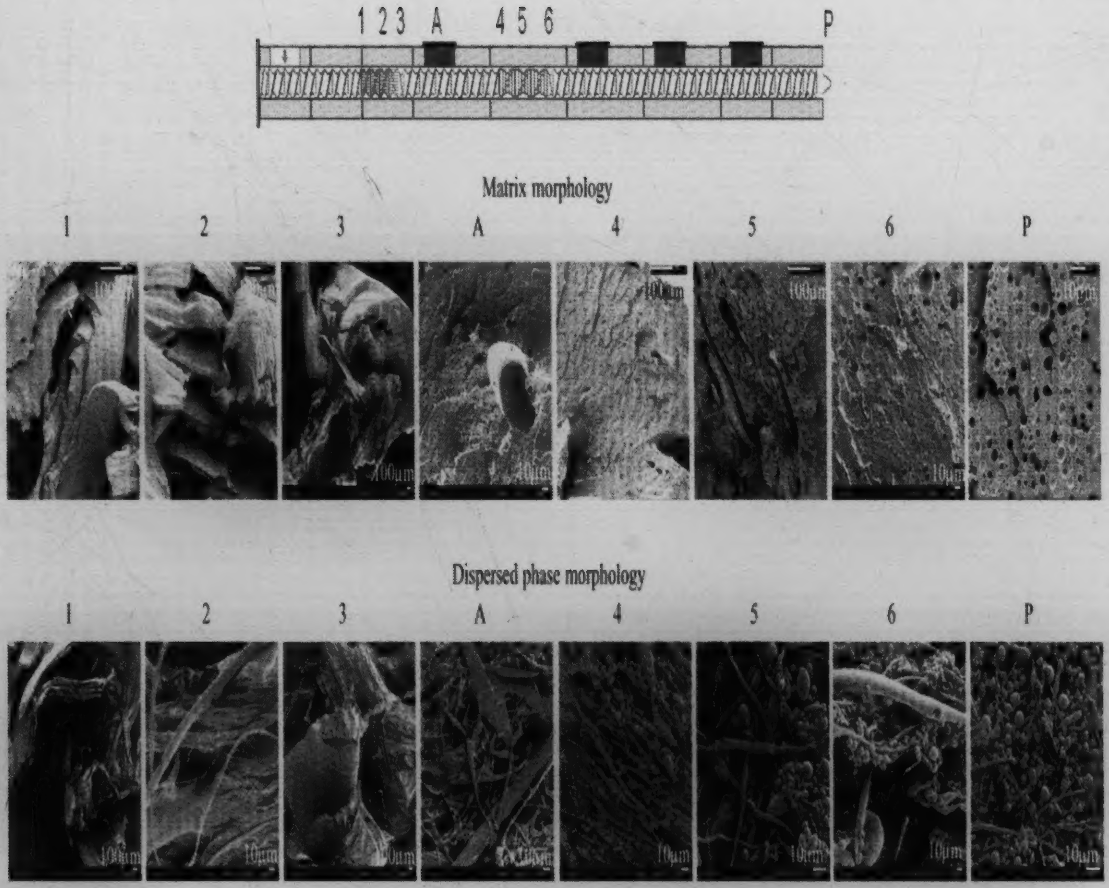

Figure 2-8 Morphology development of uncompatibilized system PS143/aPA (20 wt% aPA) at 220°C, rotation rate of 1000 rpm and a feed rate of 62.5 kg/hr in Berstorff twin screw extruder. (Note different scale bars).

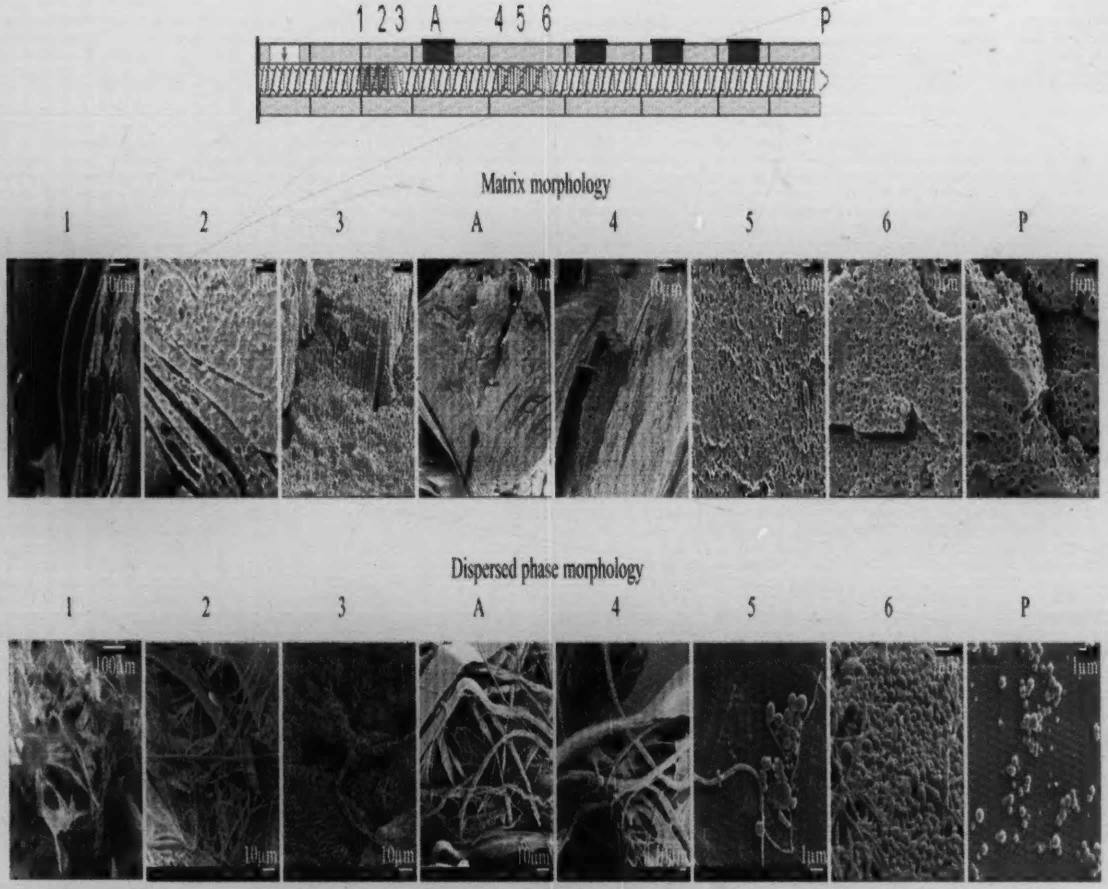

Figure 2-9 Morphology development of compatibilized system PSMA/aPA (20 wt% aPA) at 220°C, rotation rate of 1000 rpm and a feed rate of 62.5 kg/hr in Berstorff twin screw extruder. (Note different scale bars).

2.3.3 Mechanism of the effect of compatibilization on the initial morphology development

In our extrusion experiments, it has been demonstrated that compatibilized systems have better dispersion in polymer blends and that this better dispersion is due to the differences in the initial morphology development. To further understand the mechanisms underlying the dynamic dispersion process during polymer blending, it is necessary to examine the effects of different forces on the morphological change. The blending process is complex due to the complexity of the rheological properties of polymers and slip which could exist at the interface between different phases [62-64].

Viscosity measurement is usually used to detect the slip at the interface of polymer blends. Figure 2-10 shows the viscosity of the polymer blends obtained from location P of the extruder. The predicted viscosity of these blends, $\eta_{(PS143/aPA\text{-}Cal)}$ and $\eta_{(PSMA/aPA\text{-}Cal)}$, are calculated using the log-additive mixing rule:

$$\log \eta_{Cal} = \varphi_1 \eta_1 + \varphi_2 \eta_2 \tag{2.3}$$

where φ_i and η_i are the volume fraction and viscosity of the components. As seen from Figure 2-10, the viscosities of both PS143/aPA blends prepared at 400rpm and 1000rpm show significant negative deviation from the predicted viscosity calculated by log-additive mixing rule, PS143/aPA-Cal in Figure 2-10. This negative deviation means that there exists interfacial slip at the interface of PS143 and aPA [64, 65]. However, the viscosities of both PSMA/aPA blends prepared at 400rpm and 1000rpm are very close to the predicted viscosity based on the log-additive mixing rule, PSMA/aPA-Cal in Figure 2-10. The viscosities of the PSMA/aPA blends obtained at 400rpm and 1000rpm indicate that the reactive compatibilization suppresses interfacial slip.

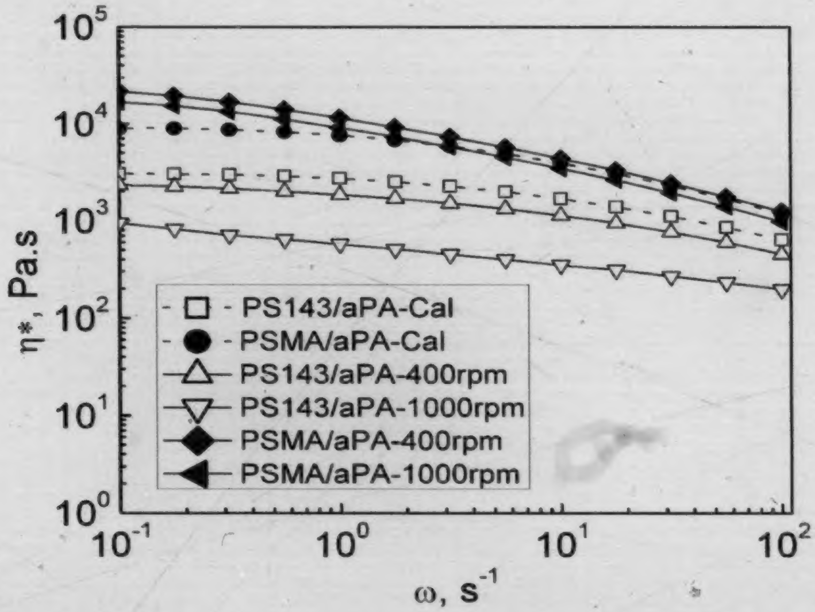

Figure 2-10 Viscosities of polymer blends obtained from location P of the extruder. Open symbols are uncompatibilized systems and closed symbols are compatibilized systems. Solid lines are measured viscosities for polymer blends obtained from location P of the extruder. Dashed lines (PS143/aPA-Cal and PSMA/aPA-Cal) denote predicted viscosities based on log-additive mixing rule (Eqn 2.3).

The initial stage of morphology development is important as it determines to a great extent the final morphology [2, 32, 33, 36, 47, 56]. The mechanism of polymer blending was further explored by performing model experiments in the internal batch mixer. The details of the batch mixer experiments were described in the experimental section. In order to investigate the effect of compatibilization on the morphology development, compatibilized and uncompatibilized polymer blend systems with similar rheological properties were selected for the model experiments. For the controlled group of PS1200/aPA and PSMA/aPA, the experiments were run at 220°C and a rotation rate of 100 rpm. The maximum shear rate in the mixer at a rotor speed of 100rpm is estimated to be 130 s^{-1} based on the minimum gap between the rotor tip and barrel of the mixer [33]. Figure 2-3 shows that PS1200 and PSMA have very similar viscosity and elastic modulus at 130 s^{-1}. As mentioned in the experimental section, no evidence was found that the grafting reaction between PSMA and aPA reduces the interfacial tension [57]. Before starting the rotor, polymers were heated in the mixer for 10 minutes. This time is long enough for the polymers to reach a steady temperature and for the in-situ reaction to complete at the interface available before mixing. Therefore, the only factor that differentiates the morphology of PS1200/aPA and PSMA/aPA is compatibilization. By investigating the difference in the initial morphology of PS1200/aPA and PSMA/aPA, we can understand how compatibilization influences the morphology development at the initial stage.

Figure 2-11 shows the optical photomicrographs of PS1200/aPA (80:20) and PSMA/aPA (80:20). After 10s mixing, the dispersed phase aPA in PS1200/aPA system appears coarse in the photomicrograph, while aPA in PSMA/aPA system forms thin layers in the PSMA matrix. At this stage, as in the extrusion experiments, the dispersed phase should have film-like morphology. The average thickness of the films in PS1200/aPA is 9.1μm, while the average thickness of the films in PSMA/aPA is 2.4μm. The films in the compatibilized system are much thinner than that in the uncompatibilized system. After 20 seconds, the dispersed phase in both blends evolves to a spherical particle shape. However, the particles in the compatibilized system (PSMA/aPA) are much finer than those in the uncompatibilized system (PS1200/aPA). Again, the morphology in the compatibilized system changes more quickly than in the uncompatibilized system.

Another controlled group is PMMA/aPA and PSMA/aPA processed at 220°C and rotation rate of 20 rpm. At these conditions, PMMA and PSMA have similar rheological properties (see Figure 2-3). Compatibilization is again the major factor influencing the initial morphology development of polymer blends. Figure 2-12 shows the optical photomicrographs of PMMA/aPA (80:20) and PSMA/aPA (80:20) obtained from internal batch mixer. After 20 seconds, the dispersed phase domains (aPA) in PMMA/aPA are very large and the size of these domains is not uniform. However, aPA forms a layered structure inside the PSMA matrix and there are also aPA particles present. Similar to Figure 2-11, the compatibilized PSMA/aPA system shown in Figure 2-12(b) has thinner films than the uncompatibilized PMMA/aPA system shown in Figure 2-12(a). After 40 seconds mixing, aPA in PMMA/aPA system also evolves to a layered structure, with films and particles distributed throughout the matrix. In PSMA/aPA system, aPA domains are thinner and more uniform. Again the morphology in the compatibilized system develops faster and gives smaller particle size than that in the uncompatibilized system.

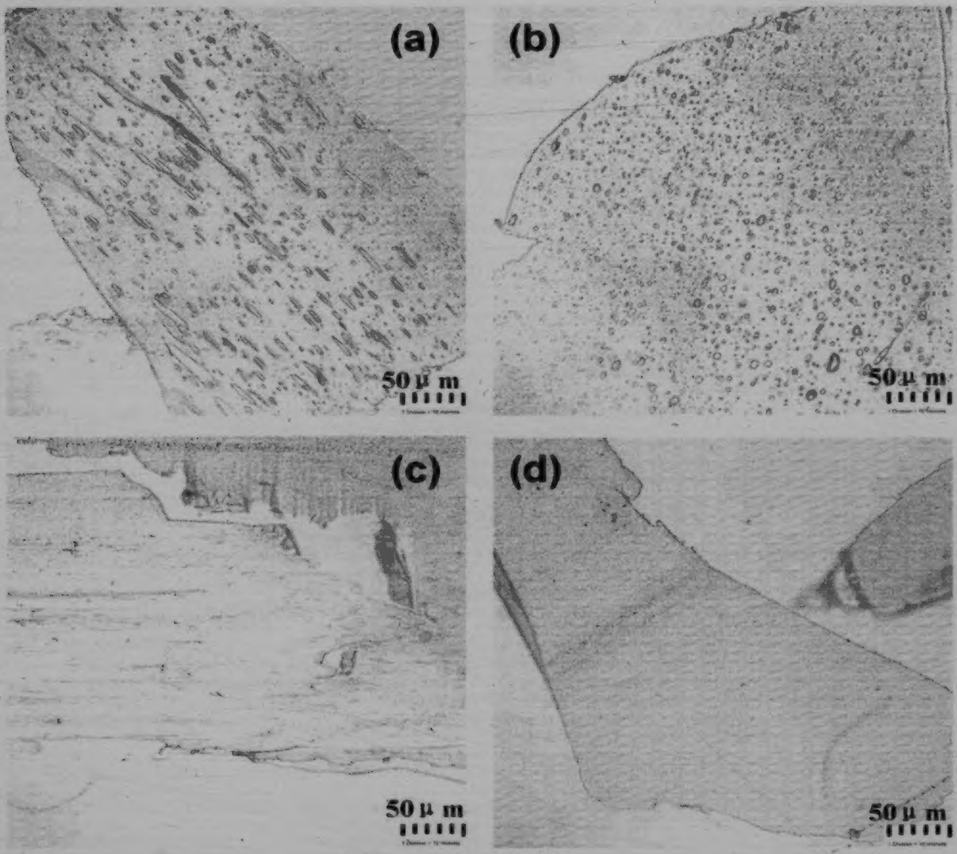

Figure 2-11 Optical photomicrographs of PS1200/aPA and PSMA/aPA obtained from internal batch mixer at 220°C and 100 rpm after mixing for 10 seconds and 20 seconds. (a) PS1200/aPA, 10 seconds, 100rpm. (b) PS1200/aPA, 20 seconds, 100rpm. (c) PSMA/aPA, 10 seconds, 100rpm. (d) PSMA/aPA, 20 seconds, 100rpm.

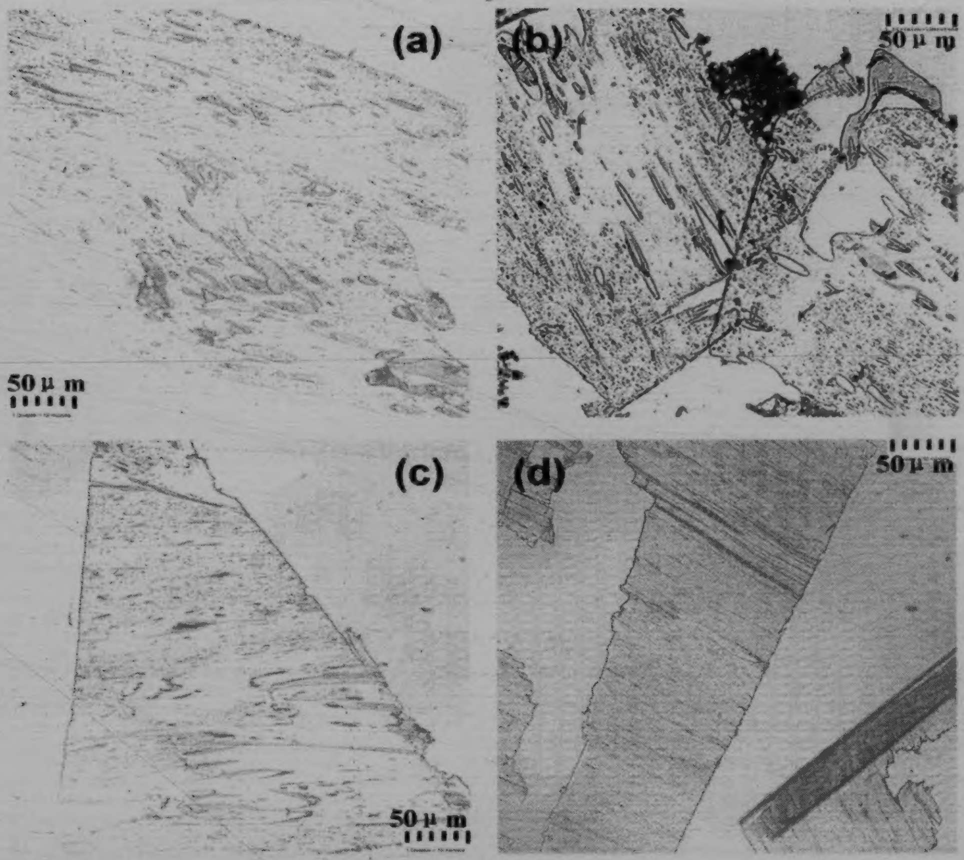

Figure 2-12 Optical photomicrographs of PMMA/aPA and PSMA/aPA obtained from internal batch mixer at 220°C and 20 rpm after mixing for 20 seconds and 40 seconds. (a) PMMA/aPA, 20 seconds, 20rpm. (b) PMMA/aPA, 40 seconds, 20rpm. (c) PSMA/aPA, 20 seconds, 20rpm. (d) PSMA/aPA, 40 seconds, 20rpm.

It is shown from Figure 2-11 and Figure 2-12 that compatibilization facilitates morphology development by extending the dispersed phase into thinner films in the initial stage. The deformation process of the dispersed phase from pellets to films is controlled by different forces exerted on the dispersed polymer, including matrix shear force, elastic forces due to the elastic nature of polymers, and interfacial tension between the matrix and dispersed phases. Sundararaj *et al.* [16, 26, 28] classified these forces into deforming forces, i.e. those forces which deform the domains of the dispersed polymers, and restoring forces, which tend to recover the shape of the dispersed domains. By this criterion, shear stress and elastic stress in the matrix phase are deforming stresses; and interfacial tension and elastic stress in the dispersed phase are restoring stresses. The stress ratio (S_r) was defined as [26]:

$$S_r = \frac{\eta_m \dot{\gamma} + N_{1m}}{\Gamma / R + N_{1d}} \tag{2.4}$$

where η, $\dot{\gamma}$, Γ and R are viscosity, shear rate, interfacial tension and drop initial radius, and subscripts *m* and *d* denote matrix and dispersed phase, respectively.

Table 2-5 shows the magnitude of these stresses assuming a no-slip interface. N_1 was approximated by 2G'. G' of the drop is calculated by assuming that the tangential stress is the same across the interface. For interfacial stress (Γ/R), the radius of pellet (R) is assumed to be 1.5 mm which is about the size of spherical aPA pellet that was processed.

Table 2-5 Magnitude of stresses and stress ratio

Controlled Group	Blends	$\dot{\gamma}$, s^{-1}	$\eta_m \dot{\gamma}$, Pa	$N_{1,m}$, Pa	$N_{1,d}$, Pa	Γ/R, Pa	S_r
1	PS1200/aPA	130	7.7×10^4	1.2×10^5	6.4×10^4	13	3.0
	PSMA/aPA	130	1.0×10^5	1.8×10^5	1.3×10^5	13	2.2
2	PMMA/aPA	26	6.6×10^4	7.8×10^4	5.4×10^4	2	2.7
	PSMA/aPA	26	5.9×10^4	9.0×10^4	5.2×10^4	13	2.9

Data in Table 2-5 demonstrate that the interfacial stress is negligible compared to other forces. Unlike Newtonian fluids, interfacial tension is not very important during the initial stages of morphology development to deform or breakup highly elastic fluids such as polymers. The shear stress and the first normal stress differences in each controlled group are relatively close. In controlled group 1, the stress ratio of PS1200/aPA is greater than that of PSMA/aPA. This means a finer dispersion should be expected in PS1200/aPA than in PSMA/aPA. The stress ratios in controlled group 2 are similar to each other, and therefore, similar morphology development is expected in the two systems. However, the morphologies shown in Figure 2-11 and Figure 2-12 contradict this analysis.

To reconcile this contradiction, the assumption made in the force analysis needs to be reexamined. The assumed no-slip condition at the interface may not be valid in our systems. It has been found that significant slip occurs at the interface of different polymers [55, 62, 64]. During blending, slip at the interface of polymers reduces the shear stress transferred from the matrix phase to the dispersed phase, i.e. there is a jump in the tangential stress. This can occur in uncompatibilized polymer blends. However, compatibilization suppresses the effect of interfacial slip since the copolymer chains formed at the interface via reaction penetrate into both phases, as shown schematically in Figure 2-13. This copolymer layer between the matrix and dispersed phases is made up of a matrix (phase A) copolymer segment that intrudes into the matrix fluid and entangles with the matrix polymer chains, and a dispersed (phase B) copolymer segment of the dispersed polymer that intrudes into the dispersed fluid and entangles with the dispersed polymer chains. The copolymer increases the interfacial width, and thus increases the adhesion between the matrix and dispersed phases [66]. Therefore, the shear stress is transferred from the matrix phase to the dispersed phase more effectively. As a result, in the initial stage, the films of the dispersed phase in the compatibilized systems are thinner than those in the uncompatibilized systems. The effect of the compatibilization on polymer blend morphology in later stages was studied by Sundararaj *et al.* [27].

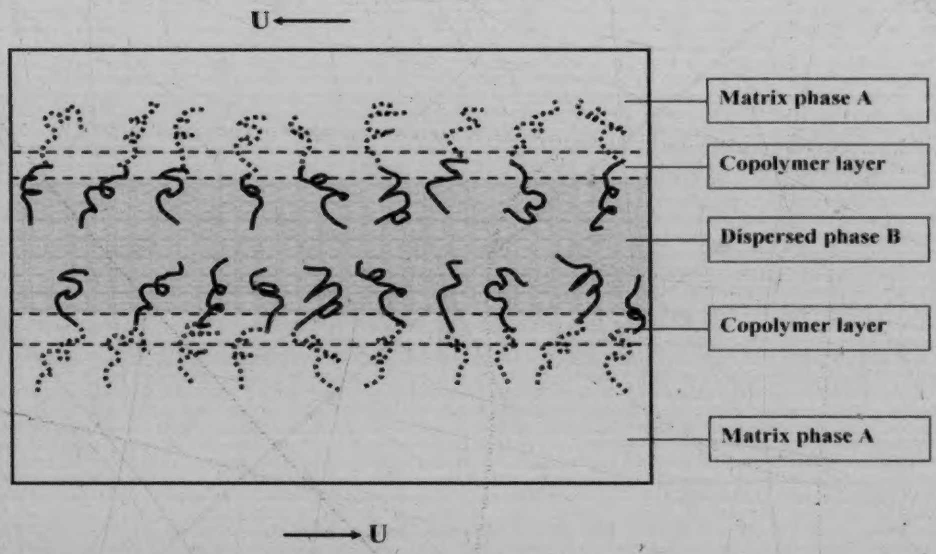

Figure 2-13 Compatibilization reduces slip at the interface of polymer blends. Chains of block copolymer formed at the interface penetrate into both phases and enhance the effective shear stress on the dispersed phase. The dashed and black curved segments denote polymer chains A and B respectively. Velocity U applies shear stress to the system.

2.3.4 Effect of rotation rate

Systems in Figure 2-5 and Figure 2-8 differ from each other only in rotation rate and feed rate. The rotation rate for Figure 2-5 is lower than that for Figure 2-8. As the rotation rate increases, the shear rate increases. The shear stress can be estimated using power law model for the polymer viscosity:

$$\tau_m = \eta_m \dot{\gamma} = M\dot{\gamma}^n. \qquad (2.5)$$

where τ_m is matrix shear stress, η_m is matrix viscosity, $\dot{\gamma}$ is shear rate, M is the power law coefficient and n is power law index ($0<n<1$). Eqn (2.5) shows that shear stress in the matrix phase always increases with increasing shear rate. If the effect of slip at the interface is neglected, a faster morphological change would be expected in the system with higher rotation rate since Q/N is kept constant for both systems. However, as seen from Figure 2-8, the dispersed phase has not completely broken up into particles for the final product (location P). There are still short fibers. Different from Figure 2-8, only spherical or slightly elongated particles are seen at the product location in Figure 2-5. This indicates that the polymer blend system in Figure 2-8 has not reached a steady state morphology at the end of the extruder. The final number average particle size of the dispersed phase is 0.7 μm for the 400 rpm run and is 2.9 μm for the 1000 rpm run. The 1000 rpm run has a higher rotation rate than the 400 rpm run at a constant Q/N, which means the residence time of the 1000 rpm run is less than that of the 400 rpm run. Therefore, the dispersed phase does not have enough time to breakup. As a result, fibers remain at the end of the extruder as shown in Figure 2-8.

For compatibilized systems, Figure 2-7 (400 rpm) and Figure 2-9 (1000 rpm), the morphology in the 400 rpm run evolves faster than the 1000 rpm run. However no big difference is seen in the final morphology at the product location. As shown in Table 2-4, the final particle size and the size distribution of the two compatibilized systems are almost the same. Both systems have reached a steady state morphology before the end of the extruder (i.e. the morphology does not change significantly between location 6 and location P). Comparing the time required for a steady state morphology for the uncompatibilized systems (Figure 2-5 and Figure 2-8) and the compatibilized group (Figure 2-7 and Figure 2-9), it is clear that compatibilization facilitates and speeds up the morphology development of polymer blends due to suppression of slip at the interface.

2.4 Conclusion

Amorphous Nylon, as dispersed phase, was intensively mixed with polystyrene or styrene-maleic anhydride copolymer under different conditions in a 25 mm Berstorff Ultraglide co-rotating twin screw extruder, which enables sampling at different locations along the length of the extruder. For all blends, the matrix phase or the dispersed phase was selectively dissolved so that the morphology of the remaining phase can be investigated with scanning electron microscopy. This study shows that the morphology of the dispersed phase evolves from films to fibers and then finally to spherical particles. In the extruder, the changing complex fluid flow fields are responsible for the morphological changes in polymer blends. Both the stretching under high shear in the kneading zones and the relaxation in the lower shear rate zones aid in dispersion of polymer blends. The morphology of compatibilized blends is found to develop faster than uncompatibilized blends. Rheological characterization reveals that slip occurs in the uncompatibilized blends and is suppressed by reactive compatibilization.

The mechanism of how compatibilization affects morphology development in the initial stage of blending is investigated in the perspective of hydrodynamic forces. Model experiments of PS/aPA, PSMA/aPA and PMMA/aPA in a laboratory internal batch mixer are employed to exclude the influence of rheological properties. A force analysis describing the phase deformation during blending indicates that compatibilization enhances dispersion of polymer blends by reducing slip at the interface between the polymer phases. Polymer segments of block copolymer formed by in-situ reaction penetrate into both the matrix and dispersed phases and entangle with the bulk polymer chains, thus improving the adhesion between the matrix phase and dispersed phase. Therefore, the shear stress from the matrix phase to the dispersed phase can be transferred more effectively.

The rotation rate of the extruder influences the morphology by changing the polymer residence time in the extruder. Higher rotation rate reduces residence time. The dispersed polymer in uncompatibilized systems does not have enough time to completely break up into particles. Therefore, higher rotation rate with inadequate residence time can result in worse dispersion. Compatibilized systems reach a steady state morphology faster than their uncompatibilized counterparts. Therefore, the final particle sizes of the compatibilized systems are almost the same regardless of the rotation rate. This result reinforces the slip-suppression mechanism of compatibilization.

2.5 References

[1] H. E. H. Meijer, P. J. Lemstra and P. H. M. Elemans, "Structured polymer blends," Makromol. Chem., Macromol. Symp. **16** 113 (1988).

[2] C. W. Macosko, "Morphology development and control in immiscible polymer blends," Macromol. Symp. **149**, 171 (2000).

[3] L. A. Utracki, "Polymer blends handbook", Kluwer Academic Publishers, Boston (2002).

[4] R. W. Flumerfelt, "Drop breakup in simple shear fields of viscoelastic fluids," Ind. Eng. Chem. Fund. **11**, 312 (1972).

[5] H. Vanoene, "Modes of dispersion of viscoelastic fluids in flow," J. Colloid Interface Sci. **40**, 448 (1972).

[6] S. H. Wu, "Formation of dispersed phase in incompatible polymer interfacial and rheological effects," Polym. Eng. Sci. **27**, 335 (1987).

[7] L. Levitt, C. W. Macosko and S. D. Pearson, "Influence of normal stress difference on polymer drop deformation," Polym. Eng. Sci. **36**, 1647 (1996).

[8] F. Mighri, A. Ajji and P. J. Carreau, "Influence of elastic properties on drop deformation in elongational flow," J. Rheol. **41**, 1183 (1997).

[9] F. Mighri, P. J. Carreau and A. Ajji, "Influence of elastic properties on drop deformation and breakup in shear flow," J. Rheol. **42**, 1477 (1998).

[10] S. Ramaswamy and L. G. Leal, "The deformation of a viscoelastic drop

subjected to steady uniaxial extensional flow of a newtonian fluid," J. Non-Newtonian Fluid Mech. **85**, 127 (1999).

[11] S. Ramaswamy and L. G. Leal, "The deformation of a newtonian drop in the uniaxial extensional flow of a viscoelastic liquid," J. Non-Newtonian Fluid Mech. **88**, 149 (1999).

[12] K. B. Migler, "Droplet vorticity alignment in model polymer blends," J. Rheol. **44**, 277 (2000).

[13] F. Mighri and M. A. Huneault, "Dispersion visualization of model fluids in a transparent couette flow cell," J. Rheol. **45**, 783 (2001).

[14] W. Lerdwijitjarud, A. Sirivat and R. G. Larson, "Influence of elasticity on dispersed-phase droplet size in immiscible polymer blends in simple shearing flow," Polym. Eng. Sci. **42**, 798 (2002).

[15] C. L. Tucker and P. Moldenaers, "Microstructural evolution in polymer blends," Annu. Rev. Fluid Mech. **34**, 177 (2002).

[16] B. Lin, F. Mighri, M. A. Huneault and U. Sundararaj, "Parallel breakup of polymer drops under simple shear," Macromol. Rapid Commun. **24**, 783 (2003).

[17] B. Lin, U. Sundararaj, F. Mighri and M. A. Huneault, "Erosion and breakup of polymer drops under simple shear in high viscosity ratio systems," Polym. Eng. Sci. **43**, 891 (2003).

[18] W. Lerdwijitjarud, A. Sirivat and R. G. Larson, "Influence of dispersed-phase elasticity on steady-state deformation and breakup of droplets in simple shearing flow of immiscible polymer blends," J. Rheol. **48**, 843 (2004).

[19] B. Lin and U. Sundararaj, "Sheet formation during drop deformation and breakup in polyethylene/polycarbonate systems sheared between parallel plates," Polymer **45**, 7605 (2004).

[20] B. Lin, F. Mighri, M. A. Huneault and U. Sundararaj, "Effect of premade compatibilizer and reactive polymers on polystyrene drop deformation and breakup in simple shear," Macromolecules **38**, 5609 (2005).

[21] H. Chen, U. Sundararaj, K. Nandakumar and M. D. Wetzel, "Erosion of polymer pellets during blending in a twin-screw extruder," AIChE Journal **52**, 1267 (2006).

[22] F. Mighri and M. A. Huneault, "In situ visualization of drop deformation, erosion, and breakup in high viscosity ratio polymeric systems under high shearing stress conditions," J. Appl. Polym. Sci. **100**, 2582 (2006).

[23] N. Aggarwal and K. Sarkar, "Deformation and breakup of a viscoelastic drop in a newtonian matrix under steady shear," J. Fluid Mech. **584**, 1 (2007).

[24] H. Li and U. Sundararaj, "Does drop size affect the mechanism of viscoelastic drop breakup? ," Phys. Fluids **20**, 053101 (2008).

[25] H. Li and U. Sundararaj, "Experimental investigation of viscoelastic drop deformation in newtonian matrix at high capillary number under simple shear flow," J. Non-Newtonian Fluid Mech. (submitted).

[26] U. Sundararaj, Y. Dori and C. W. Macosko, "Sheet formation in immiscible polymer blends: Model experiments on initial blend morphology," Polymer **36**, 1957 (1995).

[27] U. Sundararaj and C. W. Macosko, "Drop breakup and coalescence in polymer blends - the effects of concentration and compatibilization," Macromolecules **28**, 2647 (1995).

[28] P. G. Ghodgaonkar and U. Sundararaj, "Prediction of dispersed phase drop diameter in polymer blends: The effect of elasticity," Polym. Eng. Sci. **36**, 1656 (1996).

[29] M. Evstatiev, S. Fakirov, G. Bechtold and K. Friedrich, "Structure-property

relationships of injection- and compression- molded microfibrillar -reinforced pet/pa-6 composites," Adv. Polym. Technol. **19**, 249 (2000).

[30] A. Gonzalezmontiel, H. Keskkula and D. R. Paul, "Impact-modified nylon-6 polypropylene blends .1. Morphology-property relationships," Polymer **36**, 4587 (1995).

[31] U. Sundararaj and C. W. Macosko, "Evidence for inversion of phase continuity during morphology development in polymer blending," Polym. Eng. Sci. **36**, 1769 (1996).

[32] C. E. Scott and C. W. Macosko, "Morphology development during the initial stages of polymer-polymer blending," Polymer **36**, 461 (1995).

[33] C. E. Scott and C. W. Macosko, "Model experiments concerning morphology development during the initial stages of polymer blending," Polym. Bull. **26**, 341 (1991).

[34] J. T. Lindt and A. K. Ghosh, "Fluid mechanics of the formation of polymer blends. Part i: Formation of lamellar structures," Polym. Eng. Sci. **32**, 1802 (1992).

[35] U. Sundararaj, C. W. Macosko, R. J. Rolando and H. T. Chan, "Morphology development in polymer blends," Polym. Eng. Sci. **32**, 1814 (1992).

[36] R. C. Willemse, E. J. J. Ramaker, J. Van Dam and A. Posthuma De Boer, "Morphology development in immiscible polymer blends: Initial blend morphology and phase dimensions," Polymer **40**, 6651 (1999).

[37] L. A. Utracki and H. Shi, "Development of polymer blend morphology during compounding in a twin-screw extruder. 1: Droplet dispersion and coalescence-a review," Polym. Eng. Sci. **32**, 1824 (1992).

[38] H. Yang, C. C. Park, Y. T. Hu and L. G. Leal, "The coalescence of two equal-sized drops in a two-dimensional linear flow," Phys. Fluids **13**, 1087

(2001).

[39] B. Burkhart, P. Gopalkrishnan, S. Hudson, A. Jamieson, M. Rother and R. Davis, "Droplet growth by coalescence in binary fluid mixtures," Phys. Rev. Lett. **87**, 098304-1 (2001).

[40] I. Fortelny, J. Kovar and M. Stephan, "Analysis of the phase structure development during the melt mixing of polymer blends," J Elastom. Plast. **28**, 106 (1996).

[41] H. E. Burch and C. E. Scott, "Effect of viscosity ratio on structure evolution in miscible polymer blends," POLYMER **42**, 7313 (2001).

[42] J. K. Lee and C. D. Han, "Evolution of polymer blend morphology during compounding in a twin-screw extruder," Polymer **41**, 1799 (2000).

[43] S. Joseph and S. Thomas, "Morphology development and mechanical properties of polystyrene/polybutadiene blends," Eur. Polym. J. **39**, (2003).

[44] C. Harratsa, T. Omonova, G. Groeninckxa and P. Moldenaers, "Phase morphology development and stabilization in polycyclohexylmethacrylate /polypropylene blends: Uncompatibilized and reactively compatibilized blends using two reactive precursors," Polymer **45**, 8115 (2004).

[45] M. Xanthos and S. S. Dagli, "Compatibilitation of polymer blends by reactive processing," Polym. Eng. Sci. **31**, 929 (1991).

[46] A. Ajji and L. A. Utracki, "Interphase and compatibilization of polymer blends," Polym. Eng. Sci. **36**, 1574 (1996).

[47] H. Li and G.-H. Hu, "The early stage of the morphology development of immiscible polymer blends during melt blending: Compatibilized vs. Uncompatibilized blends," J. Polym. Sci., Part B: Polym. Phys. **39**, 601 (2001).

[48] S. T. Milner and H. W. Xi, "How copolymers promote mixing of

immiscible homopolymers," J. Rheol. **40**, 663 (1996).

[49] L. Y. Yang, T. G. Smith and D. Bigio, "Melt blending of linear low-density polyethylene and polystyrene in a haake internal mixer. 1. Compatibilization and morphology development," J. Appl. Polym. Sci. **58**, 117 (1995).

[50] A. K. Bhowmick, T. Chiba and T. Inoue, "Reactive processing of rubber-plastic blends - role of chemical compatibilizer," J. Appl. Polym. Sci. **50**, 2055 (1993).

[51] H. Cartier and G.-H. Hu, "Morphology development of in situ compatibilized semicrystalline polymer blends in a co-rotating twin-screw extruder," Polym. Eng. Sci. **39**, 996 (1999).

[52] G. I. Taylor, "The formation of emulsions in definable fields of flow," Proc. R. Soc. London Ser. A **146**, 501 (1934).

[53] H. P. Grace, "Dispersion phenomena in high-viscosity immiscible fluid systems and application of static mixers as dispersion devices in such systems," Chem. Eng. Commun. **14**, (1982).

[54] P. P. Varanasi, M. E. Ryan and P. Stroeve, "Experimental-study on the breakup of model viscoelastic drops in uniform shear-flow," Ind. Eng. Chem. Res. **33**, 1858 (1994).

[55] J. Zhang, P. J. Cole, U. Nagpal and C. W. Macosko, "Direct correlation between adhesion promotion and coupling reaction at immiscible polymer-polymer interfaces," J. Adhes. **82**, 887 (2006).

[56] U. Sundararaj, PhD Thesis, "Morphology development during polymer blending", University of Minnesota, Minneapolis (1994).

[57] L. Levitt and C. W. Macosko, "Extensional rheometry of polymer multilayers: A sensitive probe of interfaces," J. Rheol. **41**, 671 (1997).

[58] P. Xing, M. Bousmina and D. Rodrigue, "Critical experimental comparison between five techniques for the determination of interfacial tension in polymer blends: Model system of polystyrene/polyamide-6," Macromolecules **33**, 8020 (2000).

[59] Y. Son, "Comparative measurement of interfacial tension by transient dynamic methods," J. Appl. Polym. Sci. **99**, 1910 (2005).

[60] C. Orr, J. Cernohous, P. Gue´Gan, A. Hirao, H. K. Jeon and C. W. Macosko, "Homogeneous reactive coupling of terminally functional polymers," Polymer **42**, 8171 (2001).

[61] H. K. Jeon, C. W. Macosko, B. Moon, T. R. Hoye and Z. Yin, "Coupling reactions of end- vs mid-functional polymers," Macromolecules **37**, 2563 (2004).

[62] L. Levitt and C. W. Macosko, "Shearing of polymer drops with interface modification," Macromolecules **32**, 6270 (1999).

[63] K. B. Migler, C. Lavalle´, M. P. Dillon, S. S. Woods and C. L. Gettinger, "Visualizing the elimination of sharkskin through fluropolymer additives: Coating and polymer–polymer slippage," J. Rheol. **45**, 565 (2001).

[64] R. Zhao and C. W. Macosko, "Slip at polymer–polymer interfaces: Rheological measurements on coextruded multilayers," J. Rheol. **46**, 145 (2002).

[65] P. Van Puyvelede, Z. Oommen, P. Koets, G. Groeninckx and P. Moldenaers, "Effect of reactive compatibilization on the interfacial slip in nylon-6/epr blends," Polym. Eng. Sci. **43**, 71 (2003).

[66] R. Schach, Y. Tran, A. Menelle and C. Creton, "Role of chain interpenetration in the adhesion between immiscible polymer melts," Macromolecules **40**, 6325 (2007).

Chapter 3

Viscoelastic Drop Deformation in Newtonian Matrix at High Capillary Number under Simple Shear Flow*

3.1 Introduction

Drop deformation in immiscible liquid blends presents itself in many chemical processes, such as cosmetics, paints, food and polymer processing. In these processes, the dynamics of drop deformation, along with drop coalescence, determine the microstructure and hence the macroscopic properties of the blends [1]. The deformation of a Newtonian drop in a Newtonian matrix has been extensively investigated by both experimental and numerical approaches, providing a reasonably clear understanding of the physical mechanism [2-10]. However, drop deformation of viscoelastic fluids is much more complicated than that of pure Newtonian systems because of the complexity of their rheological properties and the modification of stresses and flow by viscoelasticity [11-23].

The steady state drop deformation (Df) in pure Newtonian system under simple shear with negligible buoyancy and inertial forces is governed by capillary number (Ca) and viscosity ratio (η_r) of the drop phase to the matrix phase [3], i.e.

$$\mathrm{Df} = f(\mathrm{Ca},\ \eta_r). \tag{3.1}$$

---

* Portions of this work are submitted to J. Non-Newtonian Fluid Mech. (in revision)

Capillary number is the ratio of shear stress to interfacial stress, which is defined as

$$Ca = \frac{\eta_m \dot{\gamma} R_0}{\Gamma}, \tag{3.2}$$

where η_m is the viscosity of the matrix phase, $\dot{\gamma}$ is the shear rate, R_0 denotes the initial radius of the drop and Γ is the interfacial tension between the drop and matrix phases. For a given Newtonian system, drops are stretched by shear stress, and the deformation increases with increasing capillary number (i.e. increasing shear rate) before they break up. Newtonian systems have been widely studied and are relatively straightforward to investigate. However, for immiscible liquid blends involving viscoelastic components, the study of drop deformation is difficult. The majority of viscoelastic materials, such as polymers, are usually elastic and shear-thinning, which result in very different drop deformation and breakup behavior [24-28].

In order to obtain a clear understanding of drop deformation in viscoelastic systems, efforts have been made to separate the effect of elasticity from that of shear-thinning by using simple rheological models such as Oldroyd-B model for numerical studies [21, 23] and by using model fluids such as Boger fluids for experimental work [16, 18, 29, 30]. Similar to Newtonian systems, an analogous relation of drop deformation in viscoelastic systems can be written as

$$Df = f(Ca,\ \eta_r,\ \text{elastic properties}). \tag{3.3}$$

The elastic properties can be represented by two parameters: (a) Deborah number (De) which is a dimensionless number defined as the ratio of the material relaxation time (λ) to the characteristic time scale of an experiment (t_c), and (b) the normal stress differences (i.e. the first normal stress difference: N_1 and the second normal stress difference: N_2). The viscoelasticity of drop phase has been demonstrated to inhibit deformation [12, 31-33]. The critical capillary number for breakup was found to be higher than that of its Newtonian counterpart [11, 12, 34]. The effects of elastic properties on drop deformation and breakup are attributed to normal stress differences in viscoelastic fluids [13, 16, 31, 33]. Aggarwal & Sarkar [23] developed a simple qualitative ordinary differential equation model on the force balance among shear stress, interfacial stress and normal stresses to depict the essential physics underlying the experimental observations and numerical results. However, when the matrix is viscoelastic and drop is Newtonian, experimental results of the deformation contradict each other. Elmendorp & Maalcke [32] and Mighri *et al.* [12] found that matrix viscoelasticity increases drop deformation, while Flumerfelt [35], Guido and coworkers [18] and Verhulst and Moldenaers [36] found that matrix viscoelasticity reduces drop deformation and hinders breakup. Yue *et al.* [21] clarified this non-monotonic behavior by investigating the modification of stresses and flow field by viscoelasticity.

Because of restrictions of experimental or computing capability, most previous work studied drop deformation in viscoelastic systems under simple shear over a limited range of small capillary numbers, typically below 1. At such low values of capillary numbers, the elastic contribution is still very weak and the deformation is small. Although Pillapakkam & Singh [17] simulated Oldroyd-B drop sheared in Newtonian matrix at high capillary number, the drop elasticity was still weak such that the drop broke up in the flow direction. However, in real industrial processes, very high capillary numbers are used. For example, the capillary numbers of polymer blending or food extrusion are on the order of 100. Drop deformation and breakup can be very different at higher capillary numbers since the normal stresses are expected to be important at high shear rate. Hobbie & Migler [13], Migler [37] and Mighri & Huneault [16] found that at high capillary numbers with strong elastic effect, viscoelastic drops under shear can elongate and break up in the vorticity direction which is the direction perpendicular to the flow direction and the velocity gradient direction. However, there is a lack of quantitative studies on drop deformation in viscoelastic systems sheared at high capillary numbers. Drop breakup is the upper limit of the steady state deformation and typically occurs at high capillary number for viscoelastic systems in many processes. Since the microstructure of immiscible liquid blends is controlled by drop deformation and breakup [1], it is necessary to investigate drop deformation under high capillary number.

In this work, we perform a quantitative investigation of viscoelastic drop deformation in a Newtonian matrix at high capillary number under simple shear flow, where the viscoelastic effects are strong and dominate the drop deformation. We separate the effect of elasticity from that of shear thinning by using Boger fluids which have shear-independent viscosities for the drop phase [38].

3.2 Experimental Section

3.2.1 Materials

Three low-viscosity polydimethylsiloxane (PDMS, Gelest, Inc.) were used as matrix phase fluids. The drop phase fluids were polymer solutions with shear-independent viscosity, also known as Boger fluids, which were prepared under slow mixing for a period of more than 5 days to ensure molecular level dissolution of the polymers. The Boger fluids used in this study were mixtures of polyisobutylene, PIB (Mw=1x10^6 kg/kmol, Sigma-Aldrich), kerosene, Ker (Fisher Scientific), and polybutene, PB (Mn=920 kg/kmol, Sigma-Aldrich). The properties and formulations of the materials are listed in Table 3-1. The interfacial tension between the Boger fluid and PDMS is 3mN/m [16]. Guido *et al.* showed that the miscibility between the drop and matrix phases is not an issue to study the drop deformation and breakup [18].

Table 3-1 Compositions of materials used in this study

Designation		Material/ Formulation*	Viscosity, Pa·s**
Matrix	M1	PDMS(DMS-T31)	0.97
	M2	PDMS(DMS-T35)	4.86
	M3	PDMS(DMS-T41)	9.74
Drop	D1	0.6%PIB+8.5%Ker+90.9%PB	13.0
	D2	0.1%PIB+4.9%Ker+95.0%PB	14.5
	D3	0.8% PIB+4.4%Ker+94.8%PB	25.0
	D4	1.0% PIB+5.8% Ker+93.2%PB	31.0
	D5	1.3%PIB+7.2%Ker+91.5%PB	40.0

* All percentages are on mass basis.

** Viscosities are measured at 20 °C.

PDMS liquids with such low viscosities exhibit Newtonian properties under the experimental conditions. Figure 3-1 shows the viscosity and the first normal stress difference (N_1) of the Boger fluids, which were obtained using a Rheometrics RMS800 rheometer operated in steady mode with cone-plate geometry at 20°C. All the Boger fluids have relatively constant viscosity and exhibit substantial elasticity. N_1 increases with increasing amount of PIB. The viscosity ratios of each drop/matrix system are shown in Table 3-2.

Table 3-2 Experimental systems and their viscosity ratios

Matrix	M1	M1	M1	M1	M2	M2	M2	M3	M3	M3
Drop	D1	D2	D4	D5	D3	D4	D5	D3	D4	D5
Viscosity ratio, η_r	13.4	14.9	32	41.2	5.1	6.4	8.2	2.6	3.2	4.1

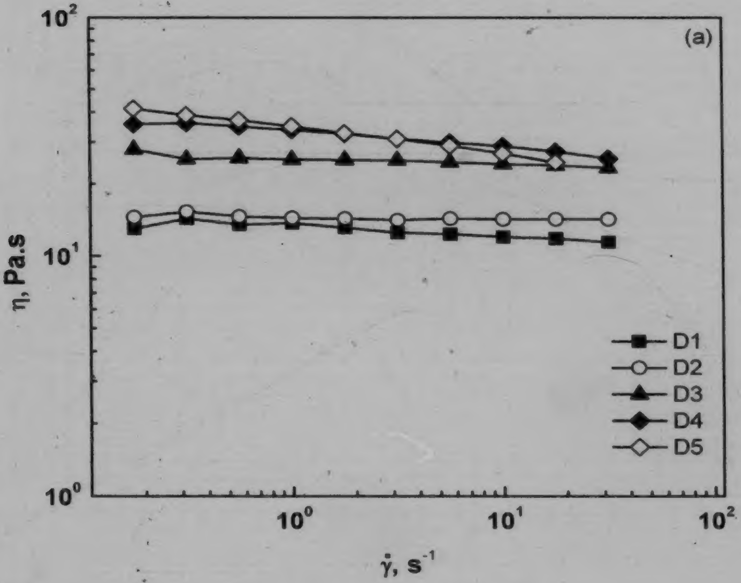

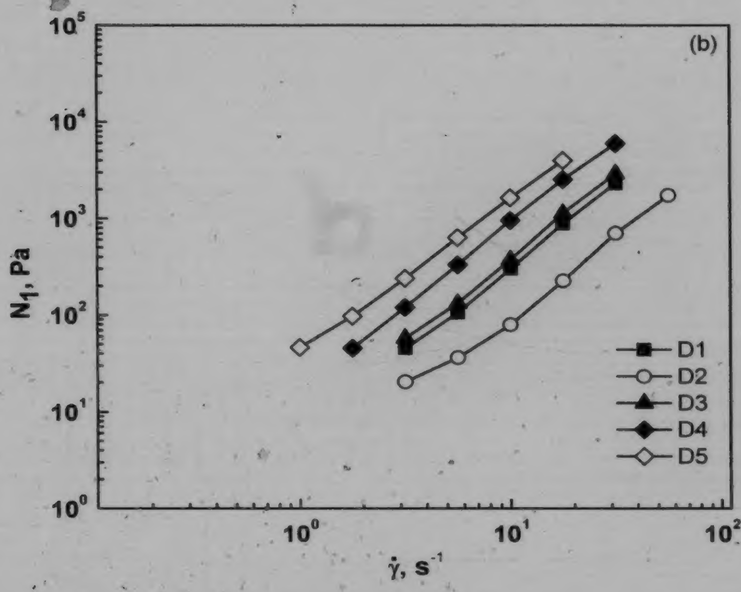

Figure 3-1 Rheological properties of Boger fluids. (a) Viscosity of Boger fluids. (b) First normal stress difference of Boger fluid.

3.2.2 Apparatus

In this study, a custom-made Couette device was used to generate simple shear flow. The apparatus consists of two concentric counter-rotating cylinders, shown in Figure 3-2. The inner cylinder is made of stainless steel and has an external diameter of 102mm. The outer cylinder is made of quartz and has an internal diameter of 110mm giving a 4mm gap between the cylinders. The height of the cylinders is 60mm. The advantage of such a narrow gap is that the apparatus can generate high shear rate without secondary flows [28] which are present in parallel plate and cone-and-plate devices, thus making it suitable to study drop deformation and breakup at high capillary numbers. Two DC motors are used to control the rotating speeds of the cylinders to provide a broad range of shear rates. The drop deformation process was recorded to a VCR with two CCD cameras (Pulnix) giving both the side view and the bottom view of the Couette device. The two views make it possible to reconstruct three dimensional photomicrographs of deformed drops by making some basic assumptions for the drop geometry (for example, assume ellipsoidal model for drops). Since the drop deformation in viscoelastic systems is not identical in the velocity gradient direction and the vorticity direction, it is important to investigate the drop deformation in three dimensions. Pillapakkam & Singh [17] also emphasized the necessity of three-dimensional simulation for drop deformation in viscoelastic systems. The shear rate was relatively uniform in the gap and can be calculated for Newtonian fluids as [39]:

$$\dot{\gamma} = (\Omega_o - \Omega_i)\frac{r_i^{-2} + r_o^{-2}}{r_i^{-2} - r_o^{-2}} \tag{3.4}$$

where Ω and r are angular rotating speed and radius, and subscripts i and o denote inner and outer cylinders.

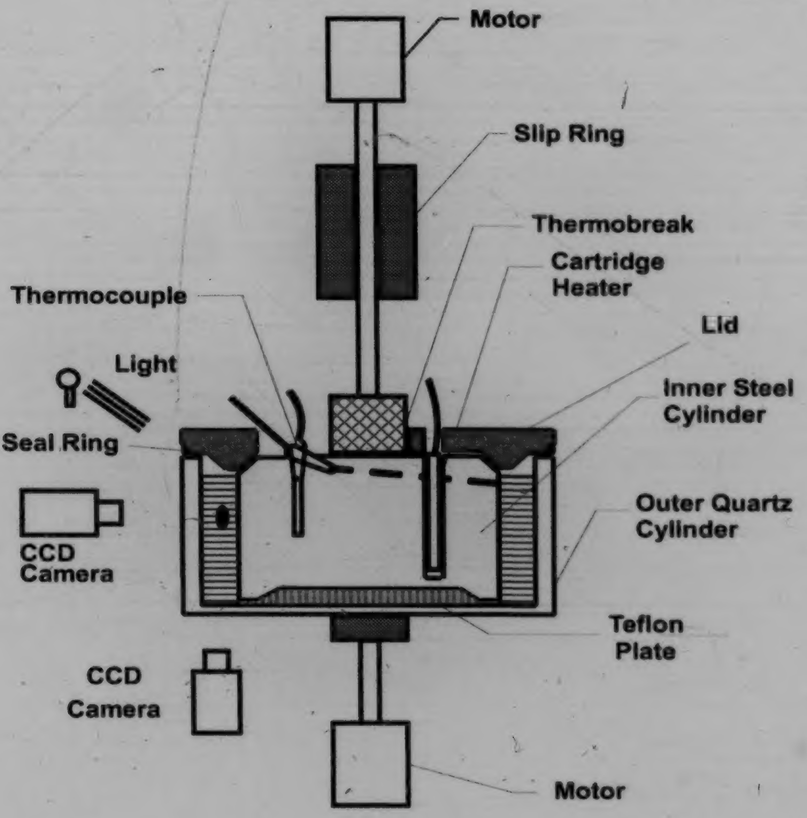

Figure 3-2 A schematic of the Couette apparatus.

3.2.3 Procedure

The 4mm gap of the Couette apparatus was first filled with PDMS. Then a Boger fluid drop was injected at the middle of the gap and at half height of the cell using a syringe. After the drop recovered a spherical shape, shear rate was increased in a stepwise manner to deform the drop. The drops were selected to be smaller than 40% of the gap width, with most of them smaller than 30% of the gap width, to minimize geometrical confinement [40]. The drop was kept in the field of view of the cameras by adjusting the rotation speeds of the two cylinders. The drop deformation process was recorded and still photomicrographs were taken from the video and are reported in this chapter. The images of drops were later analyzed using image analysis software, Sigmascan. Only data from clear photomicrographs in which the systems were at steady state were analyzed.

3.3 Results and Discussion

3.3.1 Observations of drop deformation

The schematics in Figure 3-3 define dimensions of a deformed drop; x, y and z denote the flow direction, velocity gradient direction and vorticity direction respectively. The side view and bottom view display the projections of the drop in xz plane and xy plane respectively. R_1 and R_2 are the half lengths in the major and minor axes, respectively, of the drop in the bottom view. R_3 is the half length of the drop in the vorticity direction.

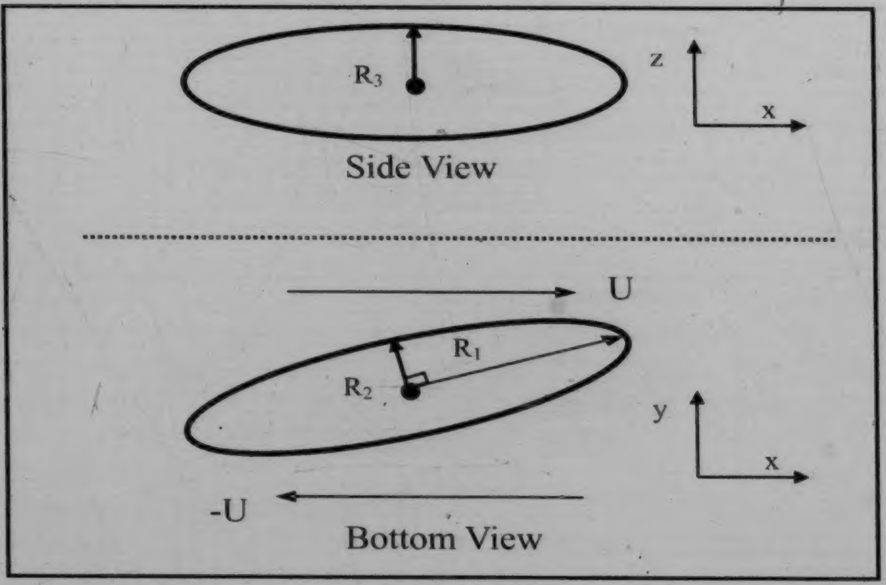

Figure 3-3 A schematic of a drop subjected to simple shear flow. • is the drop center; U is the velocity at the cylinder wall.

Two types of drop deformation were observed. Figure 3-4 shows the deformation process of system M3/D3, which is termed "flow direction deformation". The diameter of the undeformed drop (D_0) is 1.16mm. In each photomicrograph, the top part shows the side view and the bottom part shows the bottom view. Photomicrographs from side view and bottom view are denoted by S and B respectively. The side view shows the drop images in xz plane and the bottom view shows the drop images in xy plane, as depicted in Figure 3-3. All the other photomicrographs in this article are shown in the same arrangement. With increasing shear rate, Figure 3-4 shows that the drop elongates in the flow direction from spherical shape to ellipsoidal shape, and then to a long cylinder-like shape. It should be noted that the cylindrical shape in Figure 3-4 is not steady and will eventually break up.

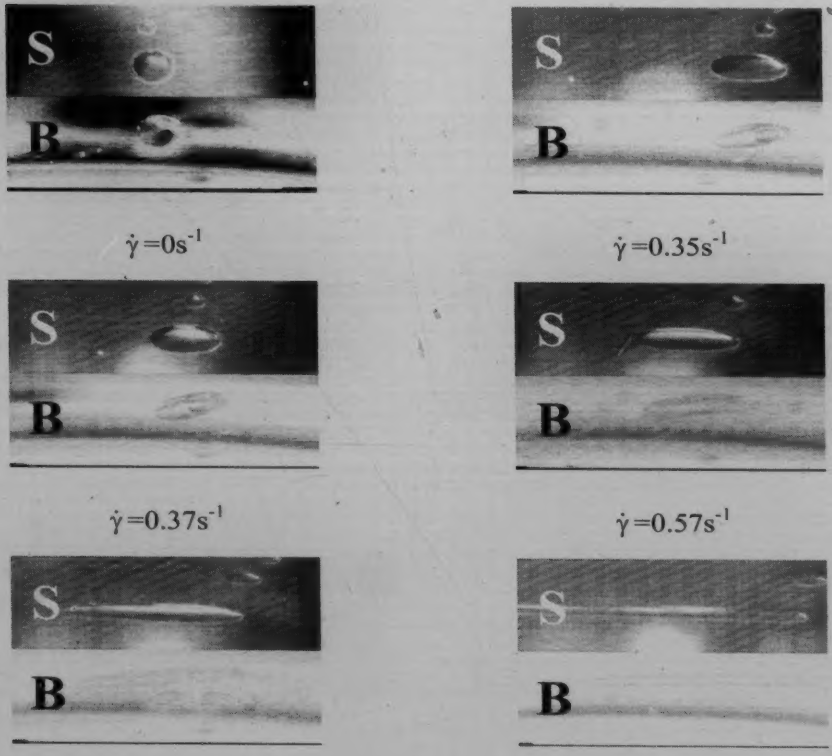

$\dot{\gamma}=0s^{-1}$ $\dot{\gamma}=0.35s^{-1}$

$\dot{\gamma}=0.37s^{-1}$ $\dot{\gamma}=0.57s^{-1}$

$\dot{\gamma}=0.73s^{-1}$ $\dot{\gamma}=0.77s^{-1}$

Figure 3-4 Flow direction deformation of system M3/D3, $\eta_r=2.6$, $D_0=1.16mm$. S and B denote side view and bottom view respectively.

Figure 3-5 shows that the reduced radius in the flow direction, R_1/R_0, monotonically increases, and the reduced radii in the other two directions, i.e. R_2/R_0 and R_3/R_0, decrease with increasing shear rate. Widening effect [33], which means R_3/R_0 increases to a value greater than 1, was not observed in this type of deformation. In this deformation mode, the effect of viscoelasticity on drop deformation is relatively weak. The flow direction deformation is similar to, though not the same as that of pure Newtonian systems. A similar drop deformation and breakup mode was observed by Flumerfelt [35] and simulated by Pillapakkam & Singh [17], Chinyoka *et al.* [41] and Aggarwal & Sarkar [23].

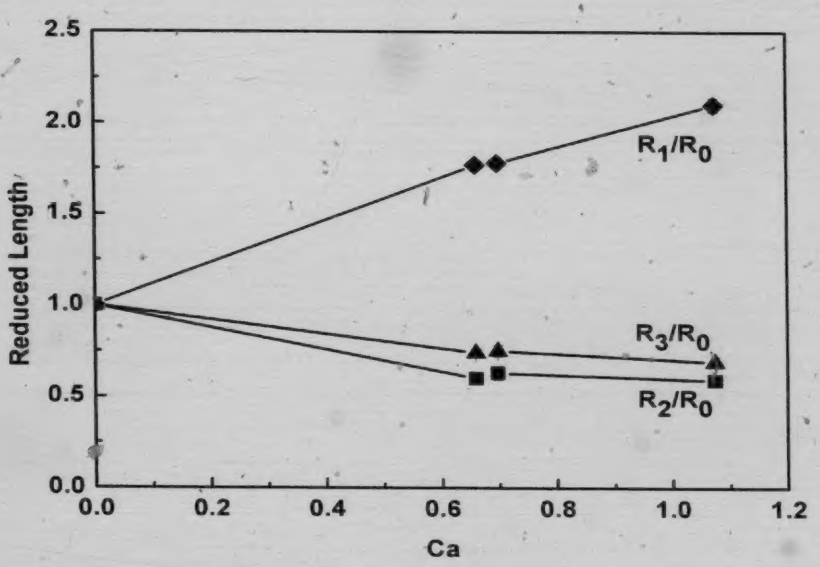

Figure 3-5 Reduced radii of M3/D3, η_r=2.6, D_0=1.16mm. Error bars are within data points.

The second type of drop deformation, which is termed "vorticity direction deformation", was seen in many of these viscoelastic drop/Newtonian matrix systems. Figure 3-6 shows this type of deformation for system M3/D4 (η_r=3.2) with initial drop diameter of 0.88 mm. The drop first elongates to an ellipsoidal shape at low shear rate, 0.79s^{-1} in the second photomicrograph of Figure 3-6 for example. With increasing shear rate, the drop contracts in the flow direction and at the same time elongates in the vorticity direction. This elongation in the vorticity direction is more pronounced at higher shear rates, 3.11 s^{-1} and 5.47 s^{-1} for example. Figure 3-6 shows that the shape of the highly deformed drop is very different from an ellipsoid which was assumed by many theoretical studies [10, 42].

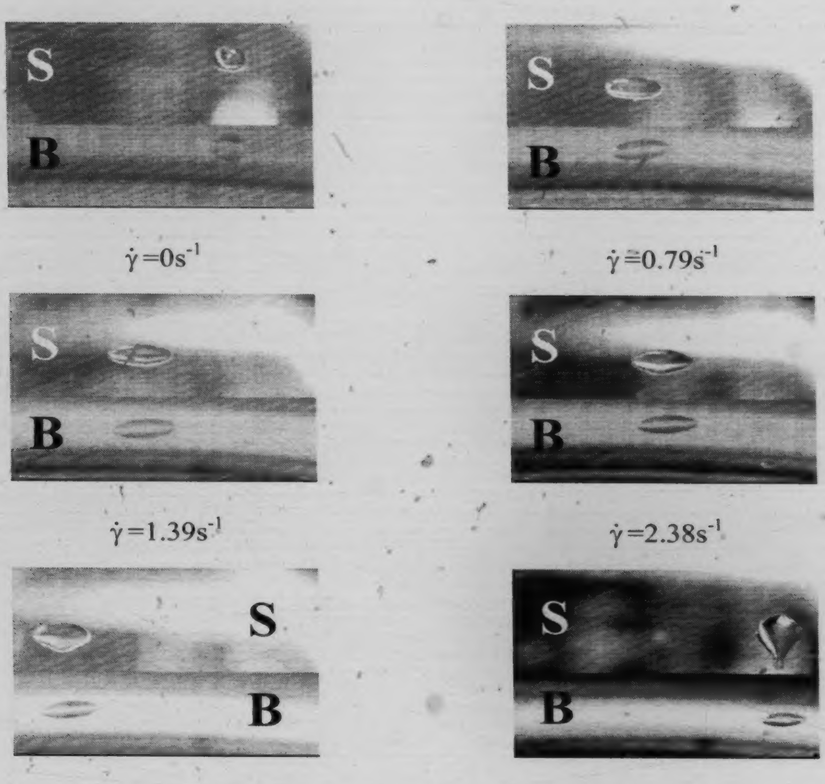

$\dot{\gamma}=0s^{-1}$ $\dot{\gamma}=0.79s^{-1}$

$\dot{\gamma}=1.39s^{-1}$ $\dot{\gamma}=2.38s^{-1}$

$\dot{\gamma}=3.11s^{-1}$ $\dot{\gamma}=5.47s^{-1}$

Figure 3-6 Vorticity direction deformation of system M3/D4, $\eta_r = 3.2$, D_0=0.88mm.

Figure 3-7 shows the reduced radii versus increasing capillary number for this system with an initial drop diameter of 0.88 mm. There is a maximum for R_1/R_0 and a minimum for R_3/R_0 at some critical point, while R_2 decreases in the entire range of capillary number. Apparent widening effect can be seen in the vorticity direction (R_3) in this type of deformation which is coupled with a decrease in dimension in the flow direction (R_1). The increase in R_3 at high shear rate is very dramatic since it can be two times the original radius. The drop elongation in vorticity direction was also observed by other researchers [13, 16, 37, 43], however, they did not perform quantitative study of the deformation with accuracy in three dimensions. This type of deformation resembles the rod-climbing phenomenon and is attributed to the viscoelastic nature of the fluid [13, 44]. It is noteworthy that even for the same system as M3/D3, drops can deform by both flow direction deformation and vorticity elongation mechanisms depending on the drop size [45]. This implies that drop size also affects the deformation mode, whereas the deformation mode is independent of drop size for Newtonian systems.

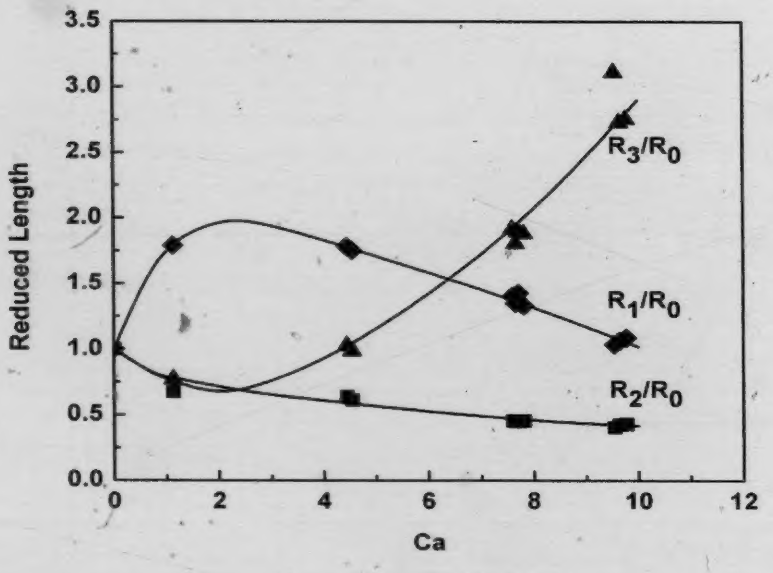

Figure 3-7 Reduced radii of M3/D4, $\eta_r = 3.2$, D_0=0.88 mm.

There is a special case of vorticity direction deformation mechanism when the viscosity ratio of the system is very high. Figure 3-8 shows the deformation of system M1/D4 with viscosity ratio of 32. Similar to Newtonian systems with high viscosity ratio, the drop deforms only slightly at low shear rate. However, the drop elongates along the vorticity direction continuously even for η_r>>4 when increasing shear rate, which is never seen in Newtonian systems. Figure 3-9 shows the reduced radii versus Ca. This kind of deformation mechanism was also found in systems M1/D2 and M1/D1.

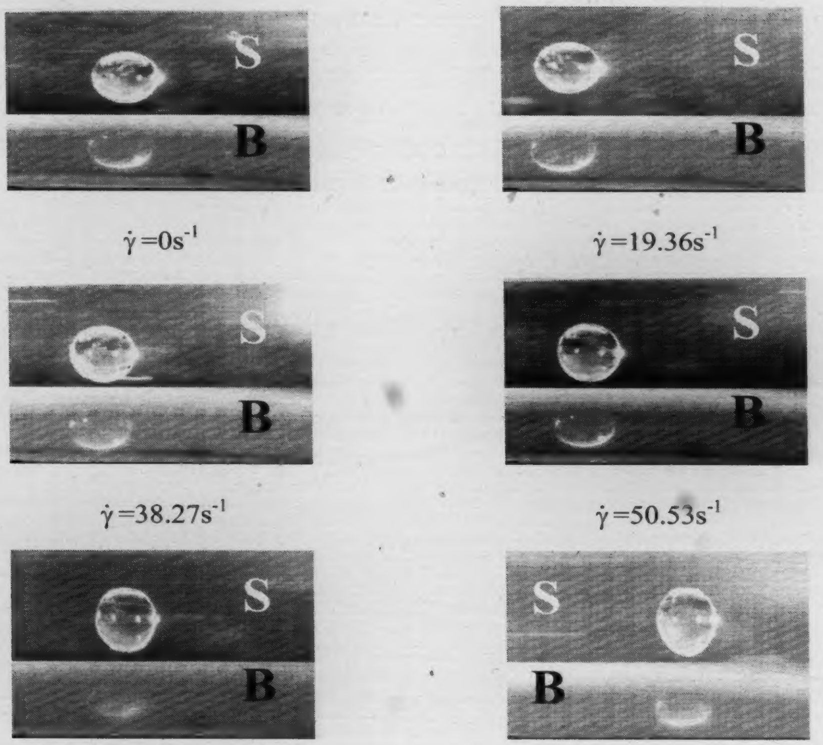

$\dot{\gamma}=0s^{-1}$

$\dot{\gamma}=19.36s^{-1}$

$\dot{\gamma}=38.27s^{-1}$

$\dot{\gamma}=50.53s^{-1}$

$\dot{\gamma}=64.37s^{-1}$

$\dot{\gamma}=69.37s^{-1}$

Figure 3-8 Vorticity direction deformation of system M1/D4, $\eta_r = 32$, D_0=1.6mm.

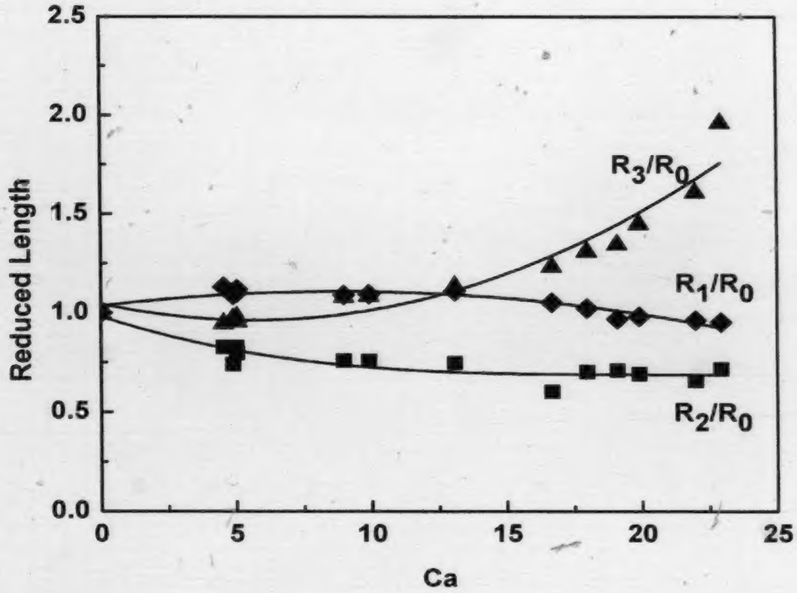

Figure 3-9 Reduced radii of M1/D4, $\eta_r = 32$, D_0=1.6mm.

3.3.2 Effect of viscolasticity

In order to quantify the drop deformation, we define two deformations, one for the side view, and the other for the bottom view. The deformation for the side view, Df_1, is defined as

$$Df_1 = \frac{R_1 - R_3}{R_1 + R_3}. \tag{3.5}$$

The deformation for the bottom view is the same as that defined by Taylor[3], which is

$$Df_2 = \frac{R_1 - R_2}{R_1 + R_2}. \tag{3.6}$$

Since R_2 and R_3 of the deformed drops are not identical, the above two deformations could provide a detailed picture about the drop deformation in three dimensions.

Unlike Newtonian fluids, the first and second normal stress differences N_1 and N_2 of viscoelastic fluids undergoing shear flow are not zero. Early research work [13, 16, 29, 31, 33, 41] attributed the difference in drop deformation between viscoelastic systems and Newtonian systems to normal stresses. For drop deformation, normal stresses are considered as extra restoring stresses in addition to interfacial stress since the normal stress differences produce tensile stress which tends to resist deformation. To determine the first normal stress difference N_1 at a particular time, the shear rate in the drop phase is first estimated by assuming the tangential stresses on both sides of the drop-matrix interface are equal. Then this shear rate is used to obtain N_1 from Figure 3-1.

Figure 3-10 shows the deformations and the development of stresses with increasing capillary number of M3/D3. Shear stress (τ) and interfacial stress ($\Gamma/R0$) are much higher than the first normal stress difference (N_1) and dominate the deformation process. Both the side deformation and bottom deformation increase monotonically for the entire deformation process before the drop breaks up. When the shear stress exceeds the combined effect of interfacial stress and normal stress to a certain extent, the drop cannot hold a stable shape and has to break up. In this type of deformation, the viscoelastic effect is relatively small. The viscoelasticity somewhat resists the drop deformation but does not change the elongation axis (i.e. the drop deforms in the flow direction).

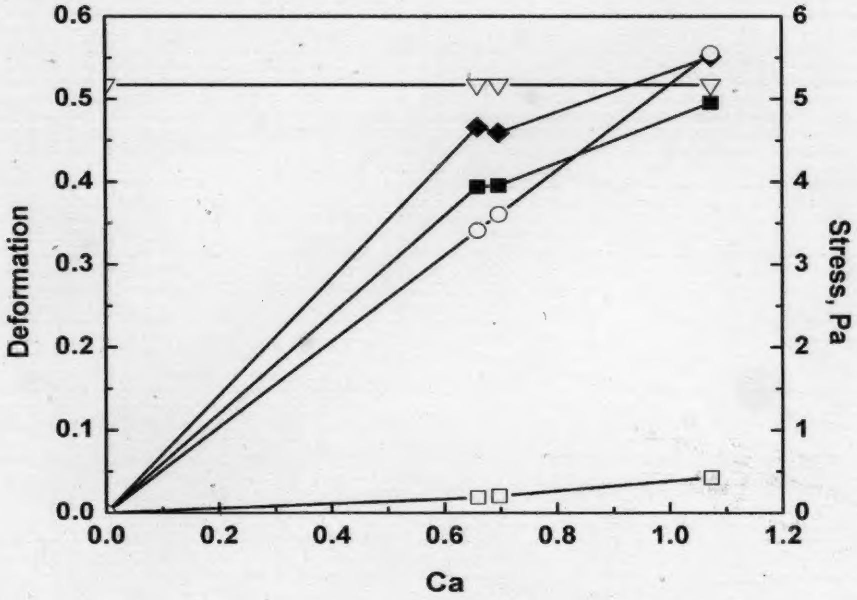

Figure 3-10 Development of stresses and deformations with increasing capillary number, M3/D3, $\eta_r = 2.6$, D_0=1.16mm. Solid symbols are deformations: Df_1 (■), Df_2 (◆); and unfilled symbols are stresses: Γ/R_0 (▽), τ (○), N_1 (□).

Figure 3-11 shows the deformations and development of stresses of system M3/D4 which has vorticity direction deformation mechanism. The bottom deformation is relatively constant at high capillary number and the side deformation increases to a maximum and then decreases. In this type of deformation, the effect of the first normal stress difference is important since its magnitude is close to the magnitude of the shear stress. Although shear stress is higher than normal stress at low shear rate, it is not strong enough to overcome the restoring effect due to the combination of interfacial stress and normal stress and the drop does not break. Instead, the normal stress increases faster than the shear stress so that the fluid inside the drop is squeezed along the vorticity direction. Previous simulation work investigated the effect of the normal stresses on drop deformation where the drop deformed in the flow direction [17, 21, 23, 41]; however, to date, no simulation work has shown drop elongation along the vorticity direction. The reason is that the drop viscoelasticity in those studies is not strong and capillary number is not high enough too see apparent squeezing effect due to the hoop stress. Since the drop deformation changes so greatly from Newtonian systems, one would expect different drop breakup mechanism for highly viscoelastic systems [16, 45]. Thus it would be necessary to simulate the drop deformation for viscoelastic systems at high capillary number incorporating strong viscoelasticity.

Figure 3-12 shows the deformation and stresses of another system M3/D5 with different drop and matrix phases. The deformation profiles are similar to Figure 3-11. In this system, the normal stress is higher than the shear stress at high capillary number and it dominates the deformation.

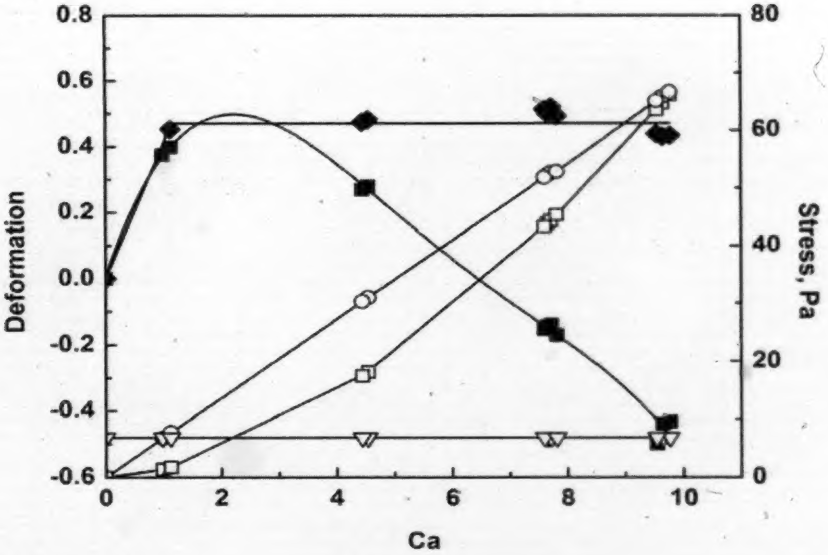

Figure 3-11 Development of stresses and deformations with increasing capillary number, M3/D4, $\eta_r = 3.2$, D_0=0.88 mm. Solid symbols are deformations: Df_1 (■), Df_2 (◆); and unfilled symbols are stresses: Γ/R_0 (▿), τ (○), N_1 (□).

From Figure 3-11 and Figure 3-12, the bottom deformation (Df_2) is relatively constant at high capillary number. This could be explained by examining the offsetting effects of increasing viscoelasiticity and increasing shear rate. Yue *et al.* [21] studied the effect of drop viscoelasticity on drop deformation by examining how the normal force modified the interface. Their results show that at the same capillary number, increasing Deborah number (De), i.e. viscoelasticity, reduces R_1 and increases R_2, and results in less deformation (Df_2). De is product of relaxation time of drop fluid and shear rate. In our experiments, for the same drop, increasing capillary number is equivalent to increasing shear rate, and increasing shear rate results in increasing N_1 and De. According to Yue [21], the increasing viscoelasticity, N_1 and/or De tends to reduce R_1 and increase R_2. On the other hand, increasing shear rate also increases the shear stress, and the increasing shear stress tends to increase R_1 and reduce R_2 and R_3 similar to Newtonian systems. These two tendencies counterbalance each other and result in a relatively constant bottom deformation (Df_2). Aggarwal & Sarkar [23] performed three-dimensional simulation of a viscoelastic drop sheared in a Newtonian matrix. Their work indicates that increasing the viscoelasticity, the normal stress in xy plane tends to reduce R_1 and increase R_2, and the normal stress in xz plane tends to reduce R_2 and R_3. However, our results show clearly that the drop increases in R_3 and decreases in R_1 and R_2. Aggarwal & Sarkar [23] speculated that the reason might be due to the zero second normal stress difference of the Oldroyd-B model which they used in their simulation work. There is significant challenge to do theoretical work to understand the evolution of the drop shape with higher order models.

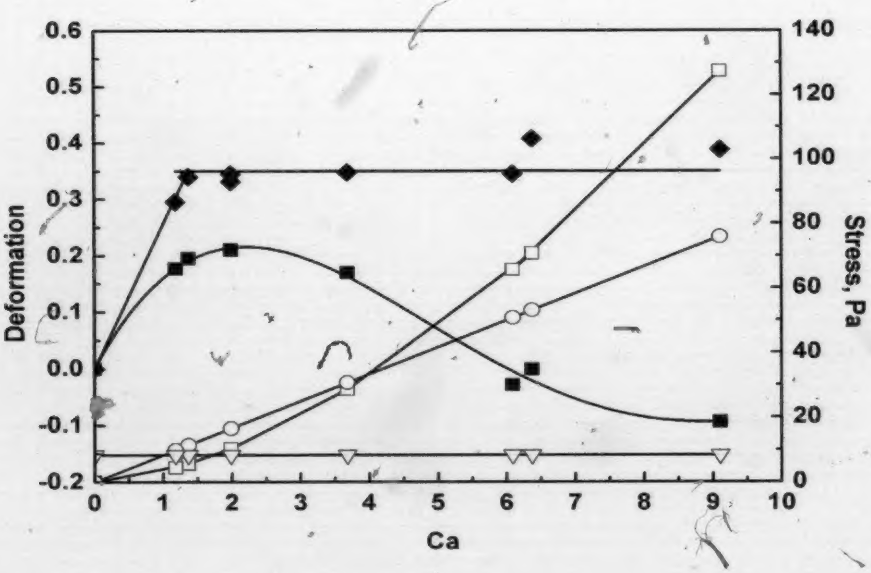

Figure 3-12 Development of stresses and deformations with increasing capillary number, M3/D5, $\eta_r = 4.1$, D_0=0.72 mm. Solid symbols are deformations: Df_1 (■), Df_2 (◆); and unfilled symbols are stresses: Γ/R_0 (▽), τ (○), N_1 (□).

3.3.3 Effect of drop size

Figure 3-13 shows the side and bottom deformations of system of M3/D4 with different drop size. Both deformations Df_1 and Df_2 show that the deformation of big drops is greater than that of small drops at the same capillary number. This result agrees with what was discussed for system M3/D3 in the observation section. In that section, we indicated that different drop size may result in different type of deformation, which supports the observations here. It is different from

Newtonian systems, in which the type of drop deformation is independent of the drop size. This difference can only be attributed to the viscoelasticity of drop phase. In Eqn (3.3), deformation is described as a function of capillary number, elastic properties and viscosity ratio. We can explain the effect of drop size using the relations between the drop size and elastic properties. If using Deborah number to represent elastic properties [21, 23], then deformation can be written as

$$\mathrm{Df} = f(\mathrm{Ca}, \eta_r, \mathrm{De}). \tag{3.7}$$

At the same capillary number, big drops will have a lower shear rate, meaning that the Deborah number is small in comparison to a small drop at the same capillary number. As proven by Yue *et al*. [21] and Aggarwal & Sarkar [23], small Deborah number results in large deformation (Df_2). In our experiments, this means that for a fixed viscosity ratio and capillary number, a big drop will have large deformation (Df_2). Aggarwal & Sarkar's results [23] showed for small capillary number, the effect of viscoelasticity is small. They expected that the effect could be significant at high capillary numbers close to the critical capillary numbers. This speculation is demonstrated by our results.

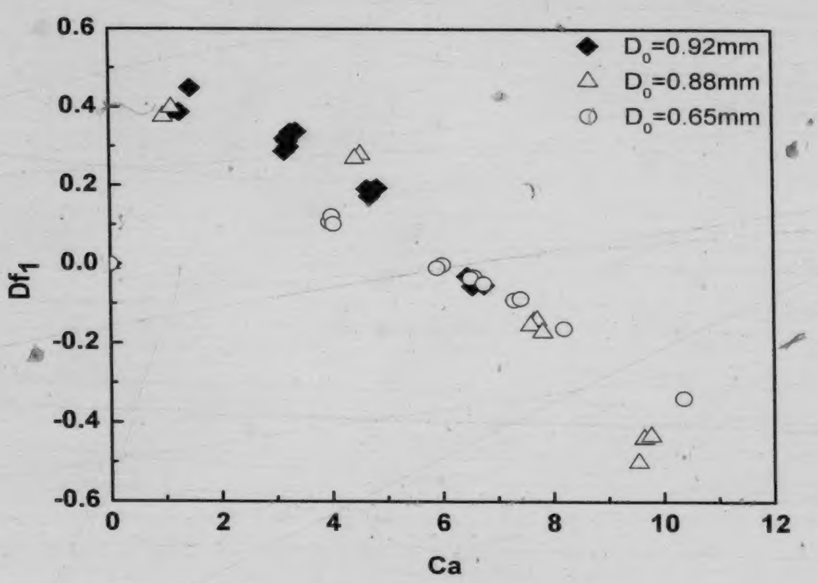

(a) Deformation from side view.

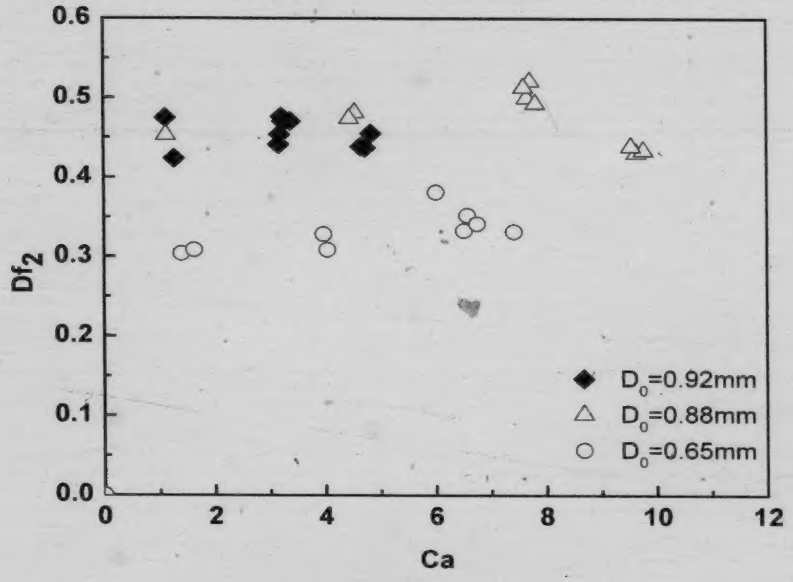

(b) Deformation from bottom side.

Figure 3-13 The effect of drop size on deformation, M3/D4, $\eta_r = 3.2$.

3.3.4 Effect of viscosity ratio

Deformations of drop D4 and PDMS matrix systems with different viscosity ratios are plotted in Figure 3-14. The deformation seen from the bottom view decreases as viscosity ratio increases from 3.2 to 32. The deformation seen from the side view follows similar trends when the deformation is above 0. However, the side deformation reduces faster with increasing capillary number for η_r=3.2 than for η_r=6.4 and 32. This means that no matter shear stress or normal stress dominates the deformation, the system with viscosity ratio of 3.2 is more easily deformed. In the range of $3.2<\eta_r<32$, both of the side deformation and bottom deformation are larger at lower viscosity ratio. Therefore, viscosity ratio gives direct indication of deformability, given the same elasticity component of the drop. A special example can be seen in Newtonian systems whose elasticity is 0. One can expect similar deformation trends regarding viscosity ratio.

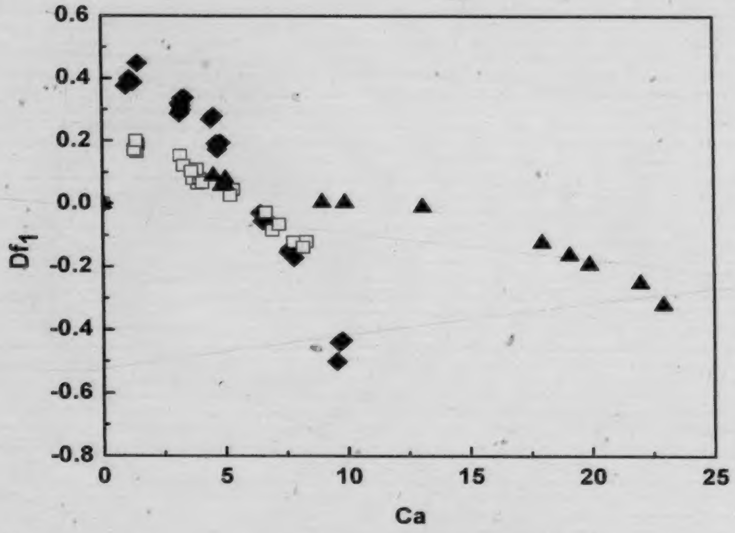

(a) Deformation from side view.

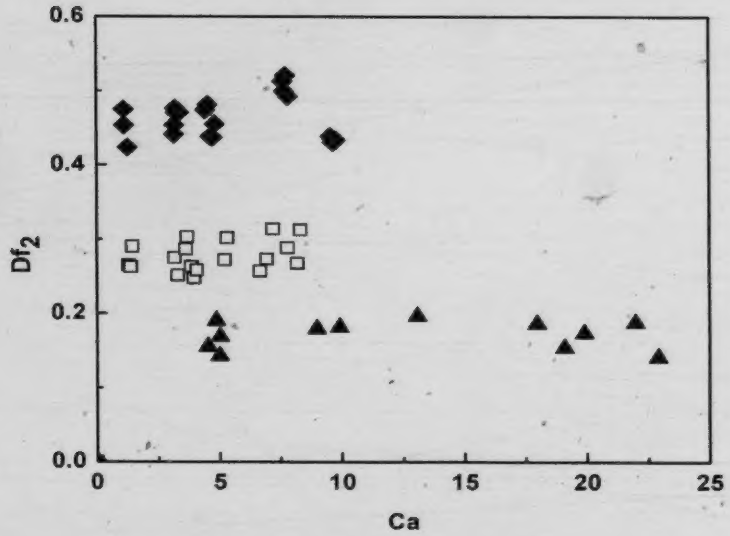

(b) Deformation from bottom view.

Figure 3-14 Drop deformation of D4 sheared in different PDMS. ◆, viscosity ratio=3.2, D_0=0.88 mm and 0.92 mm; □, viscosity ratio=6.4, D_0=0.86 mm and 0.90 mm; ▲, viscosity ratio=32, D_0=1.6 mm.

3.3.5 Short remarks on breakup

As observed, there are two types of deformation. We can expect different drop breakup modes based on these different deformation modes. For the first type of deformation "flow direction deformation", shear stress dominates the deformation and the elastic force is weak. The resultant breakup will occur in the flow direction when shear stress outbalances the elastic and interfacial stresses. This type of breakup was observed in viscoelastic systems by Flumerfelt [35] and most of simulation studies such as Pillapakkam & Singh [17], and Aggarwal & Sarkar [23]. For the second type of deformation "vorticity direction deformation", normal stresses dominate the deformation. Here, the viscoelastic drop does not break up in the flow direction as seen in Newtonian systems. However, the drop elongates in the vorticity direction and the drop rocks around its symmetrical axis. The rocking is not stable and the drop may form some local waists with increasing shear rate. Shear stress could break the drop locally at these waists. This breakup mode has been reported by Mighri & Huneault [16] and Li & Sundararaj [45].

3.4 Conclusion

In this work we have investigated the steady state deformation of a viscoelastic drop (Boger fluid) sheared in a Newtonian PDMS matrix at high capillary number by direct visualization in two perpendicular planes. Two types of deformation were found, flow direction deformation and vorticity direction deformation. For weak viscoelasticity and low capillary number, the drop elongates in the flow direction, whereas for strong viscoelasiticity and high capillary number, the drop elongates in the vorticity direction. The deformation mechanism is investigated by comparing the magnitude of the shear, normal and interfacial forces. For flow direction deformation, shear stress dominates the deformation; and for vorticity direction deformation, normal stresses dominate the deformation. Drop size is found to affect the drop deformation. This effect was studied by relating the drop size to viscoelasticity which in turn affects the drop deformation. At the same capillary number, a bigger drop has larger deformation. In the range of $3.2<\eta_r<32$, both of the side deformation and bottom deformation are larger at lower viscosity ratio.

3.5 References

[1] C.L. Tucker and P. Moldenaers, "Microstructural evolution in polymer blends," Annu. Rev. Fluid Mech. **34**, 177 (2002).

[2] G.I. Taylor, "The viscosity of a fluid containing small drops of another fluid," Proc. R. Soc. London Ser. A **138**, 41 (1932).

[3] G.I. Taylor, "The formation of emulsions in definable fields of flow," Proc. R. Soc. London Ser. A **146**, 501 (1934).

[4] R.G. Cox, "Deformation of a drop in a general time-dependent fluid flow," J. Fluid Mech. **37**, 601 (1969).

[5] E.J. Hinch and A. Acrivos, "Long slender drops in a simple shear-flow," J. Fluid Mech. **98**, 305 (1980).

[6] H.P. Grace, "Dispersion phenomena in high-viscosity immiscible fluid systems and application of static mixers as dispersion devices in such systems," Chem. Eng. Commun. **14**, 225 (1982).

[7] J.M. Rallison, "The deformation of small viscous drops and bubbles in shear flows," Annu. Rev. Fluid Me[illegible] **16**, 45 (1984).

[8] B.J. Bentley and L.G. Leal, "An experimental investigation of drop deformation and breakup in steady, two-dimensional linear flows," J. Fluid Mech. **167**, 241 (1986).

[9] H.A. Stone, "Dynamics of drop deformation and breakup in viscous fluids," Annu. Rev. Fluid Mech. **26**, 65 (1994).

[10] P.L. Maffettone and M. Minale, "Equation of change for ellipsoidal drops in viscous flow," J. Non-Newtonian Fluid Mech. **78**, 227 (1998).

[11] F. Mighri, A. Ajji, and P.J. Carreau, "Influence of elastic properties on drop deformation in elongational flow," J. Rheol. **41**, 1183 (1997).

[12] F. Mighri, P.J. Carreau, and A. Ajji, "Influence of elastic properties on drop deformation and breakup in shear flow," J. Rheol. **42**, 1477 (1998).

[13] E.K. Hobbie and K.B. Migler, "Vorticity elongation in polymeric emulsions," Phys. Rev. Lett. **82**, 5393 (1999).

[14] S. Ramaswamy and L.G. Leal, "The deformation of a viscoelastic drop subjected to steady uniaxial extensional flow of a newtonian fluid," J. Non-Newtonian Fluid Mech. **85**, 127 (1999).

[15] S. Ramaswamy and L.G. Leal, "The deformation of a newtonian drop in the uniaxial extensional flow of a viscoelastic liquid," J. Non-Newtonian Fluid Mech. **88**, 149 (1999).

[16] F. Mighri and M.A. Huneault, "Dispersion visualization of model fluids in a transparent couette flow cell," J. Rheol. **45**, 783 (2001).

[17] S.B. Pillapakkam and P. Singh, "A level-set method for computing solutions to viscoelastic two-phase flow," J. Comput. Phys. **174**, 552 (2001).

[18] S. Guido, M. Simeone, and F. Greco, "Deformation of a newtonian drop in a viscoelastic matrix under steady shear flow - experimental validation of slow flow theory," J. Non-Newtonian Fluid Mech. **114**, 65 (2003).

[19] J. Beaucourt, T. Biben, and C. Verdier, "Elongation and burst of axisymmetric viscoelastic droplets: A numerical study," Phys. Rev. E **71**, 066309-1 (2005).

[20] V. Sibillo, S. Guido, F. Greco, and P.L. Maffettone, "Single drop dynamics under shearing flow in systems with a viscoelastic phase," Macromol. Symp. **228**, 31 (2005).

[21] P.T. Yue, J.J. Feng, C. Liu, and J. Shen, "Viscoelastic effects on drop deformation in steady shear," J. Fluid Mech. **540**, 427 (2005).

[22] D. Khismatullin, Y. Renardy, and M. Renardy, "Development and implementation of vof-prost for 3d viscoelastic liquid-liquid simulations," J. Non-Newtonian Fluid Mech. **140**, 120 (2006).

[23] N. Aggarwal and K. Sarkar, "Deformation and breakup of a viscoelastic drop in a newtonian matrix under steady shear," J. Fluid Mech. **584**, 1 (2007).

[24] B. Lin, F. Mighri, M.A. Huneault, and U. Sundararaj, "Parallel breakup of polymer drops under simple shear," Macromol. Rapid Commun. **24**, 783 (2003).

[25] B. Lin, U. Sundararaj, F. Mighri, and M.A. Huneault, "Erosion and breakup of polymer drops under simple shear in high viscosity ratio systems," Polym. Eng. Sci. **43**, 891 (2003).

[26] B. Lin and U. Sundararaj, "Sheet formation during drop deformation and breakup in polyethylene/polycarbonate systems sheared between parallel plates," Polymer **45**, 7605 (2004).

[27] H. Chen, U. Sundararaj, K. Nandakumar, and M.D. Wetzel, "Erosion of polymer pellets during blending in a twin-screw extruder," AIChE J. **52**, 1267 (2006).

[28] F. Mighri and M.A. Huneault, "In situ visualization of drop deformation, erosion, and breakup in high viscosity ratio polymeric systems under high shearing stress conditions," J. Appl. Polym. Sci. **100**, 2582 (2006).

[29] P.P. Varanasi, M.E. Ryan, and P. Stroeve, "Experimental-study on the breakup of model viscoelastic drops in uniform shear-flow," Ind. Eng. Chem. Res. **33**, 1858 (1994).

[30] W. Lerdwijitjarud, A. Sirivat, and R.G. Larson, "Influence of dispersed-phase elasticity on steady-state deformation and breakup of droplets in simple shearing flow of immiscible polymer blends," J. Rheol. **48**, 843 (2004).

[31] H. Vanoene, "Modes of dispersion of viscoelastic fluids in flow," J. Colloid Interface Sci. **40**, 448 (1972).

[32] J.J. Elmendorp and R.J. Maalcke, "A study on polymer blending microrheology," Polym. Eng. Sci. **25**, 1041 (1985).

[33] L. Levitt, C.W. Macosko, and S.D. Pearson, "Influence of normal stress difference on polymer drop deformation," Polym. Eng. Sci. **36**, 1647 (1996).

[34] W. Lerdwijitjarud, A. Sirivat, and R.G. Larson, "Influence of elasticity on

dispersed-phase droplet size in immiscible polymer blends in simple shearing flow," Polym. Eng. Sci. **42**, 798 (2002).

[35] R.W. Flumerfelt, "Drop breakup in simple shear fields of viscoelastic fluids," Ind. Eng. Chem. Fund. **11**, 312 (1972).

[36] K. Verhulst and P. Moldenaers, "Drop shape dynamics of a newtonian drop in a non-newtonian matrix during transient and steady shear flow," J. Rheol. **51**, 261 (2007).

[37] K.B. Migler, "Droplet vorticity alignment in model polymer blends," J. Rheol. **44**, 277 (2000).

[38] D.V. Boger, "Highly elastic constant-viscosity fluid," J. Non-Newtonian Fluid Mech. **3**, 87 (1977).

[39] C.W. Macosko, Rheology: Principles, measurements and applications, Wiley-VCH, New York, 1994.

[40] A. Vananroye, P.V. Puyvelde, and P. Moldenaers, "Effect of confinement on the steady-state behavior of single droplets during shear flow," J. Rheol. **51**, 139 (2007).

[41] T. Chinyoka, Y.Y. Renardy, A. Renardy, and D.B. Khismatullin, "Two-dimensional study of drop deformation under simple shear for oldroyd-b liquids," J. Non-Newtonian Fluid Mech. **130**, 45 (2005).

[42] P.L. Maffettone and F. Greco, "Ellipsoidal drop model for single drop dynamics with non-newtonian fluids," J. Rheol. **48**, 83 (2004).

[43] B. Lin, F. Mighri, M.A. Huneault, and U. Sundararaj, "Effect of premade compatibilizer and reactive polymers on polystyrene drop deformation and breakup in simple shear," Macromolecules **38**, 5609 (2005).

[44] R.B. Bird, R.C. Armstrong and O. Hassager, Dynamics of polymeric liquids, Wiley, New York, 1987.

[45] H. Li and U. Sundararaj, "Does drop size affect the mechanism of viscoelastic drop breakup?" Phys. Fluids **20**, 053101-1 (2008).

Chapter 4

Visualization of Viscoelastic Drop Breakup in Shear Flow[*]

4.1 Introduction

The breakup of a liquid drop in another liquid matrix presents itself in many chemical processes, such as the formation of emulsions, food processing and polymer blending. A good understanding of the mechanism of drop deformation and breakup is crucial to control the dispersion in these processes. Most of the previous work on drop deformation and breakup has been focusing on Newtonian fluids [1-8]. For drop breakup of Newtonian systems in simple shear flow with negligible buoyancy and inertial forces, the correlation of two dimensionless parameters was found to characterize the breakup condition. The first one is the ratio of shear stress to interfacial stress, which is known as capillary number (Ca). Capillary number is defined as

$$\mathrm{Ca} = \frac{\eta_m \dot{\gamma} R}{\Gamma} \tag{4.1}$$

where η_m is the viscosity of the matrix phase, $\dot{\gamma}$ is the shear rate, R denotes the initial radius of the drop and Γ is the interfacial tension between the drop and matrix phases. The other one is viscosity ratio (η_r) of the drop phase to the matrix phase, which is defined as

---

[*] Portions of this work are published in Phys. Fluids (2008).

$$\eta_r = \frac{\eta_d}{\eta_m} \tag{4.2}$$

where η_d is the viscosity of the drop phase. Taylor [1, 2] predicted that for small deformation the maximum stable drop (D_{max}) size in a simple shear flow would be:

$$D_{max} = \frac{16\Gamma(\eta_r + 1)}{\eta_m \dot{\gamma}(19\eta_r + 16)} \quad \eta_r < 2.5 \tag{4.3}$$

He also pointed out that drops cannot break up when the viscosity ratio is above 2.5. Grace reported comprehensive experimental results of drop breakup of Newtonian systems in both simple shear flow and extensional flow [4]. These results are summarized in Figure 4-1. It shows that it is impossible to break Newtonian drop for Newtonian systems under simple shear flow when the viscosity ratio is above 4.

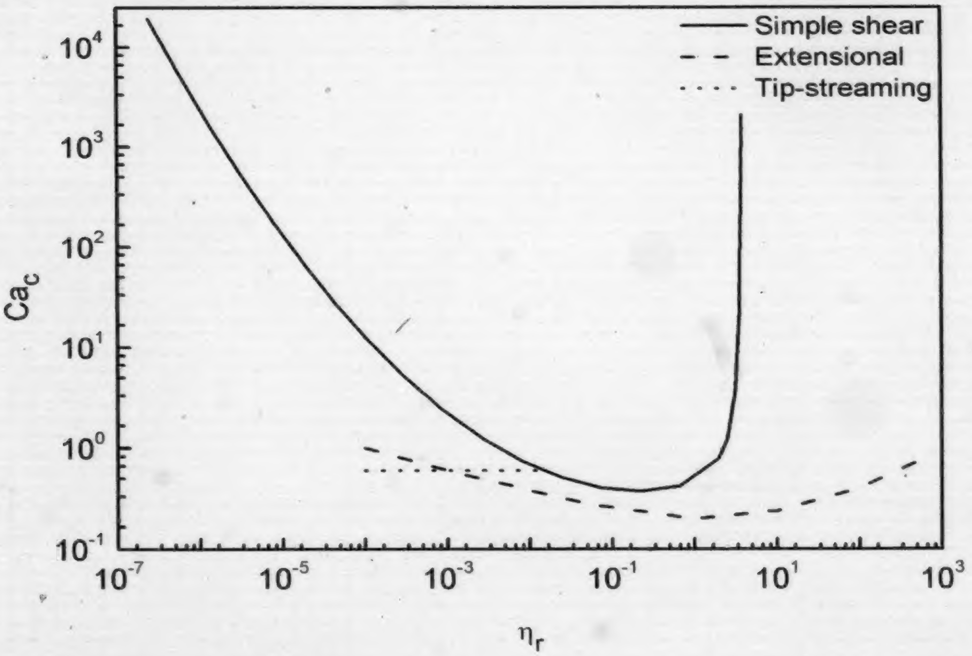

Figure 4-1 Critical capillary number versus viscosity ratio for Newtonian drop breakup (adapted from Grace[4]).

Figure 4-2 shows a typical Newtonian drop breakup process in shear flow. The shear rate is gradually increased in a quasi-steady manner. For Newtonian systems under shear flow, drops elongate and break up in the flow direction.

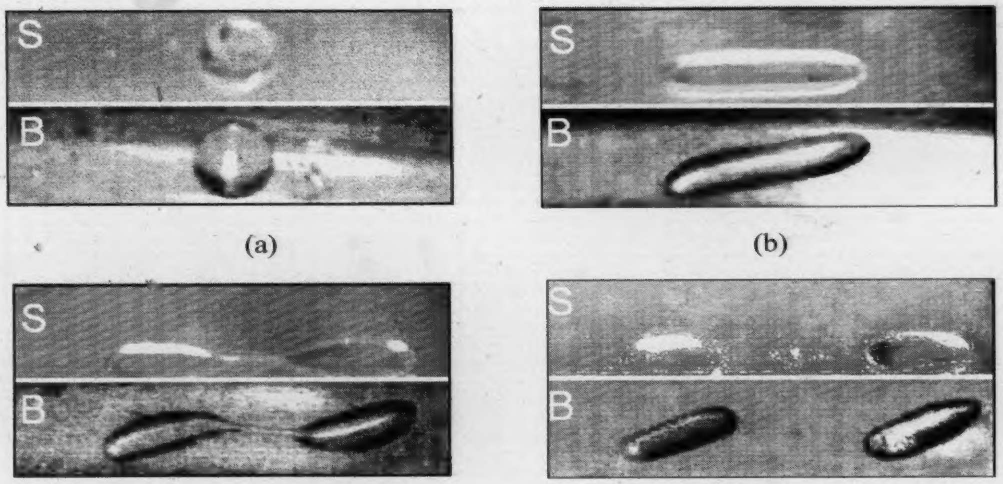

(a) (b)

(c) (d)

Figure 4-2 Deformation and breakup process of a corn syrup drop in polydimethylsiloxane (PDMS) under shear flow in a Couette device. η_r=1.1. The original drop diameter is 1.0mm. (a) Ca=0; (b) Ca=0.44; (c) Ca=0.47 (transient); (d) Ca=0.47 (transient). S and B denote the side view and bottom view of the Couette device respectively. The horizontal direction of each picture is flow direction; the vertical direction in B is the velocity gradient direction and in S is the neutral direction.

Grace's curve provides a precise characterization of Newtonian drop breakup. However, the behavior of viscoelastic systems deviates greatly from the Newtonian Ca *vs.* η_r curve [9-13]. Flumerfelt [9] studied the breakup of a Newtonian drop which was sheared in a viscoelastic matrix. The drop breakup pattern was similar to purely Newtonian systems. However, the critical capillary number of drop breakup depends not only on the viscosity ratio, but also elasticity of the matrix phase and the imposed shear rate. For a given set of drop and matrix, the critical capillary number increases linearly in the imposed shear rate. Varanasi *et al.*

investigated the breakup of a viscoelastic (Boger fluid) drop in a Newtonian fluid matrix which was under simple shear flow [12]. The critical capillary number was found to be a function of viscosity ratio and the imposed shear rate or the first normal stress difference of the drop phase, N1. If the viscosity ratio remains constant, the critical capillary number increases linearly in the imposed shear rate and N_1. Mighri *et al.* studied viscoelastic (Boger fluid) drop sheared in viscoelastic (Boger fluid) matrix [14]. They found that the ratio of the relaxation time (k') of the two phases plays a decisive role on drop breakup. The critical capillary number increases with increase in k' for k'<4, and reaches a plateau when k'>4. Lerdwijitjarud *et al.* [15] studied polymer/polymer systems and found the critical capillary number scales exponentially in the ratio of the first normal stress differences of the two phases with an exponent between 1.7 and 1.9, that is,

$$Ca_c = C(\frac{N_{1d}}{N_{1m}})^{1.7\sim1.9} \qquad (4.4)$$

where C is a constant which could be a function of viscosity ratio, d and m denote drop phase and matrix phase respectively.

The influence of elastic property on drop breakup lies in 1) it causes viscoelastic tensile stress which tends to decrease the flow-induced deformation; 2) it modifies the viscous stress by changing the flow and the pressure inside the drop, both of which tend to increase deformation [16]. The elasticity can cause different breakup phenomena from Newtonian systems. For example, viscoelastic drops can break up in shear flow when the viscosity ratio is above 4 [17-21]. The breakup modes of viscoelastic systems are also found to vary greatly from Newtonian systems. Different modes of drop deformation and breakup were reported for viscoelastic systems. Viscoelastic drops can elongate and break up in the vorticity direction which is defined as the direction perpendicular to the flow direction and the velocity gradient direction. The elongation and breakup along vorticity direction under shear flow is attributed to the normal stress differences which are unique for viscoelastic liquids [22-24]. Lin *et al.* [17-20] and Chen *et al.* [25] further found that polymer melt drops can break up via erosion, vorticity direction breakup, tip-streaming and parallel breakup.

The drop breakup of viscoelastic system is very complex especially during polymer blending process due to the elasticity and complex flow field. Inconsistency exists in the literature for viscoelatic drop breakup. In this chapter, experiments are conducted to understand the effect of viscoelasticity on drop breakup. The systems have been designed as Boger fluid drops sheared in Newtonian matrices.

4.2 Experimental Section

4.2.1 Materials

The matrix phase fluids in the experiments were polydimethylsiloxane (PDMS, Gelest, Inc.) with different viscosities. Boger fluids were used as drop phase, which were prepared using a low-speed mixer for a period of more than 5 days to ensure molecular level mixing. The Boger fluids consist of small amount of polyisobutylene (PIB, Mw=1X10^6 kg/kmol, Sigma-Aldrich) and kerosene (Ker, Fisher Scientific), and a high fraction of viscous polybutene (PB, Mn=920 kg/kmol, Sigma-Aldrich). The viscosity and formulations of the materials are listed in Table 4-1. The interfacial tension between these Boger fluids and PDMS liquids is 3mN/m [24]. Guido *et al.* showed that the miscibility between the drop and matrix phases is not an issue for the study of the drop deformation and breakup [26].

Table 4-1 Viscosity and formulations of material used in the study

Designation		Material Formulation*	Viscosity, Pa·s**
Matrix	M1	PDMS (DMS-T31)	0.97
	M2	PDMS (DMS-T35)	4.86
	M3	PDMS (DMS-T41)	9.74
	M4	PDMS (DMS-T51)	97.7
	M5	PDMS (20%T51+80%T35)	30.5
Drop	D1	0.6%PIB+8.5%Ker+90.9%PB	13.0
	D2	0.1%PIB+4.9%Ker+95.0%PB	14.5
	D3	0.8% PIB+4.4%Ker+94.8%PB	25.0
	D4	1.0% PIB+5.8%Ker+93.2%PB	31.0
	D5	1.3%PIB+7.2%Ker+91.5%PB	40.0

* DMS-T31, T35, T41 and T51 are commercial names of PDMS. All percentages are on mass basis.

** Viscosities are measured at 20 °C.

The rheological properties were obtained with a Rheometrics RMS800 rheometer using cone-and-plate geometry by steady mode at 20°C. All PDMS liquids used in this study exhibit Newtonian fluid properties under the experimental conditions.

Figure 4-3 shows the shear rate dependence of the viscosity (η) and the first normal stress difference (N_1) of the Boger fluids. All the Boger fluids have nearly constant viscosity and exhibit substantial elasticity. With different amount of PIB used, the Boger fluids have different elasticity.

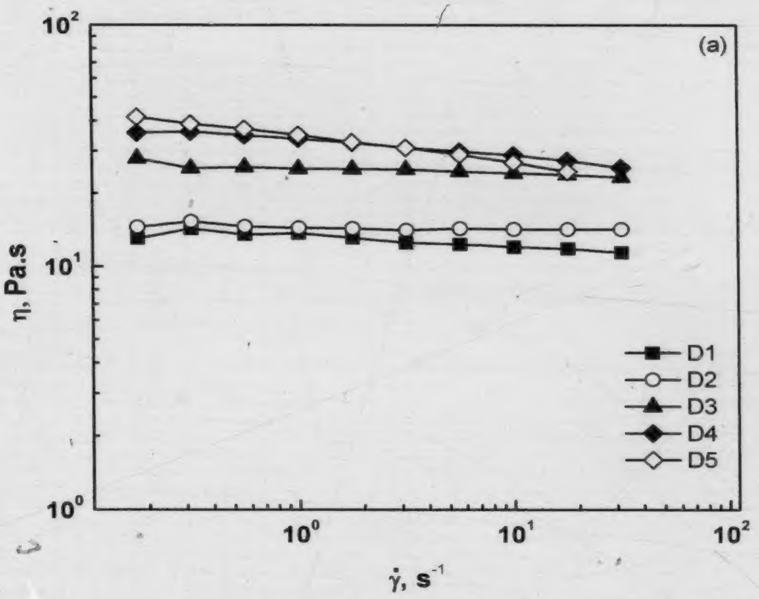

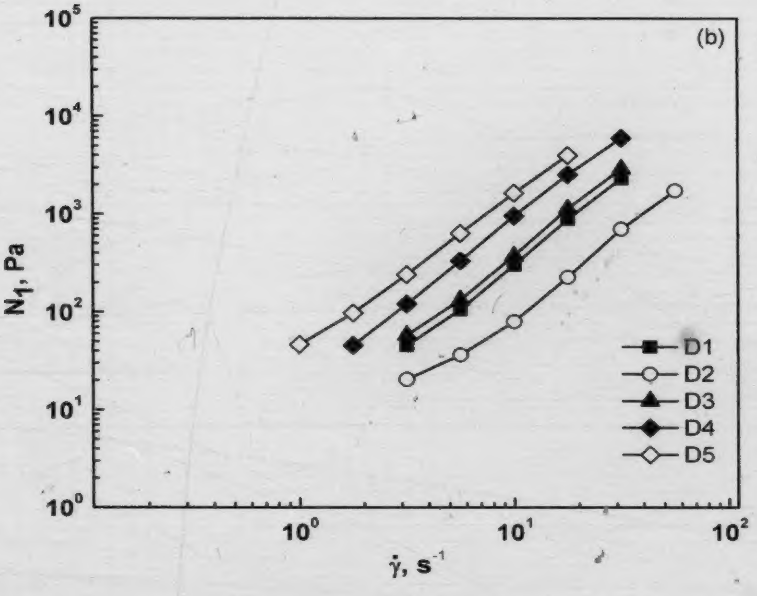

Figure 4-3 Steady rheology properties of Boger fluids. (a) Viscosity of Boger fluids. (b) First normal stress difference of Boger fluid.

The relaxation time (λ) of Boger fluid is calculated as [27, 28]:

$$\lambda = \frac{\psi_{01}}{2\eta_p} \tag{4.5}$$

where ψ_{01} is the coefficient of the first normal stress difference at zero shear rate, and η_p is the polymeric contribution to viscosity. ψ_{01} is obtained by fitting N_1 using power law. η_p is obtained by

$$\eta_p=\eta-\eta_s \tag{4.6}$$

where η is the viscosity of Boger fluid and η_s is the viscosity of the solvent for the Boger fluid. To obtain η_s, mixtures of PB and Kerosen were prepared using the same mass fraction as in Table 4-1 and their viscosities were measured using the same method as for the Boger fluids. The viscoelasticity of the solvent is negligible. The relaxation times of the Boger fluids are listed in Table 4-2.

Table 4-2 Relaxation time of Boger fluids

Boger fluid	η, Pa.s	η_s, Pa.s	η_p, Pa.s	Ψ_{01}, Pa.s^2	λ, s
D1	13.0	7.6	5.4	4.8	0.44
D2	14.5	13.2	1.3	1.3	0.50
D3	25	12.3	12.7	7.3	0.28
D4	31	10	21	18.1	0.43
D5	40	7.8	32.2	42.0	0.65

4.2.2 Setup

A specially designed Couette flow cell was used to generate simple shear flow.

Figure 4-4 shows the schematic of the device. The inner cylinder is made of stainless steel and has a diameter of 102mm. The outer cylinder is made of quartz and has an internal diameter of 110mm. Thus a 4mm gap is formed by the two cylinders. The height of the gap is 60mm. This geometry enables a relatively uniform shear rate within the gap without forming secondary flows [21]. Two DC motors are used to control the rotating speeds of the cylinders to provide a broad range of shear rates. The drop deformation process was recorded to a VCR with two CCD cameras (Pulnix) giving both the side view and the bottom view of the Couette device. The two views make it possible to reconstruct three dimensional photomicrographs of deformed drops by making some basic assumptions for the drop geometry (for example, assume ellipsoidal model for drops). The shear rate was relatively uniform in the gap and can be calculated for Newtonian fluids as [29]:

$$\dot{\gamma} = (\Omega_o - \Omega_i)\frac{r_i^{-2} + r_o^{-2}}{r_i^{-2} - r_o^{-2}} \qquad (4.7)$$

or can be estimated as

$$\dot{\gamma} = \frac{\Omega_o r_o - \Omega_i r_i}{r_o - r_i} \qquad (4.8)$$

where Ω and r are angular rotating speed and radius, and subscripts i and o denote inner and outer cylinders.

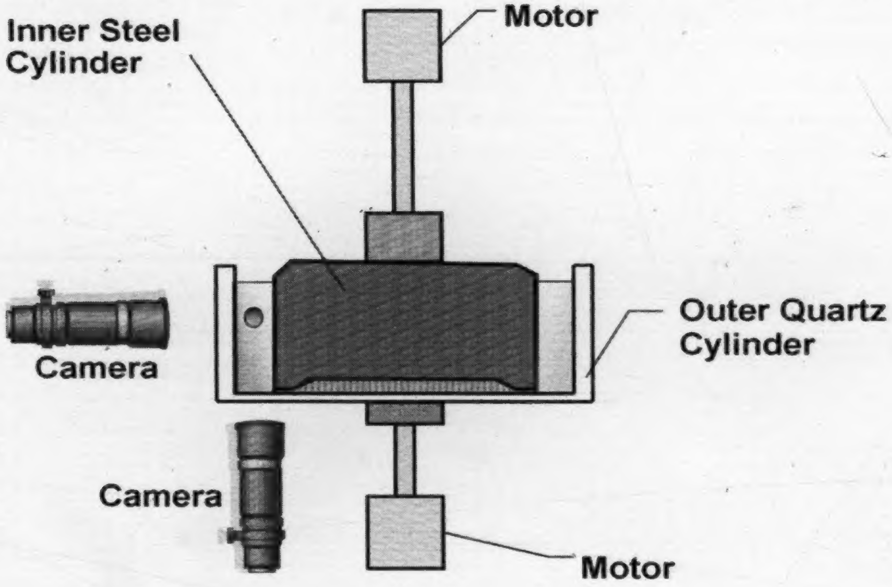

Figure 4-4 Couette apparatus diagram.

4.2.3 Procedure

The gap between the cylinders of the Couette cell was first filled with PDMS. Then a Boger fluid drop was introduced at the middle of the gap and at half height of the cell using a syringe. The apparatus was kept stationary to allow the drop to recover a spherical shape. Then the shear rate was increased gradually to deform the drop in a quasi-steady process. The drops were selected to be smaller than 40% of the gap width, with most of them smaller than 30% of the gap width, to minimize geometrical confinement [30]. The drop deformation and breakup process was recorded. The images and shear rates were later retrieved to analyze the drop breakup conditions.

4.3 Results and Discussion

4.3.1 Breakup modes

As shown in the *Introduction* section in this chapter, drops in Newtonian systems elongate and break up in the flow direction. However, the deformation and breakup modes of viscoelastic drops in Newtonian matrix under shear flow are quite different from those of Newtonian systems. Figure 4-5 shows the deformation and breakup modes of viscoelastic drops in Newtonian matrix under shear flow. Generally, the breakup modes can be classified into two classes: breakup in the flow direction (Figure 4-5(a)) and breakup in the vorticity direction (Figure 4-5(b) and (c)). As indicated by Grace's results, drops in Newtonian systems cannot break up in shear flow when the viscosity ratio is higher than 4. However, viscoelastic drops in Newtonian matrix can break up when the viscosity ratio is above 4. When $\eta_r > 4$, drops break up in vorticity direction. When $\eta_r < 4$, drops may break up in either the flow direction or the vorticity direction. The breakup in the vorticity direction can be further classified in two types as observed: breakup with a waist (Figure 4-5(b)) and breakup with tips (Figure 4-5(c)).

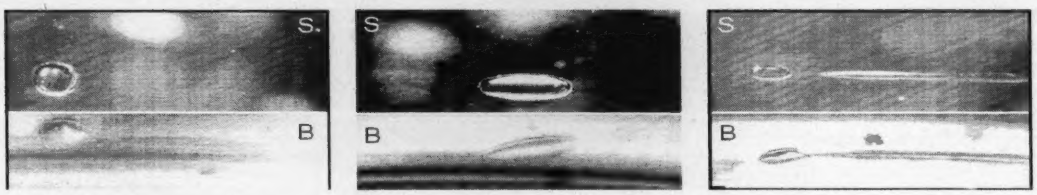

$\dot{\gamma} = 0\,\mathrm{s}^{-1}$ $\dot{\gamma} = 0\ .49\mathrm{s}^{-1}$ $\dot{\gamma} = 0\ .68\mathrm{s}^{-1}$

(a) Drop breakup in the flow direction: M3/D3, η_r=2.6, D_0=1.16mm

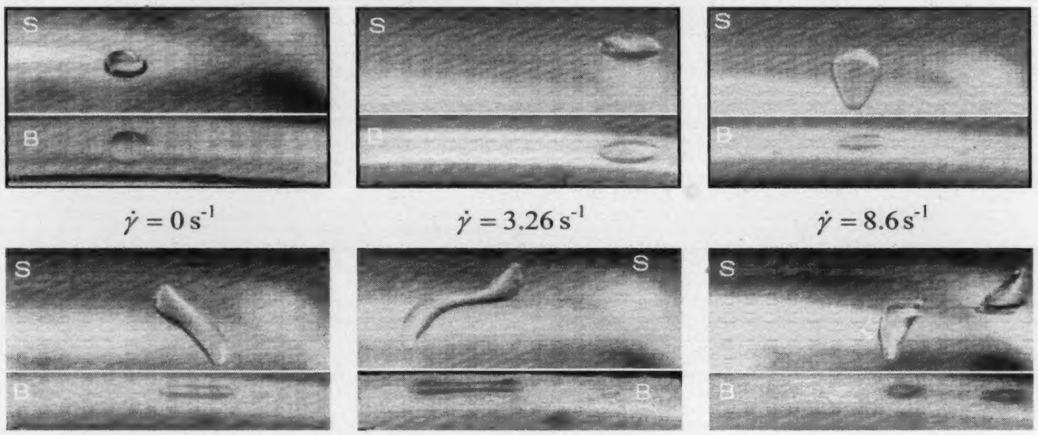

$\dot{\gamma} = 0\,\mathrm{s}^{-1}$ $\dot{\gamma} = 3.26\,\mathrm{s}^{-1}$ $\dot{\gamma} = 8.6\,\mathrm{s}^{-1}$

$\dot{\gamma} = 10.39\,\mathrm{s}^{-1}$ $\dot{\gamma} = 13.41\,\mathrm{s}^{-1}$(transient) $\dot{\gamma} = 13.39\,\mathrm{s}^{-1}$

(b) Breakup in vorticity direction with a waist: M2/D4, η_r=6.4, D_0=1.06mm

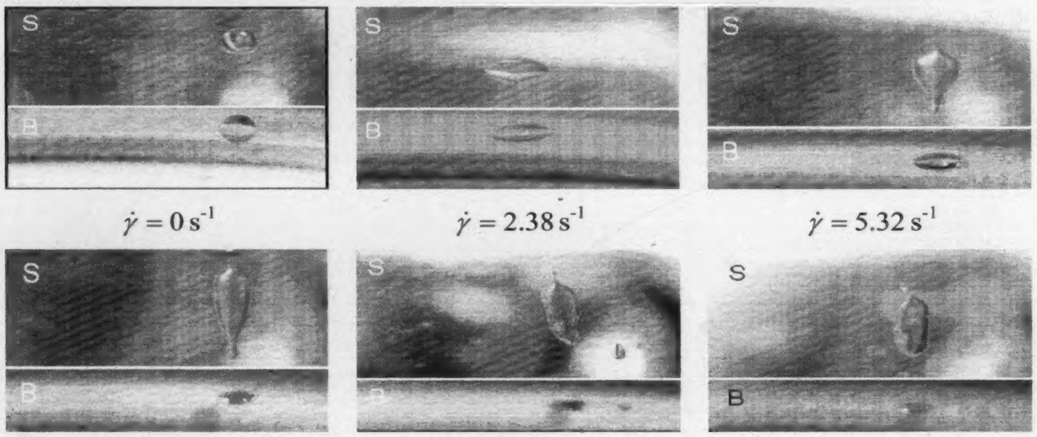

$\dot{\gamma} = 0\,\mathrm{s}^{-1}$ $\dot{\gamma} = 2.38\,\mathrm{s}^{-1}$ $\dot{\gamma} = 5.32\,\mathrm{s}^{-1}$

$\dot{\gamma} = 6.75\,\mathrm{s}^{-1}$(transient) $\dot{\gamma} = 6.79\,\mathrm{s}^{-1}$(transient) $\dot{\gamma} = 6.75\,\mathrm{s}^{-1}$(transient)

(c) Tip breakup in vorticity direction: M3/D4, η_r=3.2, D_0=1.45mm

Figure 4-5 Drop deformation and breakup modes. For each image, S and B denote the side view and bottom view, respectively.

5

Drop breakup is unsteady process of drop deformation. For a viscoelastic drop under shear flow, Hobbies and Migler [23], and Mighri and Huneault [24] showed that the first normal stress difference (N_1) exerts as an extra restoring stress which resists the drop elongation in the flow direction. The relation of stress development and drop deformation was discussed in detail in Chapter 3. The deforming stress, i.e. the shear stress, may outbalance the combining restoring effect of the interfacial stress and N_1. In such cases, the drop will break up in the flow direction (Figure 4-5(a)). However, in many cases the shear stress does not outbalance the restoring stresses. This means the drop cannot break up in the flow direction. On the contrary, with the increase in shear rate, N_1 increases rapidly and a resultant "hoop force" squeezes the drop fluid toward the vorticity direction. Thus the drop elongates in the vorticity direction. When the shear rate reaches a certain value, the drop may form a waist in the middle or small tips at the top and bottom ends along the vorticity direction. The flow will eventually break the drops at the "necked" positions. A further investigation helped us distinguish these two modes. High values in drop size and shear rate steps usually result in a breakup with a waist while lower values cause a breakup at the tips. This implies that the breakup with a waist is more likely caused by disturbance since the vorticity-elongated drop is not stable. Figure 4-6 gives a schematic explanation of the drop breakup with a waist. Drop breakup with tips should be closer to a quasi-steady critical breakup mode without/with small disturbance. However, the mechanism of the formation of the necks between the tips and the bulk drop is unknown.

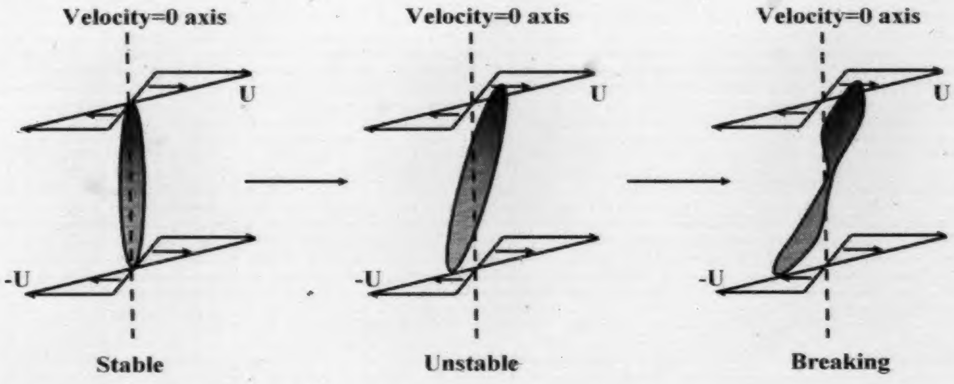

Figure 4-6 Disturbance causes instability of vorticity-elongated drop. U is velocity.

4.3.2 Effect of drop size

It has been found in our experiments that for some Boger drop/Newtonian matrix systems, drops can break up either in the flow direction or in the vorticity direction depending on the drop size. Figure 4-7 shows different breakup modes for system M3/D3. A drop with initial diameter (D_0) of 1.16 mm broke up in the flow direction when the shear rate was 0.68 s^{-1}, as shown in Figure 4-7(a). The critical capillary number was close to that of Newtonian systems with the same viscosity ratio. Figure 4-7 (b) gives the breakup of a relatively small drop with initial diameter of 0.57 mm. The drop initially stretched in the flow direction but later changed its stretching axis to the vorticity direction. With increasing shear rate, it continued to elongate in the vorticity direction and eventually broke up in the same direction when the shear rate reached 42 s^{-1}. The critical capillary number is much higher than that of Newtonian counterparts. We speculated that the drop size affected the drop breakup mechanism and the critical conditions. This speculation was proved by the result shown in Figure 4-7 (c) in which the breakup of a big drop was traced and one of its daughter drops. The initial drop diameter ($D2_0$) was 0.64 mm and this drop broke up in the flow direction at a shear rate of 1.81 s^{-1}. The breakup mode was similar to that shown in Figure 4-7 (a). After this breakup, shearing was stopped and the Couette cell was kept motionless to let the daughter drops recover to a spherical shape, shown in the third image of Figure 4-7 (c). Then one of the daughter drops was followed and the shear rate was increased in a quasi-steady manner. The diameter of the daughter drop ($D1_0$) was 0.46 mm. The daughter drop showed similar breakup behavior as that of the drop depicted in Figure 4-7 (b). It eventually broke up in the vorticity direction at a shear rate of 55 s^{-1}. It is important to note the drastic difference in critical shear rate between these two drop breakup modes for relatively similar sized drops (approximately 2 s^{-1} for $D2_0$=0.64 mm compared to 55 s^{-1} for $D1_0$=0.46 mm). This has significant consequences for equipment design and process conditions for mixing operations. We extended this study to other systems, M3/D1 and M5/D5. The same breakup phenomena were identified. The results are summarized in Table 4-3. The breakup mechanism of viscoelastic drops in simple shear flow depends greatly on the drop size. The effect of the drop size on the drop breakup mechanism can also be seen from the dependence of the critical shear rate on the drop size. Figure 4-8 gives the critical shear rate versus drop size of systems M3/D3 and M3/D1. There is a big jump in the critical shear rate when the mechanism changes from breakup in the flow direction to breakup in the vorticity direction.

Table 4-3 The effect of drop size on breakup mode and condition

Matrix/Drop	η_r	D_0, mm	Breakup mode[a]	$\dot{\gamma}_c$[b], s^{-1}	Ca_c	τ, Pa	N_1, Pa
M3/D1	1.3	1.71	F	0.50	1.4	4.9	1.7
		0.50	F	1.57	1.3	15.3	10.7
		0.34	V	17.6	9.9	171	531
M3/D3	2.6	1.16	F	0.53	1.0	5.2	0.8
		1.19	F	0.75	1.4	7.3	1.4
		0.64	F	1.81	1.9	17.6	5.9
		0.57	V	42.0	38.5	409	902
		0.46	V	55.0	41.0	536	1390
M5/D5	1.3	1.37	F	0.70	4.9	21.4	19.0
		0.54	V	5.5	15.1	168	420

a. F: breakup in flow direction; V: breakup in vorticity direction.

b. $\dot{\gamma}_c$: critical shear rate at breakup.

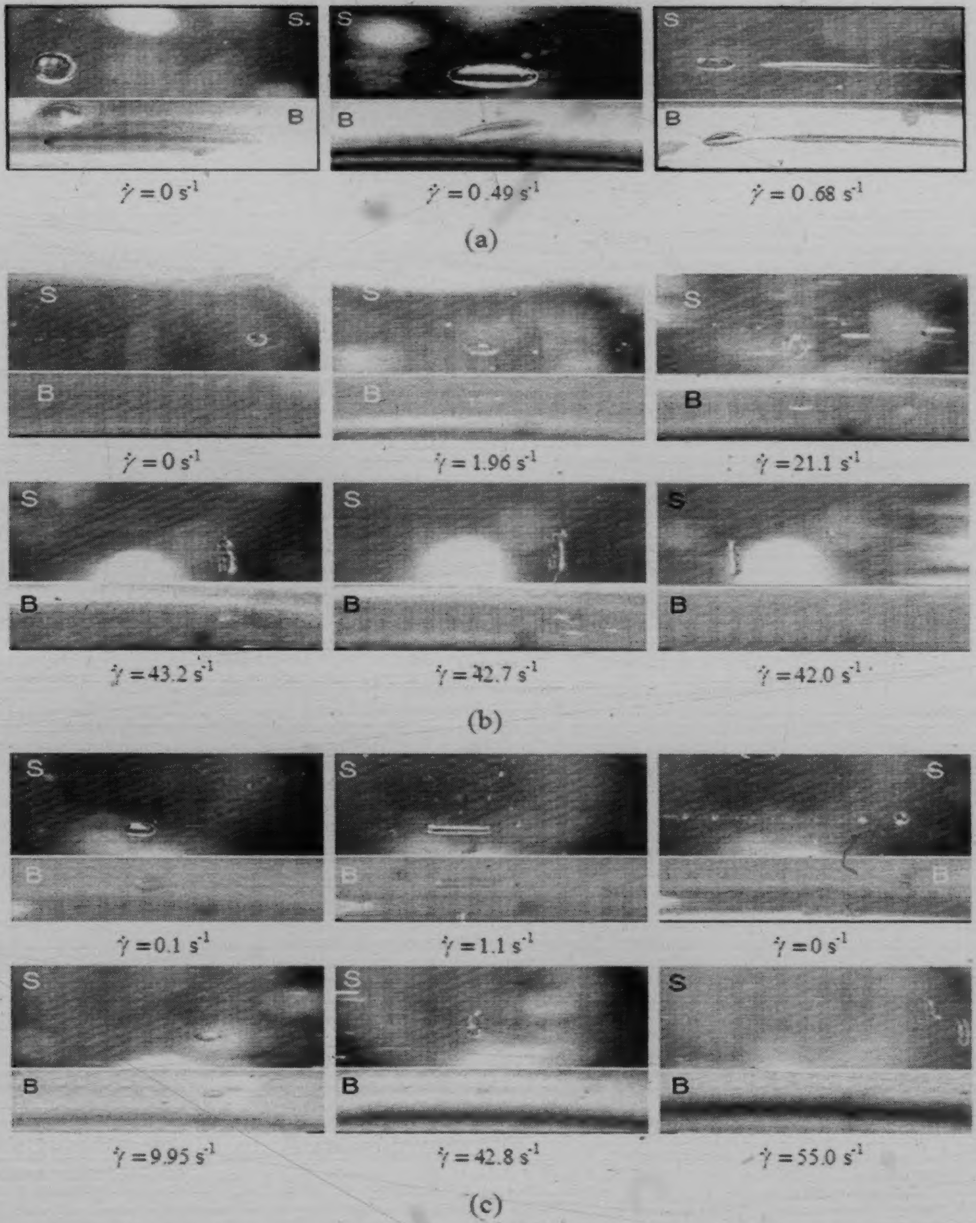
S
B
$\dot{\gamma}=0\ s^{-1}$
$\dot{\gamma}=0.49\ s^{-1}$
$\dot{\gamma}=0.68\ s^{-1}$
(a)
$\dot{\gamma}=0\ s^{-1}$
$\dot{\gamma}=1.96\ s^{-1}$
$\dot{\gamma}=21.1\ s^{-1}$
$\dot{\gamma}=43.2\ s^{-1}$
$\dot{\gamma}=42.7\ s^{-1}$
$\dot{\gamma}=42.0\ s^{-1}$
(b)
$\dot{\gamma}=0.1\ s^{-1}$
$\dot{\gamma}=1.1\ s^{-1}$
$\dot{\gamma}=0\ s^{-1}$
$\dot{\gamma}=9.95\ s^{-1}$
$\dot{\gamma}=42.8\ s^{-1}$
$\dot{\gamma}=55.0\ s^{-1}$
(c)

Figure 4-7 Breakup modes of M3/D3, η_r=2.6, for different drop sizes. (a) Elongation and breakup in the flow direction: D_0=1.16 mm; (b) Elongation and breakup in the vorticity direction: D_0=0.57 mm; (c) Transition from flow direction to vorticity direction, $D2_0$=0.64 mm; $D1_0$=0.46 mm. S and B denote side view and bottom view respectively.

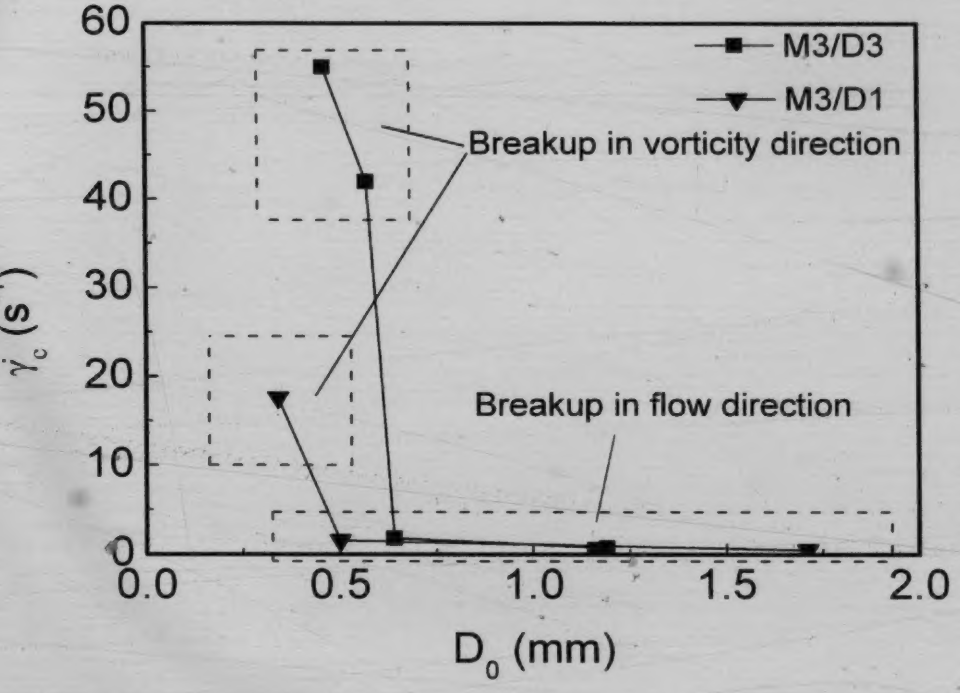

Figure 4-8 The critical shear rate jumps when the breakup mechanism changes.

It should be noted that the critical shear rate also changes with variable drop size in Newtonian systems. However, for Newtonian systems, the critical capillary number is constant if the viscosity ratio is given. Hence the critical shear rate for a Newtonian system is inversely proportional to the drop size. It would not change as much as what was observed in the viscoelastic systems. The critical capillary number of viscoelastic system is no longer a single-variable function of viscosity ratio. Table 4-3 shows that for different viscosity ratios, the drop size always affects the breakup mode and the critical shear rate.

The effect of drop size is attributed to the elastic properties of Boger fluids. Since the breakup is the consequence of deformation, the influence of the drop elasticity is seen throughout the deformation until breakup. When a viscoelastic drop stretches in the flow direction, regardless of the subsequent breakup mode, the length in the velocity gradient direction is smaller than that in the vorticity direction. Similar widening phenomenon, i.e. when the drop length in vorticity direction exceeds the original drop diameter, was discussed by Levitt *et al.* [31] by relating the deformation to normal stress. Big drops stretch significantly before breaking in the flow direction. The widening effect is more evident when the drops elongate in the vorticity direction. Figure 4-7 (b) and (c) show that the length in the vorticity direction is much larger than those in the velocity gradient direction.

These special deformation and breakup patterns of viscoelastic systems and the drop size effect indicate that there must be forces pushing the fluid along the vorticity direction, similarly to the "rod-climbing" phenomenon [23]. Different from Newtonian systems, the three normal stresses of viscoelastic fluids undergoing shear flow are not equal. It is believed that the first normal stress difference N_1 plays a key role in the drop elongation along the vorticity axis [10, 23, 24]. Sundararaj *et al.* [32, 33] grouped stresses into deformation stress and restoring stress to study the drop deformation of polymer systems and indicated that the drop deformation was related to the stress ratio between the deformation stress and restoring stress. In our experiments, during the elongation in the flow direction, the deformation stress is the shear stress τ and the restoring stress is approximated as the sum of the first normal stress N_1 and the interfacial stress Γ / R. τ is proportional to shear rate $\dot{\gamma}$, N_1 is proportional to $\dot{\gamma}^2$ at low shear rate and Γ / R is independent of $\dot{\gamma}$. We define the stress ratio S_r as:

$$S_r = \frac{N_1 + \Gamma / R}{\eta_m \dot{\gamma}} \tag{4.9}$$

Figure 4-9 gives the development of the stress ratio as shear rate increases for different drop diameter (D_0) of system M3/D3, as well as the critical stress ratio for Newtonian system with the same viscosity ratio (η_r=2.6) which is $1/Ca_c$. For drop size below D_0=0.46 mm, the stress ratio is above the critical stress ratio of the Newtonian system. This means that for drop diameter below 0.46 mm, it is impossible to break the drop in the flow direction in simple shear flow. This result agrees with our experiments.

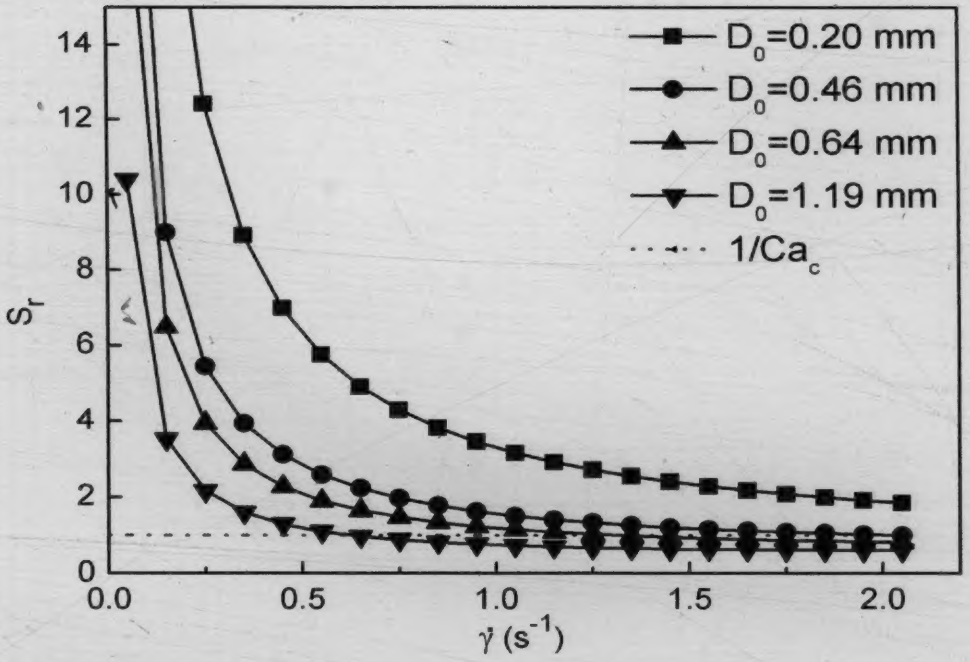

Figure 4-9 Dependence of stress ratio on shear rate for different drop sizes for system M3/D3.

The critical stresses at breakup are shown in Figure 4-10. Compared to the shear stress and interfacial stress, N_1 is negligible when the shear rate is very low as shown in Figure 4-10 (a). However, it increases dramatically with increasing shear rate, resulting in high restoring stress, as shown in Figure 4-10 (b). At high shear rate, the interfacial stress is relatively small and the restoring stress is dominated by N_1. If the drop is big enough, the drop can break up in the flow direction at a low shear rate, similar to Newtonian-type breakup. In this case, the stress ratio can be considered close to the capillary number since the shear rate is low and N_1 is negligible. This is also indicated by the results in Table 4-3. However, smaller drops require higher shear rate to reach the value of the critical capillary number for Newtonian-type breakup. But at this shear rate, the normal stress N_1 cannot be neglected. As a restoring stress, N_1 resists the deformation in the flow direction and tends to contract the drop. With further increases in the shear rate, the normal stress grows faster than the shear stress. A resultant "hoop force" squeezes the fluid in the vorticity direction and the drop begins to elongate in the vorticity direction and eventually breaks up. In this case, the critical capillary numbers at breakup are much larger than those of flow direction breakup. To further understand the effect of drop size on drop breakup mechanism, one can simply imagine an extremely big viscoelastic drop and a very small drop subjected to shear flow. The big one must deform and break up like a pure Newtonian drop, while the deformation of the small one must be greatly affected by normal stresses.

Our findings of the effect of drop size on the drop breakup mode shed light on the mechanism of mixing process of immiscible viscoelastic liquids. For example, in polymer blending process, normally at the beginning of mixing, the dispersed phase particles are several millimeters in size; and at the end of mixing, the particle size reduces to micrometers. During the blending process, the drops may initially break up in the flow direction to reduce the dispersed phase dimensions and will later break up in the vorticity direction when the drop sizes are below the critical drop size. Furthermore, knowing that a jump in shear rate exists for different breakup modes may facilitate the design of polymer blending processes in that the process can be designed so that shear rate is variable along the length of the process equipment.

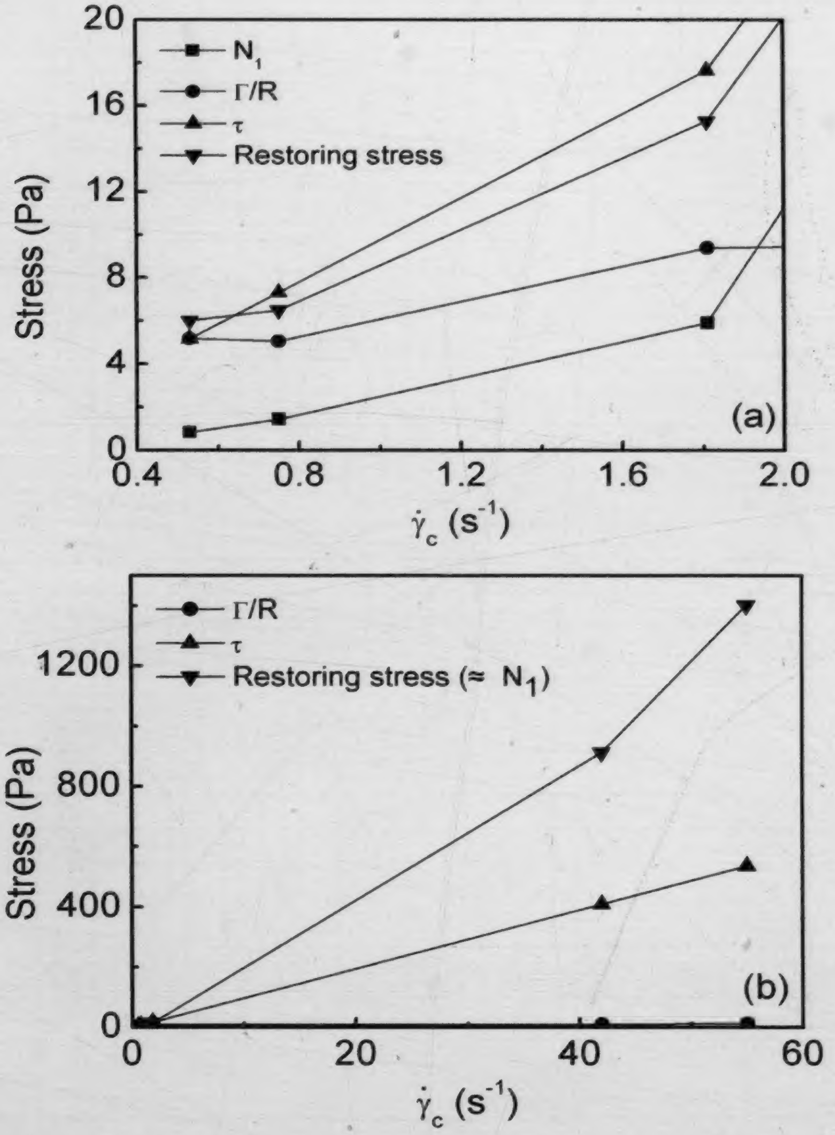

Figure 4-10 Drop size effect on the stresses at breakup, M3/D3. (a) Stresses at low shear rates; (b) Stresses in the whole range of shear rate in this study.

From the above discussion, one would expect a critical drop size above which the drop breaks up in the flow direction but below which it breaks up in the vorticity direction. If the drop breaks up in the flow direction, the breakup must happen before the drop contracts in the flow direction. On the contrary, if the drop breaks up in the vorticity direction, it must happen after the drop contracts. Aggarwal and Sarkar [34] gave a simple model based on force balance to describe deformation of a viscoelastic drop sheared in a Newtonian matrix. De Bruijn [35] also gave a qualitative model to predict the critical drop size of viscoelastic drop breakup based on force balance. Here we construct a similar model to explain the effect of drop size on the drop breakup mode. This model assumes the shear force is equal to the sum of interfacial force and elastic force caused by N_1, i.e.

$$\Gamma R_0 \hat{X} + N_1 R_0^2 \hat{X} = \eta_m R_0^2 \dot{\gamma} \qquad (4.10)$$

where $\hat{X}$ is a characteristic drop deformation. The first and second terms on the left-hand side represent interfacial force and elastic force. The right-hand side represents the shear force. When the drop starts to contract in the flow direction, the deformation $\hat{X}$ as a function of $\dot{\gamma}$ is at its maximum, which means

$$\frac{\partial \hat{X}}{\partial \dot{\gamma}} = 0 \text{ at } \hat{X} = \hat{X}_{\max} \qquad (4.11)$$

Differentiating Eqn (4.10) with respect to shear rate and substituting Eqn (4.11), we got

$$\frac{dN_1}{d\dot{\gamma}} = \frac{\eta_m}{\hat{X}_{max}} \quad \text{at} \quad \hat{X} = \hat{X}_{max} \tag{4.12}$$

N_1 is a function of the shear rate within the drop ($\dot{\gamma}_d$), which is

$$N_1 = \psi_1 \dot{\gamma}_d^2 \tag{4.13}$$

$\dot{\gamma}_d$ can be approximated by assuming the tangential stress is continuous across the interface, which gives

$$\eta_m \dot{\gamma} = \eta_d \dot{\gamma}_d \tag{4.14}$$

From Eqn (4.13) and Eqn (4.14) we have

$$N_1 = \frac{\psi_1 \dot{\gamma}^2}{\eta_r^2} \quad \text{where} \quad \eta_r = \frac{\eta_d}{\eta_m} \tag{4.15}$$

If we assume ψ_1 is constant, then from Eqn (4.12) and Eqn (4.15) we got the shear rate at the starting point of contraction ($\dot{\gamma}_{ct}$) as:

$$\dot{\gamma}_{ct} = \frac{\eta_m \eta_r^2}{2\psi_1 \hat{X}_{max}} \tag{4.16}$$

For a drop to break up in the flow direction, it must continuously elongate in the flow direction until breakup. In cases where drop breaks up in the flow direction, there may be a point where the drop would contract if it had not broken up at $\dot{\gamma}_c$. In other words, if we assume a virtual contraction point for this drop, the shear rate for contraction should be higher than the critical shear rate for breakup, that is

$$\dot{\gamma}_{ct} \geq \dot{\gamma}_c \tag{4.17}$$

which means

$$\eta_m \dot{\gamma}_{ct} D / 2\Gamma \geq Ca_c \tag{4.18}$$

For the drop to break up in the flow direction, the drop size must be such that

$$D \geq \frac{4Ca_c \Gamma \psi_1 \hat{X}_{max}}{\eta_d^2} \tag{4.19}$$

If D is less than the predicted size in Eqn (4.19), the drop could not break up in the flow direction.

This model gives reasonable explanation for the effect of drop size on drop breakup mode. However, it is important to note that this model is only qualitative. The parameters, Ca_c and $\hat{X}_{max}$ depend on the viscoelastic properties.

4.3.3 Effect of viscoelasticity

Similar to the breakup criterion for Newtonian system, Figure 4-11 plots the critical capillary number *versus* viscosity ratio for the viscoelastic drop breakup in this work. The breakup conditions for viscoelastic systems do not fall on the same curve as Newtonian systems. There are several differences between viscoelastic drop/Newtonian matrix and Newtonian drop/Newtonian matrix systems: 1) Viscoelastic drop can breakup at $\eta_r > 4$. This breakup occurs when the drop elongates in the vorticity direction. 2) The critical capillary number for viscoelastic drop/Newtonian matrix is higher than or close to purely Newtonian systems with the same viscosity ratio. This is apparently due to the resistance of

N_1 to drop elongation in the flow direction. To break the drop, the capillary number has to exceed the critical capillary number for purely Newtonian systems.

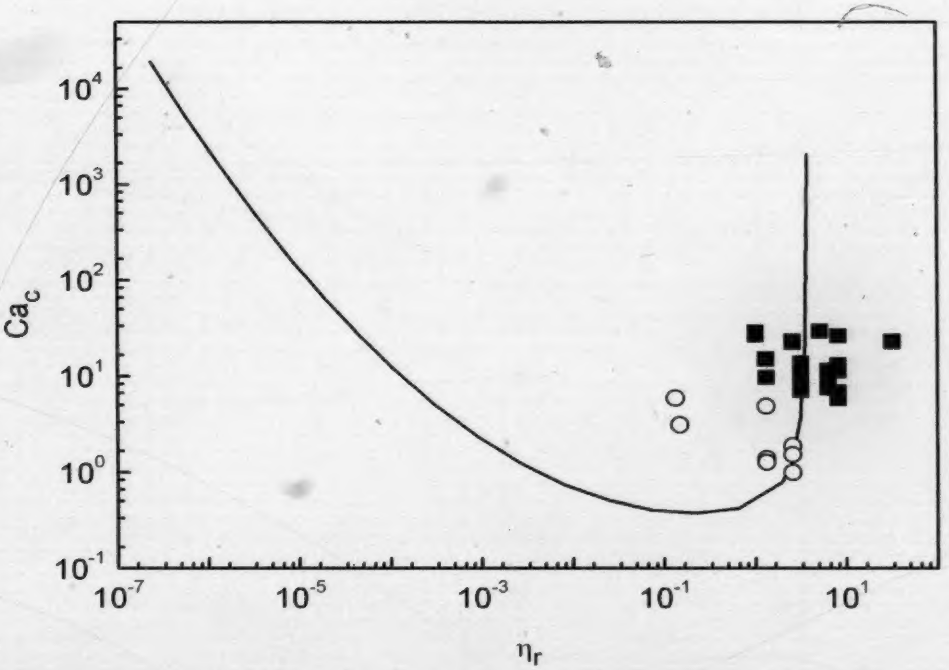

Figure 4-11 The relationship between Ca_c and η_r for viscoelastic drop breakup. The dashed line is the correlation for Newtonian drop breakup adapted from de Bruijn [35]. Solid squares are for vorticity breakup and empty circles are for breakup in the flow direction.

Unlike the Ca_c vs. η_r correlation for Newtonian systems, there is at least one more parameter should be taken into consideration to characterize the breakup criterion for viscoelastic drop suspended in Newtonian matrix under shear flow. This parameter should represent the elasticity of the drop phase fluid. The Deborah number (De) is widely used to represent elastic property of viscoelastic fluids.

Deborah number is dimensionless group which is the product of relaxation time λ and shear rate $\dot{\gamma}$. Table 4-4 shows the effect of elasticity on the drop breakup. For systems M4/ D2 and M4/ D1, their drop size and viscosity ratios are very close. In both systems, drops break up in the flow direction. The critical capillary number increases with increase in the Deborah number, which means that it is harder to break the drop in the flow direction with higher elasticity. For system M3/ D1, a drop with a diameter of 0.5mm in M3/D1 breaks up in the flow direction at Ca_c=1.3. However, a similar sized drop (D_0=0.54mm) in system M5/D5 with the same viscosity ratio cannot break up in the flow direction but break up in the vorticity direction at Ca_c=15.1. The critical capillary number, as well as the critical Deborah number increases a lot for M5/D5 system. The critical breakup conditions are affected by the drop size. For all experiments, their critical capillary numbers are higher than their Newtonian counterpart. This again demonstrates that the elasticity of the drop phase resists drop breakup.

Table 4-4 Critical capillary number and viscosity ratio.

Matrix	Drop	η_r	Drop diameter (mm)	De_c	Ca_c
M4	D1	0.13	0.91	0.2	5.9
M4	D2	0.15	0.87	0.1	3.1
Newtonian system*		0.13	--	--	0.38
M3	D1	1.3	0.5	0.7	1.3
M5**	D5	1.3	0.54	3.6	15.1
Newtonian system*		1.3	--	--	0.54

* Ca_c calculated based on de Bruijn's 5-parameter equation [35].

** The drop in this system breaks up in the vorticity direction.

4.4 Conclusion

In this chapter, the breakup of a viscoelastic drop (Boger fluid) sheared in a Newtonian PDMS matrix was investigated. The drop deformation and breakup was found to be very different from purely Newtonian systems. Two different breakup modes were identified for viscoelastic drops. When the viscosity ratio is above 4, drops break up in the vorticity direction. When the viscosity ratio is below 4, drops break up either in the flow direction or the vorticity direction.

For a specified viscoelastic drop/Newtonian matrix system, there is coexistence of drop breakup in the flow direction breakup and drop breakup in the vorticity direction. Drop size is found to play a decisive role in the transition between different breakup mechanisms. A dramatic change in the critical shear rate was found when going from one breakup mode to another. The critical drop size determining the drop breakup mechanism is found to be related to interfacial tension, the elastic property (the coefficient of the first normal stress different), and the viscosities of the matrix and drop phase.

The elastic property has great influence on the viscoelastic drop breakup. Drops can break up in simple shear flow for viscoelastic systems with viscosity ratio higher than 4. The critical capillary for viscoelastic drop suspended in Newtonian matrix under simple shear flow is higher/close to that of Newtonian systems with the same viscosity ratio. For constant viscosity ratio and drop size, drops with higher Deborah number break up at higher capillary number.

4.5 References

[1] G.I. Taylor, "The viscosity of a fluid containing small drops of another fluid," Proc. R. Soc. London Ser. A **138**, 41 (1932).

[2] G.I. Taylor, "The formation of emulsions in definable fields of flow," Proc. R. Soc. London Ser. A **146**, 501 (1934).

[3] A. Acrivos and T.S. Lo, "Deformation and breakup of a single slender drop in an extensional flow," J. Fluid Mech. **86**, 641 (1978).

[4] H.P. Grace, "Dispersion phenomena in high-viscosity immiscible fluid systems and application of static mixers as dispersion devices in such systems," Chem. Eng. Commun. **14**, 225 (1982).

[5] B.J. Bentley and L.G. Leal, "An experimental investigation of drop deformation and breakup in steady, two-dimensional linear flows," J. Fluid Mech. **167**, 241 (1986).

[6] H.A. Stone and L.G. Leal, "The effects of surfactants on drop deformation and breakup," J. Fluid Mech. **220**, 161 (1990).

[7] J. Li, Y.Y. Renardy, and M. Renardy, "Nuemerical simulation of breakup of a viscous drop in simple shear flow through a volume-of-fluid method," Phys. Fluids **12**, 269 (2000).

[8] V. Cristini, B. J., and M. Loewenberg, "An adaptive mesh algorithm for evolving surfaces: Simulations of drop breakup and coalescence," J. Comput. Phys. **168**, 445 (2001).

[9] R.W. Flumerfelt, "Drop breakup in simple shear fields of viscoelastic

fluids," Ind. Eng. Chem. Fund. **11**, 312 (1972).

[10] H. Vanoene, "Modes of dispersion of viscoelastic fluids in flow," J. Colloid Interface Sci. **40**, 448 (1972).

[11] S.H. Wu, "Formation of dispersed phase in incompatible polymer interfacial and rheological effects," Polym. Eng. Sci. **27**, 335 (1987).

[12] P.P. Varanasi, M.E. Ryan, and P. Stroeve, "Experimental-study on the breakup of model viscoelastic drops in uniform shear-flow," Ind. Eng. Chem. Res. **33**, 1858 (1994).

[13] W. Lerdwijitjarud, A. Sirivat, and R.G. Larson, "Influence of dispersed-phase elasticity on steady-state deformation and breakup of droplets in simple shearing flow of immiscible polymer blends," J. Rheol. **48**, 843 (2004).

[14] F. Mighri, P.J. Carreau, and A. Ajji, "Influence of elastic properties on drop deformation and breakup in shear flow," J. Rheol. **42**, 1477 (1998).

[15] W. Lerdwijitjarud, A. Sirivat, and R.G. Larson, "Influence of elasticity on dispersed-phase droplet size in immiscible polymer blends in simple shearing flow," Polym. Eng. Sci. **42**, 798 (2002).

[16] S. Ramaswamy and L.G. Leal, "The deformation of a newtonian drop in the uniaxial extensional flow of a viscoelastic liquid," J. Non-Newtonian Fluid Mech. **88**, 149 (1999).

[17] B. Lin, F. Mighri, M.A. Huneault, and U. Sundararaj, "Parallel breakup of polymer drops under simple shear," Macromol. Rapid Commun. **24**, 783 (2003).

[18] B. Lin, U. Sundararaj, F. Mighri, and M.A. Huneault, "Erosion and breakup of polymer drops under simple shear in high viscosity ratio systems," Polym. Eng. Sci. **43**, 891 (2003).

[19] B. Lin and U. Sundararaj, "Sheet formation during drop deformation and breakup in polyethylene/polycarbonate systems sheared between parallel plates," Polymer **45**, 7605 (2004).

[20] B. Lin, F. Mighri, M.A. Huneault, and U. Sundararaj, "Effect of premade compatibilizer and reactive polymers on polystyrene drop deformation and breakup in simple shear," Macromolecules **38**, 5609 (2005).

[21] F. Mighri and M.A. Huneault, "In situ visualization of drop deformation, erosion, and breakup in high viscosity ratio polymeric systems under high shearing stress conditions," J. Appl. Polym. Sci. **100**, 2582 (2006).

[22] K.B. Migler, "Droplet vorticity alignment in model polymer blends," J. Rheol. **44**, 277 (2000).

[23] E.K. Hobbie and K.B. Migler, "Vorticity elongation in polymeric emulsions," Phys. Rev. Lett. **82**, 5393 (1999).

[24] F. Mighri and M.A. Huneault, "Dispersion visualization of model fluids in a transparent couette flow cell," J. Rheol. **45**, 783 (2001).

[25] H. Chen, U. Sundararaj, K. Nandakumar, and M.D. Wetzel, "Erosion of polymer pellets during blending in a twin-screw extruder," AIChE J. **52**, 1267 (2006).

[26] S. Guido, M. Simeone, and F. Greco, "Deformation of a newtonian drop in a viscoelastic matrix under steady shear flow - experimental validation of slow flow theory," J. Non-Newtonian Fluid Mech. **114**, 65 (2003).

[27] D.V. Boger and M.E. Mackayb, "Continuum and molecular interpretation of ideal elastic fluids " J. Non-Newtonian Fluid Mech. **41**, 133 (1991).

[28] C.P. Carroll and Y.L. Jooa, "Electrospinning of viscoelastic boger fluids: Modeling and experiments," Phys. Fluids **18**, 053102-1 (2006).

[29] C.W. Macosko, Rheology: Principles, measurements and applications,

Wiley-VCH, New York, 1994.

[30] A. Vananroye, P.V. Puyvelde, and P. Moldenaers, "Effect of confinement on the steady-state behavior of single droplets during shear flow," J. Rheol. **51**, 139 (2007).

[31] L. Levitt, C.W. Macosko, and S.D. Pearson, "Influence of normal stress difference on polymer drop deformation," Polym. Eng. Sci. **36**, 1647 (1996).

[32] U. Sundararaj, Y. Dori, and C.W. Macosko, "Sheet formation in immiscible polymer blends: Model experiments on initial blend morphology," Polymer **36**, 1957 (1995).

[33] P.G. Ghodgaonkar and U. Sundararaj, "Prediction of dispersed phase drop diameter in polymer blends: The effect of elasticity," Polym. Eng. Sci. **36**, 1656 (1996).

[34] N. Aggarwal and K. Sarkar, "Deformation and breakup of a viscoelastic drop in a newtonian matrix under steady shear," J. Fluid Mech. **584**, 1 (2007).

[35] R.A. De Bruijn, PhD Thesis, "Deformation and breakup of drops in simple shear flows", Eindhoven University of Technology, Eindhoven (1989).

Chapter 5
Polymer Blends under Shear Flow

5.1 Introduction

It is widely known that the morphology of polymer blends greatly determines the properties of the final products, while the morphology is the result of the blending process. During a typical blending process, the dispersed polymer morphology evolves from pellets to submicron particles in a matrix composed of the major polymer phase. The major size reduction of the dispersed domain occurs during the initial mixing stages [1-7] and the balance between drop breakup and coalescence dominates the final stages [8-10]. The blending process is the combination of (1) the breaking process of a single fluid body of the dispersed polymer which can be in all shapes such as drop, fiber or film, and (2) the interaction of multiple fluid bodies, both of which take place inside the major polymeric fluid. The morphology of polymer blends results from this blending process and is largely determined by the rheological properties of polymer components. Due to the complexities of the processing flow fields and rheological properties of polymers, the morphology development during polymer blending remains mystery to scientists working in areas ranging from polymer blending to fluid mechanics.

Polymer blending process is just one type of liquid dispersion processes.

During liquid dispersion, one fluid phase is continuously broken into smaller droplets until a critical condition is reached. Most liquid dispersion processes involve Newtonian liquids. The breakup of Newtonian liquid drop has been extensively investigated both theoretically and experimentally since Taylor's work [11, 12]. The drop breakup of Newtonian system is controlled by the flow field which the drop experiences, the viscosity ratio of the dispersed phase and the matrix phase, and capillary number which is a dimensionless number representing the ratio of the viscous force to the interfacial force [13, 14]. There are a huge number of publications on this topic. Interested readers are referred to the review articles by Rallison [15] and Stone [16].

However, polymers are viscoelastic and shear-thinning. The dispersion of molten polymers is quite different from the Newtonian drop breakup theories. Wu found that the correlation between capillary number and viscosity ratio for polymer blending in an extruder differed greatly from Grace's monumental experimental results on Newtonian drop breakup [14, 17]. Sundararaj and Macosko attributed the discrepancy between polymer drop breakup and Newtonian drop breakup to the viscoelastic nature of polymers [8]. Other researchers found the normal stress differences affected the dispersion in polymer blends [18-22]. Model viscoelastic fluids such as polymer solution and Boger fluid were also used to mimic molten polymers. The drop deformation and breakup of model fluids subjected to a controlled flow field was extensively investigated. It also showed that the viscoelasticity affected drop deformation and breakup [23-38].

The studies based on the final morphology of polymer blends and the studies based on model fluids do not reveal the truth about how polymer pellets evolve to submicron particles. The former misses information about the mechanisms of polymer drop deformation and breakup. Although the latter studies the relations among the flow field, fluid properties and drop deformation and breakup, the model fluids do not represent real molten polymers used in polymer blending. Model fluids typically have much lower viscosity and elastic properties than real polymers. Based on the results obtained from the extruder and batch mixer, Macosko's group proposed a morphology evolution path for polymer blends that the dispersed polymer is first stretched into sheets and then the sheets break up into fibers and subsequently particles [1-3]. This mechanism of morphology development has not been observed in the studies using model viscoelastic fluids. Sundararaj *et al.* visualized the deformation and breakup of a polymer pellet sheared in another polymer matrix. Polymer pellets can be sheared into thin films and the films can be broken with holes [39, 40]. A masterplot of the stress ratio versus the Deborah number was used to judge the stability of the films [20]. Levitt *et al.* found that polymer widened in the vorticity direction during shearing [19]. Lin and Sundararaj performed experiments in parallel plates and found that a polymer drop breaks up by either stretching into a thin thread or a sheet with cylindrical tip [41]. All these experiments were done under low shear rate (typically around 1 s^{-1}) in parallel-plate device. However, during polymer blending in extruders or batch mixers, typical shear rates are over 50 s^{-1}. Lin *et al.* also visualized polymer drop breakup in a Couette device by increasing the shear rate in a quasi-steady manner, and observed that the drop broke up by complex mechanisms such as erosion, parallel breakup, tip-streaming and vorticity direction breakup [42-44]. The erosion mechanism was also visualized during polymer blending in a twin-screw extruder by Chen *et al.* [45]. These complex breakup mechanisms are very different from those found in Newtonian systems and model viscoelastic fluids. It is noteworthy that the results of Lin and Sundararaj for parallel plates are not exactly the same as Lin *et al.*'s results from the Couette device for the same polymers.

In a real blending process, polymer pellets may experience different shear rate profile such as start-up and high shear rates. Most previous studies have focused on the morphology evolution at the range of low shear rate. To model the real polymer blending process, we visualized the deformation and breakup of polymer pellets using a home-made parallel-plate-type device which can provide high shear rates. The effects of viscoelasticity, shear rate and patterns of shear rate increase on polymer deformation and breakup were investigated. These types of model experiments are helpful to understand the morphology development during blending, and thus to design morphology for polymer blend products.

5.2 Experimental Section

5.2.1 Materials

Polyethylene (PE, Petromont DMDA-8907), Polystyrene (PS, Styrochem T28) and two types of polycarbonates (PC140 and PC1050, Sabic Innovative Plastics) were used in this work. PE and PC140 were used as matrix phases, and PS and PC1050 were used as drop phases. PE and PC were provided in pellet form. PS was in bead form with a diameter of 0.38 mm. These PS beads were used directly as the drop phase in the experiments. To make PC1050 particles, PC1050 threads were first made in a melt flow indexer (Folio Instruments INC., Galaxy I) and then cut into pellets with an effective diameter of 0.4mm. The interfacial tensions of PE/PS, PE/PC and PC/PS are 4.9 mN/m, 17.2 mN/m and 6.4 mN/m, respectively [46-48].

Dynamic rheological properties of the polymers were obtained with a Rheometrics RMS800 Rheometer at 220°C. The complex viscosities (η^*) and elastic moduli (G’) of the polymers are plotted *versus* frequency (ω) in Figure 5-1 and Figure 5-2.

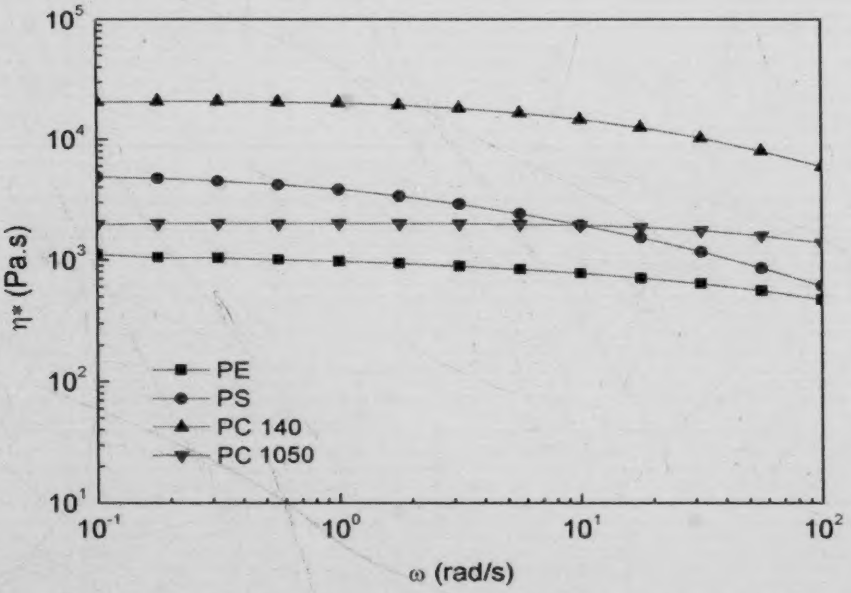

Figure 5-1 Complex viscosity (η^*) versus frequency (ω) for polymers at 220°C.

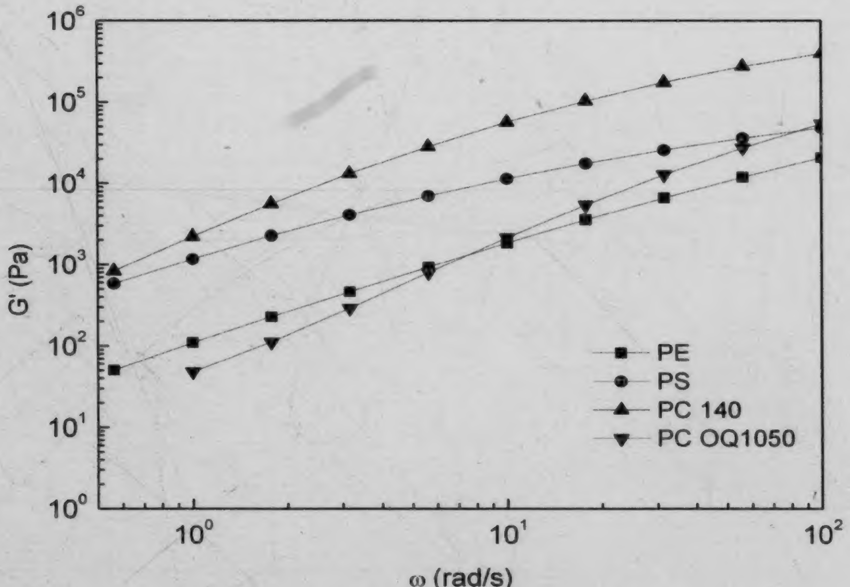

Figure 5-2 Elastic modulus (G') versus frequency (ω) for polymers at 220°C.

5.2.2 Experimental Setup

A home-made device based on the modification of the Haake Rheomix 600 internal mixer was used to generate shear flow. Figure 5-3 shows the schematics of the device. The motor drive is Haake System 90. We made two cylindrical rotors to fit in the Haake drive. The diameters of the rotors are 35 mm. The gear ratio is 2:3. We built a front plate with a quartz window to visualize the polymer pellet deformation and breakup. The gap between the front surface of the rotors and the front plate is 2.3mm. The rotation rate of the rotors and the temperatures of the back plate, middle barrel and the front plate can be set using the Rheocord90 program. When running the rotors, the front surface of the rotors and the front quartz plate act as parallel plates which generate shear flow in the gap. A Pulnix CCD camera was used to visualize the polymer pellet deformation and breakup. The drop deformation and breakup under shear was recorded.

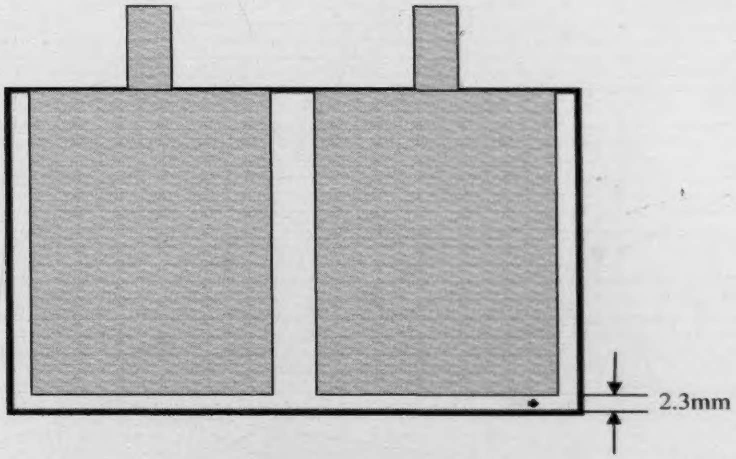

(a) Lateral view

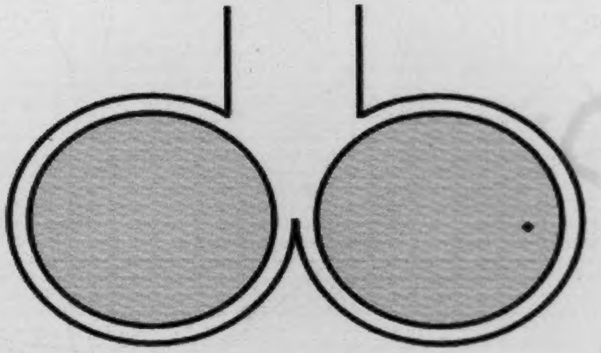

(b) Front view

Figure 5-3 Schematics of the parallel-plate device. The black dot denotes a pellet of the dispersed phase.

5.2.3 Procedure

The polymers were weighed to have enough material fully fill the free volume of the mixer in order to avoid air bubbles occurring in the gap. The mass percent of the dispersed polymer was around 1% to ensure there were not so many particles of the dispersed phase in the gap between the rotor surface and the front plate in order to avoid the interactions between the dispersed spheres. It should be noted that these mass fractions are for the material added to the whole mixer. The actual mass fraction for the polymers in the gap may be different.

Polymers were premixed by hand in a glass cup. The temperature of the whole chamber of the mixer was preheated to 220°C before adding the polymers. After the temperature of the mixer reached the set value, polymers were added to the mixer through a chute. A 5kg steel plate was used to press the polymer to fill the free volume of the mixer. The rotors were kept motionless in order to heat the polymers to the set temperature before starting the device. After the temperature of the mixer reached the set values, the motor was then started at a specified rotation rate. The behavior of the polymer pellet was recorded. The radial positions of the dispersed drops were found by comparing the spheres with marks on the surface of the rotors. The shear rate that the drop was subject to is then calculated as

$$\dot{\gamma} = \frac{\Omega X}{d} \tag{5.1}$$

where Ω is the rotation rate, X is the radial position of the drop and d is the gap width. The systems and runs are summarized in Table 5-1.

Table 5-1 Polymer systems used for parallel plate blending experiments

System (matrix/drop)	Drop size (mm)	Ω^* (rpm)	Increasing pattern of rotation rate**
PE/PS	0.38	1	Start-up
	0.38	2	Start-up $\Delta\Omega$=1 rpm/min
	0.38	5	Start-up $\Delta\Omega$=1 rpm/min
	0.38	10	Start-up $\Delta\Omega$=1 rpm/min
	0.38	20	Start-up $\Delta\Omega$=1 rpm/min
	0.38	30	Start-up $\Delta\Omega$=1 rpm/min
	0.38	50	Start-up $\Delta\Omega$=1 rpm/min
PC140/ PS	0.38	1	Start-up
	0.38	2	Start-up
PE/PC1050	0.4	2	Start-up
	0.4	5	$\Delta\Omega$=1 rpm/min
	0.4	20	Start-up

* The rotation rate is for the master rotor.

** Start-up means the rotation rate jumps from 0 to the set value directly. $\Delta\Omega$=1 rpm/min means the rotation rate is increased stepwise by 1 rpm per minute from 0.

5.3 Results

5.3.1 PE/PS system under different shear rates

PS spheres are sheared in PE matrix. The average diameter of PS sphere is 0.38mm. The rotation rate of the rotors is increased abruptly from 0 to a specified value. Figure 5-4 shows the deformation and breakup of PS spheres sheared in PE matrix at a rotation rate of 1 rpm for the master rotor. Figure 5-4 (a)-(d) are morphologies of the same sphere after being sheared for different times. The applied shear rate on this PS sphere is 0.2 s^{-1}. The sphere is stretched along the flow direction at both ends while the major part of the drop at the center remains a slightly deformed spherical shape. The whole drop is like a bulb with two long threads at its ends, shown in Figure 5-4(c). Figure 5-4(d) shows that the extended threads continue to stretch and eventually break up into small elongated droplets via fiber instability. Figure 5-4(e) shows a different PS drop develops a thread-like tail. The shear rate applied is 0.2 s^{-1}. This is similar to the first drop but the deformation is asymmetric. Figure 5-4(f) shows another PS drop under a shear rate of 0.4 s^{-1}. Unlike the previous two drops, the ends of this drop do not stretch, but tiny threads are seen to peel off the surface of the drop.

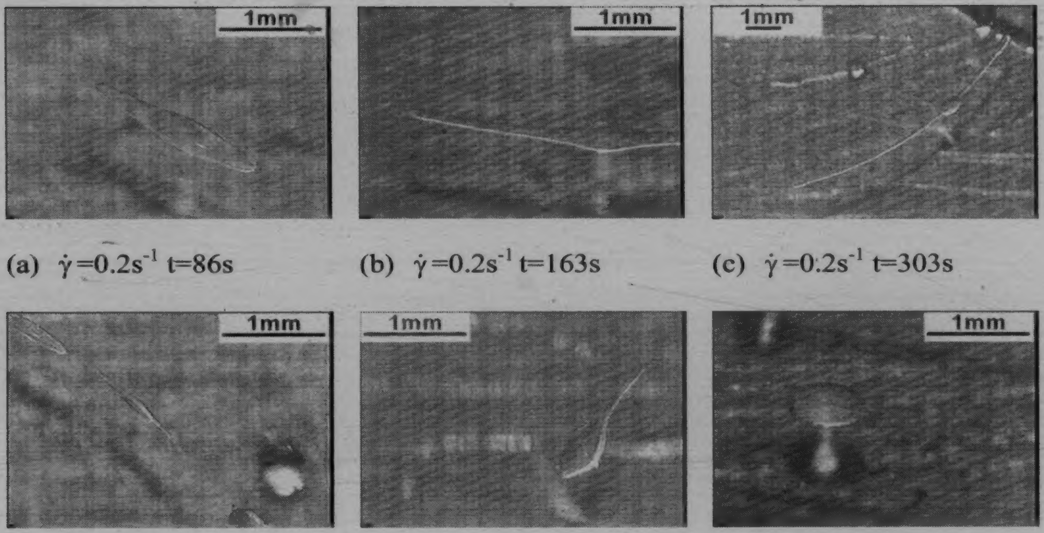

(a) $\dot{\gamma}=0.2s^{-1}$ t=86s (b) $\dot{\gamma}=0.2s^{-1}$ t=163s (c) $\dot{\gamma}=0.2s^{-1}$ t=303s

(d) $\dot{\gamma}=0.2s^{-1}$ t=497s (e) $\dot{\gamma}=0.2s^{-1}$ t=365s (f) $\dot{\gamma}=0.4s^{-1}$ t=408s

Figure 5-4 PS sphere sheared in PE matrix at a rotation rate of 1rpm of the master rotor. (a), (b), (c) and (d) show the morphology of the same PS drop after shearing for different time. (e) and (f) show the morphology of another two PS spheres. The shear rates are shown below each micrograph.

Figure 5-5 shows PE/PS system at a rotation rate of 5 rpm. Figure 5-5(a) shows two drops close to the center. The applied shear rate is 0.4 s^{-1}. The ends of the drops are elongated in the flow direction and thin threads are stretched out and break into small droplets. This type of deformation and breakup mode is also seen for another PS drop under a shear rate of 0.6 s^{-1}, as shown in Figure 5-5(b). Figure 5-5(c) shows a drop that develops many tiny threads from the surface, which is the same deformation mode seen in Figure 5-4(f). A new deformation mode is also found in this system. As shown in Figure 5-5(d), a PS drop elongated along the vorticity direction, i.e. the radial direction. This drop developed a waist in the middle and may be later broken by the shear flow. There are also many small droplets and strings peeling off from the vorticity elongated drop. This mechanism was named "erosion" by Lin *et al.* [43]. The vorticity direction elongation depends greatly on the shear rates. Figure 5-5(e) shows a picture containing several drops at different locations. Drops deform slightly at locations close to the center where the shear rate is low; however, drops elongate in the vorticity direction at locations far from the center where the shear rate is high.

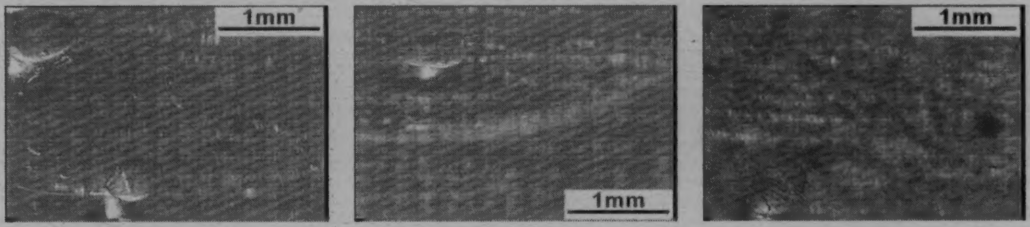

(a) $\dot{\gamma}=0.4s^{-1}$ t=1351s (b) $\dot{\gamma}=0.6s^{-1}$ t=925s (c) $\dot{\gamma}=1.7s^{-1}$ t=334s

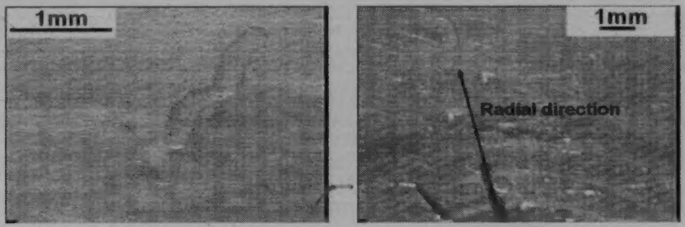

(d) $\dot{\gamma}=1.7s^{-1}$ t=1114s (e) t=1221s

Figure 5-5 PE/PS sheared at a rotation rate of 5rpm of the master rotor. (a) and (b): threads developed at the drop ends. (c): threads developed at the drop surface. (d): drop elongates in the vorticity direction. (e): drops elongates in the high shear rate zones. The shear rates are shown below each micrograph.

PE/PS systems under rotation rates from 10rpm to 50rpm are summarized in

Figure 5-6. The same drop deformation and breakup modes as shown in Figure 5-4 and Figure 5-5 are found for these runs. Thin threads are found to develop at the ends or at the surface of the drop. Erosion and vorticity elongation modes are also seen in these systems. At 50rpm, the PS drop elongates in the vorticity direction with two tips. This drop does not develop a waist in the middle as shown in Figure 5-5(d). The tips can break away continuously from the mother drop. The same vorticity elongation modes were discussed in Chapter 3 and 4 for Newtonian matrix/Boger drop systems. Drops break up faster under high shear rate than they do under low shear rate. This can be easily seen from the pictures at different rotation rate.

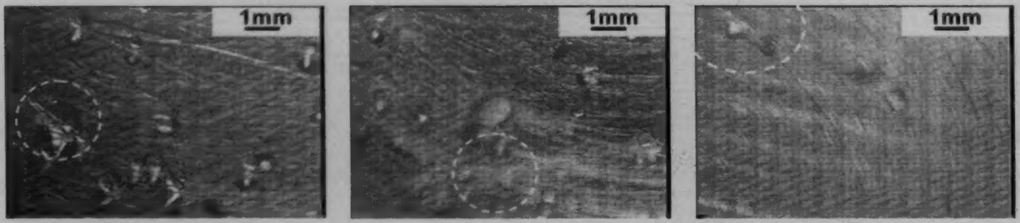

(10 rpm) $\dot{\gamma}=3.1s^{-1}$ t=34s **(10 rpm)** $\dot{\gamma}=3.5s^{-1}$ t=156s **(20rpm)** $\dot{\gamma}=5.8s^{-1}$ t=23s

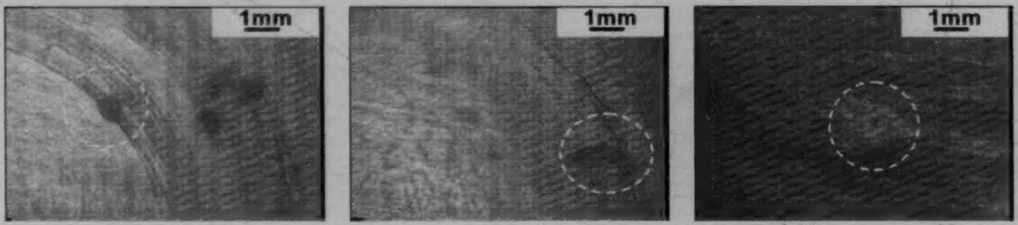

(20rpm) $\dot{\gamma}=3.5s^{-1}$ t=264s **(20rpm)** $\dot{\gamma}=5.9s^{-1}$ t=650s **(30rpm)** $\dot{\gamma}=12.3s^{-1}$ t=198s

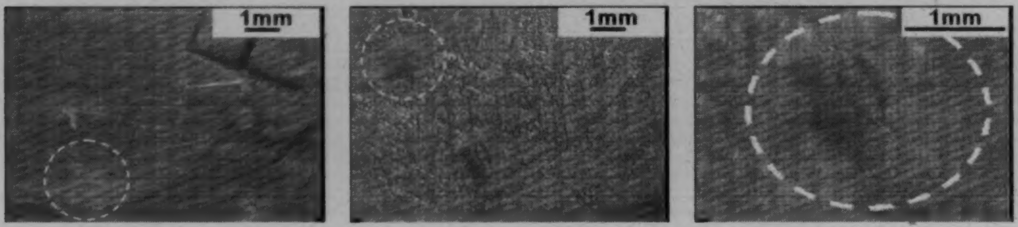

(30rpm) $\dot{\gamma}=4.2s^{-1}$ t=285s **(50rpm)** $\dot{\gamma}=9s^{-1}$ t=74s **(50rpm)** $\dot{\gamma}=15s^{-1}$ t=74s

Figure 5-6 PE/PS sheared at a rotation rate of 10 to 50 rpm of the master rotor. The shear rates shown in the figure are the shear rate for the drops in white circles.

The effect of different protocols for shear rate on drop deformation and breakup mechanism is also investigated. Besides the start-up mode, the rotation rate is also increased stepwise by 1rpm/min. Figure 5-7 shows the drop morphology development under 2, 5 and 20rpm. In general, the same modes of drop deformation and breakup are found as in the start-up runs. This means that the mechanisms identified here are not caused by the abrupt change in shear rate.

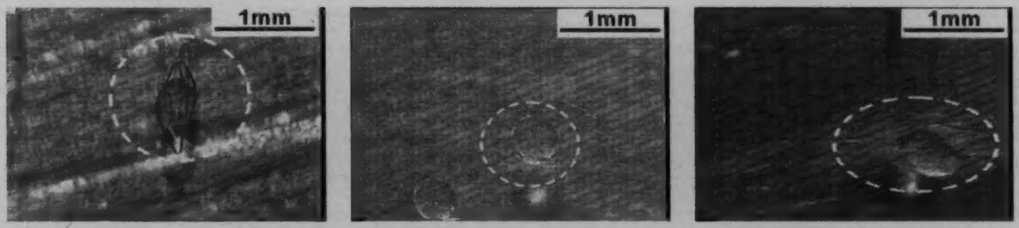

(2 rpm) $\dot{\gamma}=0.4s^{-1}$ t=1089s **(2 rpm)** $\dot{\gamma}=0.7s^{-1}$ t=325s **(5 rpm)** $\dot{\gamma}=1.4s^{-1}$ t=751s

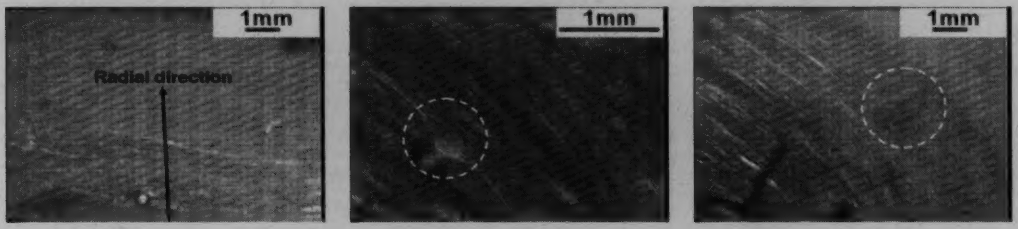

(5 rpm) t=1752s **(20rpm)** $\dot{\gamma}=2.3s^{-1}$ t=603s **(20rpm)** $\dot{\gamma}=6.5s^{-1}$ t=1129s

Figure 5-7 PS drops are sheared in PE matrix while the rotation rate is increased stepwise by 1 rpm/min. The shear rates shown in the figure are the shear rate for the drops in white circles.

5.3.2 PC140/PS and PE/PC1050 systems

In order to investigate the effect of viscoelasitic properties on drop deformation and breakup, the matrix phase or the drop phase is changed for the breakup experiments. Figure 5-8 shows PS drops sheared in PC140 matrix. Unlike the PE/PS system, the PS drops deform into films when sheared in PC140 matrix even when the shear rate is very low. Figure 5-8 shows the morphologies of PS drops in PC140 matrix. As shown by the arrows in Figure 5-8(a), holes formed in the film. The films can break up via these holes. Figure 5-8(b) shows a PS film more clearly. Holes can also be seen for this film. Figure 5-8(c) shows a film tearing and breaking into pieces. The fracture process is very erratic. It looks like that there is little cohesion among the polymer chains and films are very loose in structure. This is somewhat similar to the "parallel breakup mechanism" described by Lin and Sundararaj [42]. In the "parallel breakup mechanism", the polymer drop is also sheared into film before breakup.

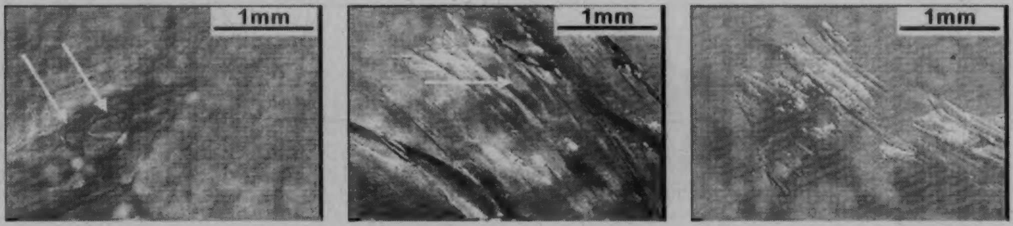

(a) $\dot{\gamma}=0.2s^{-1}$ t=37s (b) $\dot{\gamma}=0.34s^{-1}$ t=170s (c) $\dot{\gamma}=0.29s^{-1}$ t=821s

Figure 5-8 PS drops are deformed into films in PC140 matrix at 1 rpm. (a) film with holes deformed from a PS drop with a diameter of 0.38mm. (b) and (c) films are from the breakup of a bigger PS cylindrical pellet (diameter=1.9mm and length=2.5mm).

Figure 5-9 shows PC1050 drops sheared in PE matrix. At rotation rate of 2 rpm (Figure 5-9(a) and (b)), PC1050 drops are elongated in the flow direction and are stretched into thin fibers. Most of the fibers are stable while some of the fibers break up into small particles. The diameter of the fibers in Figure 5-9(b) is around

30 to 50μm. When the rotation rate is 20 rpm increased by start-up mode (Figure 5-9(c) and (d)), drops may first have a film-like morphology as shown in Figure 5-9(c). Then these film-like particles are further stretched and the edges of these ribbons pull in to create thin fibers. At high shear rate zones, the fibers break up into smaller particles, as shown in Figure 5-9(d). Figure 5-9(e) shows fibers are formed when the shear rate is increased stepwise. After shearing is stopped, these fibers break up into small particles with diameter of 50 to 100μm as shown in Figure 5-9(f). This indicates that relaxation is more effective in breaking fibers. The development of fibers by shearing one type of polymer drops in another polymer matrix provides a potential method to produce polymer microfibers, and even nanofibers. Wang *et al.* fabricated polymer nanofibers using this approach [49].

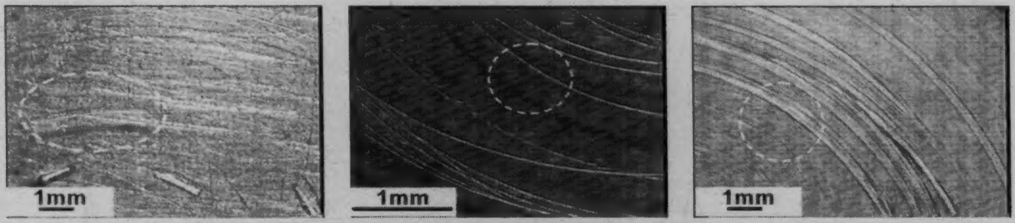

(a) $\dot{\gamma}=0.4s^{-1}$ t=402s (b) $\dot{\gamma}=0.3s^{-1}$ t=3358s (c) $\dot{\gamma}=5.5\ s^{-1}$ t=7s

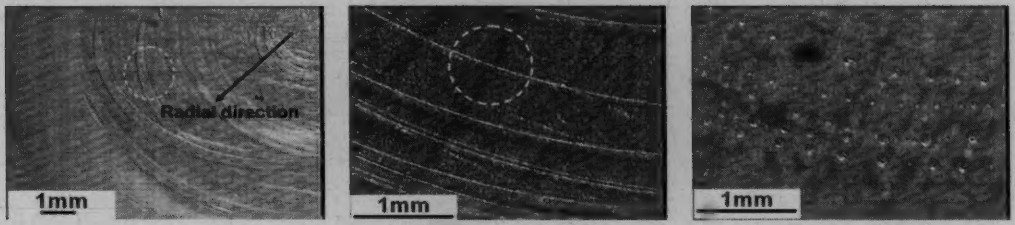

(d) $\dot{\gamma}=3.6s^{-1}$ t=327s (e) $\dot{\gamma}=1.0s^{-1}$ t=300s (f) after stopped for 138s

Figure 5-9 PC1050 drops are sheared in PE matrix at different shear rates. (a) and (b): the rotation rate is 2 rpm by start-up mode. (c) and (d): the rotation rate is 20 rpm by start-up mode. (e): the rotation rate is increased to 5 rpm stepwise by 1 rpm/min. (f): after (e) stopped for 138s, the fibers break up into spheres. The shear rates shown in the figure are the shear rate for the drops in white circles.

5.4 Discussion

5.4.1 Surface instability

The instability of PS drop sheared in PE matrix can occur at very low shear rate. The drop may have highly stretched ends with the main drop remains as a bulb, or have tiny threads or particles peeling off the surface. A close investigation of these modes of morphology change indicates that all these modes may be caused by the instability of the surface, which means that part of the surface is removed from the main drop. This surface instability can be seen from the pictures in the *Results* section. Figure 5-10 gives schematics of different types of surface instability found in the experiments. For PE/PS systems in this work, the drop behaves like a soft shell encapsulating a hard core. The shell is stretched or removed under shear from the core. At high shear rate, drops may also elongate in the vorticity direction while eroding.

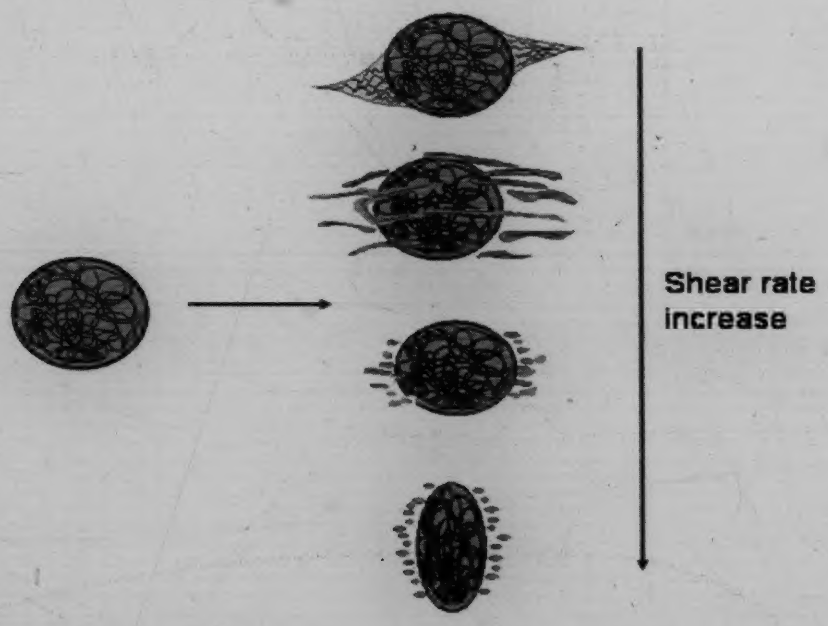

Figure 5-10 Surface instability of polymer drop during shearing.

Yue *et al.* simulated the deformation of an Oldroyd-B drop sheared in Newtonian matrix [23]. The results show that the shear rates within the drop phase is not uniform. Inside the drop, the shear rate is higher in areas close to the drop/matrix interface, and it is lower in the part close to the drop center. If this is also true for polymer drop/polymer matrix system, the viscosity of the drop is lower at the interface and higher close to the center since polymers are usually shear-thinning. In this work, PS is highly shear-thinning as demonstrated from rheological test. The non-uniform distribution of viscosity means the polymer drop possesses a soft shell/hard core structure. Previous work in our group by Chen *et al.* [45] confirmed this soft shell/hard core model by simulating a polycarbonate drop sheared in polyethylene matrix. Their result shows that the shear stress is much higher at the interface than that at the center of the drop, which is consistent with our analysis. The PE/PC1050 systems have similar viscosity ratio to the PE/PS systems. However, PC1050 has a relatively constant viscosity in the processing range. It is not easy to have surface instability in the PE/PC1050 systems.

The surface instability mechanism of the soft shell/hard core structure is twofold: 1) for PE/PS system, the lower viscosity ratio of the shell/matrix means the shell is easier to deform; 2) the high stress at the interface tends to deform the surface and peel off the surface. In this mechanism, the drop itself is not easy to deform given high viscosity ratio, however the surface can be peeled off the main drop. After part of the surface is removed from the main drop, a new surface forms. The new drop is subject to the same condition and its surface continues to be peeled off. From this analysis, the original drop size is supposed to have little influence on the minimum shear rate required to have the surface instability. This is supported by previous work in our research group [43].

5.4.2 Film, fiber and vorticity elongation

In different systems, drops deform via different mechanisms as shown in the *Results* section. In the PE/PS system, drops elongate in vorticity direction; in the PC140/PS system, drops deform into films; and in the PE/PC1050 system, drops deform into fibers. The morphology of drops depends greatly on the viscoelastic nature of the polymers. The morphology of drops usually evolves from sphere to ellipsoid or cylinder with increasing shear rate. When the shear rate is increased further, the drops may have different morphology depending on the viscoelastic properties of the matrix and drop fluids. Table 5-2 shows the morphology of different systems after the ellipsoid/cylinder stage. The shear rate inside the drop is calculated by assuming the tangential stress is equal at both sides of the matrix/drop interface. Then we calculate the viscosity ratio (η_r). The elasticity ratio (λ_r) is defined as the ratio of the relaxation time (λ) of the drop phase to the matrix phase. The relaxation time was obtained from the complex viscosity versus frequency data. The intersection of the line representing the zero shear viscosity limit at low frequency and the line representing the power law viscosity at high frequency was determined to be the critical frequency (ω_c) and $\lambda=1/\omega_c$. The relaxation times of PE, PS, PC140 and PC1050 are 0.15s, 0.69s, 0.17s and 0.05s, respectively. To calculate the capillary number (Ca), we use 0.38mm for the diameter of PS spheres and 0.4mm for the diameter of PC1050 spheres. Capillary number is defined as

$$Ca = \frac{\eta_m \dot{\gamma} R}{\Gamma} \tag{5.2}$$

where η_m is the viscosity of the matrix phase, $\dot{\gamma}$ is the shear rate, R is the radius of the drop and Γ is the interfacial tension between the drop and matrix phase.

Table 5-2 Polymer systems and morphology

System (matrix/drop)	shear rate (s^{-1})	η_r	λ_r	Ca	Morphology*
PE/PS	1.7	4.8	4.6	62	vor+ero
	3.5	4.0	4.6	118	vor+ero
	5.9	3.4	4.6	190	vor+ero
	12.3	2.8	4.6	362	vor+ero
	15	2.8	4.6	424	vor+ero
PC140/ PS	0.2	0.15	4.1	124	film
	0.85	0.08	4.1	512	film
	0.54	0.10	4.1	330	film
PE/ PC1050	0.25	1.9	0.33	3.0	fiber
	0.36	2.0	0.33	4.3	fiber
	0.67	2.0	0.33	7.8	fiber
	3.6	2.3	0.33	36	fiber
	4.6	2.3	0.33	46	fiber
	1.3	2.1	0.33	14	fiber

* vor+ero = vorticity elongation and erosion.

Figure 5-11 shows that drops tend to deform into films when the viscosity ratio is low and elasticity ratio is high. When the viscosity ratio is around 2 and elasticity ratio is low, drops are easily deformed into fibers. When the viscosity ratio is high (especially higher than 4) and the elasticity ratio is high, drops can elongate in vorticity direction.

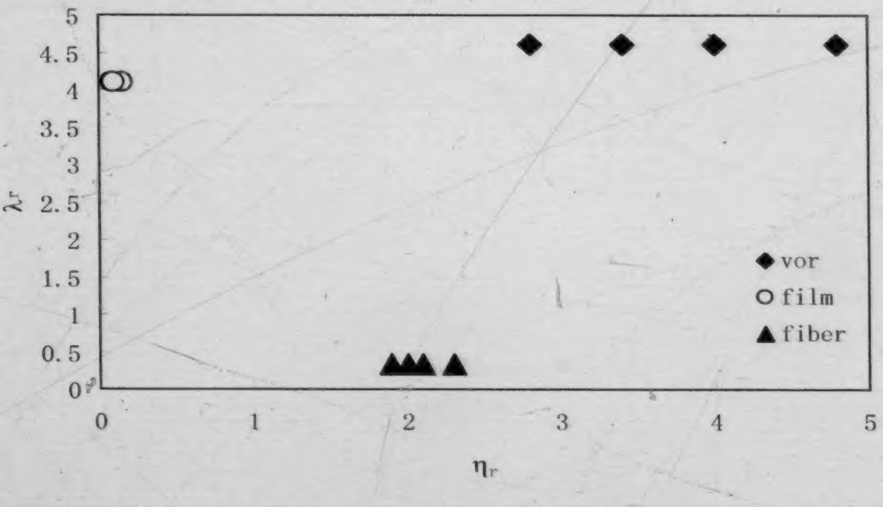

Figure 5-11 The effect of viscoelastic properties on morphology.

Viscosity ratio serves as an indicator of the deformability of the drops [31] and the elasticity ratio indicates the extent that the drop is elongated in the vorticity direction. Typically for systems showing film morphology, the viscosity ratio is low and the drop is easy to stretch in the flow direction. As the volume of the drop is conserved, the stretch in the flow direction will cause a decrease in dimension in the other two dimensions. However, since the elasticity is strong in the case of film morphology, the length in the vorticity direction would not reduce as much as that in the velocity gradient direction. As a result, a film morphology is generated. For the systems exhibiting fiber morphology, the drop is easy to deform in the flow direction. Since the elasticity is not strong in this case, the length in the vorticity direction reduces similarly to that in the velocity gradient direction. Therefore a fiber morphology is obtained. For systems showing vorticity elongation morphology, the drop is not easy to stretch in the flow direction since the viscosity ratio is high. With increasing shear rate, the elasticity becomes important and results in vorticity elongation.

5.4.3 Morphology development during blending

The morphology development during blending is complicated. Based on our experiments with PE/PS, PC140/PS and PE/PC1050 systems, we proposed a morphology development mechanism for polymer blending as shown in Figure 5-12. In all cases, our discussion is limited to drop breakup, and drop coalescence is not considered. When both the viscosity ratio and elasticity ratio are high, the dispersed polymer is not easy to deform in the flow direction. The dispersed polymer breaks up mainly by vorticity elongation and/or surface instability depending on the shear-thinning viscosity. When the viscosity ratio is low and the elasticity ratio is high, the dispersed polymer easily deforms into films, since low viscosity ratio tends to stretch the polymer drop in the flow direction and high elasticity ratio tends to extend the polymer drop in the vorticity direction. These films may break up into smaller pieces of films. When the viscosity ratio is at a medium level and elasticity ratio is low, the dispersed polymer easily stretches in the flow direction only and thin fibers are obtained. These fibers break up into smaller fibers and particles. Via these mechanisms, the dispersed polymer evolves from millimeter scale to micrometer/submicrometer scale. This discussion gives a qualitative picture of the overall morphology development during polymer blending. However, more experiments need be done by varying viscoelastic properties of polymer systems to complete this understanding.

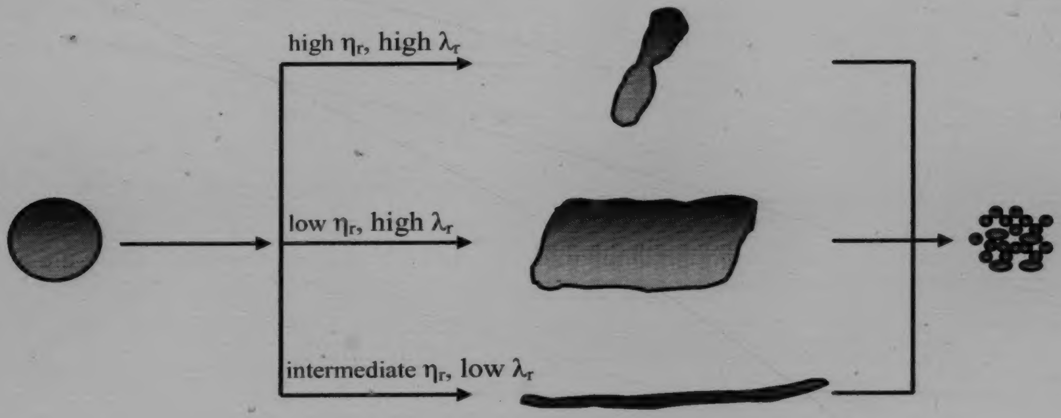
high η_r, high λ_r
low η_r, high λ_r
intermediate η_r, low λ_r

Figure 5-12 Morphology development mechanism during blending.

5.5 Conclusion

Morphology development during polymer blending depends greatly on the viscoelastic properties of both the matrix and dispersed phases. The dispersed polymer breaks up via different modes depending on different viscosity ratio and elasticity ratio. When both the viscosity ratio and elasticity ratio are high, and the dispersed polymer is shear-thinning, the dispersed polymer breaks up mainly by surface instability. Material on the surface of the dispersed polymer can be removed from the main drop as films, strings or particles. Under high shear rate, the drop elongates in the vorticity direction and can be broken by the shear flow. The surface instability is determined by the shear-thinning property of the dispersed phase. A soft shell/hard core model is proposed to explain this phenomenon. For systems with low viscosity ratio and high elasticity ratio, the dispersed phase forms films under shear. These films break up erratically into smaller films. For systems with medium viscosity ratio and low elasticity ratio, the dispersed polymer is deformed into fibers and the fibers can break up via fiber instability.

In our observations, increasing shear rate does not change the drop breakup modes qualitatively. However, high shear rate results in faster change in the morphology. A mechanism is proposed to describe morphology development of real polymer blends based on visualizations under high processing temperatures.

5.6 References

[1] C. E. Scott and C. W. Macosko, "Model experiments concerning morphology development during the initial stages of polymer blending," Polymer Bulletin **26**, 341 (1991).

[2] C. E. Scott and C. W. Macosko, "Morphology development during the initial stages of polymer-polymer blending," Polymer **36**, 461 (1995).

[3] U. Sundararaj, C. W. Macosko, R. J. Rolando and H. T. Chan, "Morphology development in polymer blends," Polym. Eng. Sci. **32**, 1814 (1992).

[4] J. T. Lindt and A. K. Ghosh, "Fluid mechanics of the formation of polymer blends. Part i: Formation of lamellar structures," Polym. Eng. Sci. **32**, 1802 (1992).

[5] D. Bourry and B. D. Favis, "Morphology development in a polyethylene/polystyrene binary blend during twin-screw extrusion," Polymer **39**, 1851 (1998).

[6] R. C. Willemse, E. J. J. Ramaker, J. Van Dam and A. Posthuma De Boer, "Morphology development in immiscible polymer blends: Initial blend morphology and phase dimensions," Polymer **40**, 6651 (1999).

[7] H. Li and G.-H. Hu, "The early stage of the morphology development of immiscible polymer blends during melt blending: Compatibilized vs. Uncompatibilized blends," J. Polym. Sci., Part B: Polym. Phys. **39**, 601 (2001).

[8] U. Sundararaj and C. W. Macosko, "Drop breakup and coalescence in polymer blends - the effects of concentration and compatibilization," Macromolecules **28**, 2647 (1995).

[9] L. A. Utracki and H. Shi, "Development of polymer blend morphology during compounding in a twin-screw extruder. Part i: Droplet dispersion

and coalescence-a review," Polym. Eng. Sci. **32**, 1824 (1992).

[10] B. Majumdar, D. R. Paul and A. J. Oshinski, "Evolution of morphology in compatibilized vs uncompatibilized polyamide blends," Polymer **38**, 1787 (1997).

[11] G. I. Taylor, "The viscosity of a fluid containing small drops of another fluid," Proc. R. Soc. London Ser. A **138**, 41 (1932).

[12] G. I. Taylor, "The formation of emulsions in definable fields of flow," Proc. R. Soc. London Ser. A **146**, 501 (1934).

[13] B. J. Bentley and L. G. Leal, "An experimental investigation of drop deformation and breakup in steady, two-dimensional linear flows," J. Fluid Mech. **167**, 241 (1986).

[14] H. P. Grace, "Dispersion phenomena in high-viscosity immiscible fluid systems and application of static mixers as dispersion devices in such systems," Chem. Eng. Commun. **14**, 225 (1982).

[15] J. M. Rallison, "The deformation of small viscous drops and bubbles in shear flows," Annu. Rev. Fluid Mech. **16**, 45 (1984).

[16] H. A. Stone, "Dynamics of drop deformation and breakup in viscous fluids," Annu. Rev. Fluid Mech. **26**, 65 (1994).

[17] S. H. Wu, "Formation of dispersed phase in incompatible polymer interfacial and rheological effects," Polym. Eng. Sci. **27**, 335 (1987).

[18] W. Lerdwijitjarud, A. Sirivat and R. G. Larson, "Influence of elasticity on dispersed-phase droplet size in immiscible polymer blends in simple shearing flow," Polym. Eng. Sci. **42**, 798 (2002).

[19] L. Levitt, C. W. Macosko and S. D. Pearson, "Influence of normal stress difference on polymer drop deformation," Polym. Eng. Sci. **36**, 1647 (1996).

[20] U. Sundararaj, Y. Dori and C. W. Macosko, "Sheet formation in immiscible polymer blends: Model experiments on initial blend morphology," Polymer **36**, 1957 (1995).

[21] H. Vanoene, "Modes of dispersion of viscoelastic fluids in flow," J. Colloid Interface Sci. **40**, 448 (1972).

[22] E. K. Hobbie and K. B. Migler, "Vorticity elongation in polymeric emulsions," Phys. Rev. Lett. **82**, 5393 (1999).

[23] P. T. Yue, J. J. Feng, C. Liu and J. Shen, "Viscoelastic effects on drop deformation in steady shear," J. Fluid Mech. **540**, 427 (2005).

[24] R. W. Flumerfelt, "Drop breakup in simple shear fields of viscoelastic fluids," Ind. Eng. Chem. Fund. **11**, 312 (1972).

[25] H. Li and U. Sundararaj, "Does drop size affect the mechanism of viscoelastic drop breakup? ," Phys. Fluids **20**, 053101-1 (2008).

[26] F. Mighri, A. Ajji and P. J. Carreau, "Influence of elastic properties on drop deformation in elongational flow," J. Rheol. **41**, 1183 (1997).

[27] F. Mighri, P. J. Carreau and A. Ajji, "Influence of elastic properties on drop deformation and breakup in shear flow," J. Rheol. **42**, 1477 (1998).

[28] F. Mighri and M. A. Huneault, "Dispersion visualization of model fluids in a transparent couette flow cell," J. Rheol. **45**, 783 (2001).

[29] P. P. Varanasi, M. E. Ryan and P. Stroeve, "Experimental-study on the breakup of model viscoelastic drops in uniform shear-flow," Ind. Eng. Chem. Res. **33**, 1858 (1994).

[30] S. Guido, M. Simeone and F. Greco, "Deformation of a newtonian drop in a viscoelastic matrix under steady shear flow - experimental validation of slow flow theory," J. Non-Newtonian Fluid Mech. **114**, 65 (2003).

[31] H. Li and U. Sundararaj, "Experimental investigation of viscoelastic drop deformation in newtonian matrix at high capillary number under simple shear flow," J. Non-Newtonian Fluid Mech. (submitted).

[32] J. J. Elmendorp and R. J. Maalcke, "A study on polymer blending microrheology," Polym. Eng. Sci. **25**, 1041 (1985).

[33] K. Verhulst and P. Moldenaers, "Drop shape dynamics of a newtonian drop in a non-newtonian matrix during transient and steady shear flow," J. Rheol. **51**, 261 (2007).

[34] S. Ramaswamy and L. G. Leal, "The deformation of a viscoelastic drop subjected to steady uniaxial extensional flow of a newtonian fluid," J. Non-Newtonian Fluid Mech. **85**, 127 (1999).

[35] S. Ramaswamy and L. G. Leal, "The deformation of a newtonian drop in the uniaxial extensional flow of a viscoelastic liquid," J. Non-Newtonian Fluid Mech. **88**, 149 (1999).

[36] N. Aggarwal and K. Sarkar, "Deformation and breakup of a viscoelastic drop in a newtonian matrix under steady shear," J. Fluid Mech. **584**, 1 (2007).

[37] J. Beaucourt, T. Biben and C. Verdier, "Elongation and burst of axisymmetric viscoelastic droplets: A numerical study," Phys. Rev. E **71**, 066309-1 (2005).

[38] T. Chinyoka, Y. Y. Renardy, A. Renardy and D. B. Khismatullin, "Two-dimensional study of drop deformation under simple shear for oldroyd-b liquids," J. Non-Newtonian Fluid Mech. **130**, 45 (2005).

[39] U. Sundararaj, Y. Dori and C. W. Macosko. Visualization of morphology development in polymer blends. in Antec. 1994. San Francisco, CA, USA.

[40] U. Sundararaj, PhD Thesis, "Morphology development during polymer blending", University of Minnesota, Minneapolis (1994).

[41] B. Lin and U. Sundararaj, "Sheet formation during drop deformation and breakup in polyethylene/polycarbonate systems sheared between parallel plates," Polymer **45**, 7605 (2004).

[42] B. Lin, F. Mighri, M. A. Huneault and U. Sundararaj, "Parallel breakup of polymer drops under simple shear," Macromol. Rapid Commun. **24**, 783 (2003).

[43] B. Lin, U. Sundararaj, F. Mighri and M. A. Huneault, "Erosion and breakup of polymer drops under simple shear in high viscosity ratio systems," Polym. Eng. Sci. **43**, 891 (2003).

[44] B. Lin, PhD Thesis, "Visualization of polymer blending and drop breakup", University of Alberta, Edmonton (2005).

[45] H. Chen, U. Sundararaj, K. Nandakumar and M. D. Wetzel, "Erosion of polymer pellets during blending in a twin-screw extruder," AIChE J. **52**, 1267 (2006).

[46] P. H. M. Elemans, J. M. H. Janssen and H. E. H. Meijer, " The measurement of interfacial-tension in polymer-polymer systems - the breaking thread method," J. Rheol. **34**, 1311 (1990).

[47] N. Chapleau, B. D. Favis and P. J. Carreau, "Measuring the interfacial tension of polyamide/polyethylene and polycarbonate/polypropylene blends: Effect of temperature," Polymer **41**, 6695 (2000).

[48] K. Okamoto, M. Takahashi and H. Yamane, "Shape recovery of a dispersed droplet phase and stressrelaxation after application of step shear strains in a polystyrene/polycarbonate blend melt," J. Rheol. **43**, 951 (1999).

[49] D. Wang, G. Sun, B.-S. Chou and J. P. Hinestroza, "Controllable fabrication and properties of polypropylene nanofibers," Polym. Eng. Sci. **47**, 1865 (2007).

Chapter 6

Conclusions and Future Work

6.1 General Discussion and Conclusions

Microstructures of polymer blends are generated by the processing flow in polymer blending mixers. This thesis deals with the mechanisms of microstructure development in polymer blends. The mechanisms are investigated by studying

1) the morphology development of polymer blends (*real polymer melts*) in extruder and internal batch mixer (*real industial processing flows*);

2) drop deformation and breakup of Boger fluid (*model viscoelastic fluid*) under simple shear flow (*model processing flow*); and

3) polymer blend (*real polymer melts*) under shear flow (*model processing flow*).

In all cases, the major effort was placed on the drop breakup process in this work, though it should be noted drop coalescence also has important effect on the microstructure of polymer blends[1].

6.1.1 Polymer melts in industrial mixers

The processing flow in industrial mixers, typically extruders and internal batch mixers, is complex. Polymers exhibit complex rheological properties. Thus it is difficult to investigate the mechanism of polymer blend morphology evolution in industrial mixers. A realistic method is to sample at different location along an extruder or at different mixing times from a batch mixer, and then image these samples microscopically. The micrographs obtained at different locations or different mixing times represent the polymer blend morphology at a certain stage. Polymer morphology development in mixers is then envisaged by connecting these micrographs. The model polymer blend systems, amorphous Nylon/Polystyrene and amorphous Nylon/Polystyrene-maleic anhydride, give us representative dispersion processes of polymer blending for non-reactive and reactive systems, respectively. The dispersed phase evolves from pellet to film, then to fibers and eventually to spherical particles. Both stretching and relaxation flows can facilitate the breakup of the dispersed phase. These observations are later confirmed by visualizing polymer blends under shear flow. It should be noted that in this process, we were limited to visualizing the breakup phenomenon, and other blending phenomena such as the development of co-continuous morphology and phase inversion during blending are not included in this thesis. This typical breakup process during polymer blending triggered the latter research of viscoelastic fluids and polymer melts under shear flow in order to understand the underlying fundamental blending mechanisms.

Compatibilization is commonly used in industry to enhance dispersion of polymer blends. Compatibilizer may be considered as surfactant. In Newtonian systems, an important effect of surfactant is the reduction of interfacial tension which facilitates drop breakup. However, the major effect of compatibilizer during polymer blending is different. A widely accepted opinion is that compatibilization improves dispersion of polymer blends by resisting coalescence between the dispersed particles [1, 2]. This is also confirmed in this thesis. This conclusion is obtained by comparing the final micrometer sized particles with and without compatibilizers. However, the effect of compatibilization during the initial stages of polymer blending is rarely discussed. In this thesis, it is found by inspecting the whole morphology evolution process that the morphology of compatibilized blends develops faster than uncompatibilized blends. In order to investigate the mechanism of how compatibilization affects morphology development in the initial stage of blending, compatibilized and uncompatibilized polymer blend systems with similar rheological properties are selected and blended in an internal batch mixer. Based on force analysis, it is found that major mechanism of compatibilization in improving dispersion of polymer blends is to reduce slip at the interface between the polymer phases. The chains of compatibilizer, i.e. block copolymer formed at the interface, penetrate into both the matrix and dispersed phases and entangle with the bulk polymer chains. In fact, when the copolymers form, the respective copolymer chain segments will already be entangled with their respective homopolymer chains. The effective shear stress transferred from the matrix to the dispersed phase is thus enhanced.

In a real blending process, there are many factors affecting the morphology development of polymer blends. The residence time in extruder is one of them. In this thesis, the residence time is changed by changing the rotation rate of the extruder. A higher rotation rate reduces the residence time and the dispersed phase polymer in the uncompatibilized systems did not have enough time to completely break up into particles. Therefore, a higher rotation rate with inadequate residence time can result in worse dispersion even though the shear rate is higher. Compatibilized systems require less time to reach a steady state morphology than their uncompatibilized counterparts. Therefore, the final particle sizes of the compatibilized systems in this thesis are not found to be affected by the rotation rate.

The morphology development of polymer blends in industrial mixers is determined by many influencing factors, and a dynamic picture of the whole process is not yet available. Information on how the morphology jumps from one stage to another stage is missing. Moreover, morphology might change during sampling and freezing samples even if the sampling time is minimized. Other alternative approaches should be used to overcome these obstacles. Visualization of model viscoelastic fluids and polymer melts in a well-defined flow is thus proposed to obtain a more precise picture of the polymer dispersion process.

6.1.2 Model viscoelastic fluids under simple shear flow

The dispersion of polymer blends in mixers is essentially deformation and breakup of viscoelastic drops in a certain flow field. In this thesis, the drop deformation and breakup of model viscoelastic fluid (Boger fluid) under shear flow is investigated to understand the effect of viscoelasiticity on the morphology development of polymer blends.

The drop deformation and breakup of viscoelastic systems is different from

Newtonian systems. Two general types of deformation and breakup modes are found for Boger fluid drops sheared in Newtonian matrices: drop elongation and breakup in the flow direction; and drop elongation and breakup in the vorticity direction. Additional breakup modes may be found within the two general categories. Viscoelasticity plays an important role in the drop deformation and breakup. With weak viscoelasticity, drops elongate and may break up in the flow direction. For strong viscoelasticity, drops elongate and break up in the vorticity direction. The breakup in the flow direction is caused by the deforming force (shear stress) greatly exceeding the restoring force (elastic tensile stress and interfacial tension). The breakup in the vorticity direction is mainly caused by the disturbance in the flow. Unlike Newtonian systems, viscoelastic drops can break up even when the viscosity ratio is higher than 4.

It is found that the first normal stress difference N_1 acts as a restoring stress in the viscoelastic drop deformation and breakup. The magnitude of N_1 determines the drop deformation and breakup mode. For drop elongation in the flow direction, the elastic stress N_1 is weak and shear stress dominates the deformation. For drop elongation in the vorticity direction, N_1 becomes stronger than the shear stress and plays a dominant role in the deformation.

Drop size is found to affect the drop breakup condition. For a given viscoelastic drop/Newtonian matrix system, the two different breakup modes can occur depending on the drop size. A big drop can break up in the flow direction while a small drop may break up in the vorticity direction. This special phenomenon is directly associated with the degree of viscoelasticity. For a big drop at a relatively low shear rate, the elastic stress is not strong. When the shear stress exceeds the restoring stresses (the combination of elastic tensile and interfacial stress) to a certain extent, the drop breaks up in the flow direction. For a small drop, a low shear rate and low shear stress cannot break the drop. As shear rate increases, a strong N_1 squeezes the drop along the vorticity direction. Thus drop breakup occurs in the vorticity direction. A dramatic change in the critical shear rate was found when going from one breakup mode to another. There exists a critical drop size for a given system which separates these two breakup modes. The critical drop size determining the drop breakup mechanism is found to be related to interfacial tension, the elastic property (the coefficient of the first normal stress different), and the viscosities of the matrix and drop phase. It is interesting to note that De Bruijn indicated that there is a minimum drop size for viscoelastic drop to breakup in shear flow [3]. Since his observation is confined to flow direction breakup because of the relatively low shear rate used, this minimum drop size could be the same as the critical drop size in this thesis, if he had increased the shear rate to achieve vorticity direction breakup.

The investigation of viscoelastic drop deformation and breakup under shear flow is to simulate the industrial polymer blending process. It has uncovered different dispersion modes and the decisive role of viscoelasticity. Furthermore, the effect of drop size on drop breakup mode implies that during polymer blending process, pellets may first elongate and break up in the flow direction to reduce the size, and then the small sized particles can elongate and break up in the vorticity direction.

6.1.3 Polymer blends under shear flow

In this thesis, the processing of polymer melts under shear flow over a large range of shear rate is investigated to simulate the morphology development in industrial mixers. Morphology of polymer blends depends greatly on both the viscosity ratio and elastic ratio of the dispersed phase to the matrix phase. The dispersed polymer breaks up via different modes depending on different viscoelastic ratio. When both the viscosity ratio and elasticity ratio are high, the dispersed polymer breaks up mainly by vorticity elongation and/or surface instability. Surface instability is unique to polymer melts. It has not been found in other model viscoelastic fluid such as Boger fluids and polymeric solutions. The dispersed polymer particle possesses a hard-core/soft-shell structure. The surface of the dispersed polymer is stretched uniformly and can be removed from the main drop as films, strings or particles. Under high shear rate, the surface instability is concurrent with vorticity elongation and breakup. For systems with low viscosity ratio and high elasticity ratio, the dispersed phase forms films under shear. These films break up erratically into smaller films. For systems with medium viscosity ratio and low elasticity ratio, the dispersed polymer is deformed into fibers and the fibers can break up via fiber instability or during relaxation.

Figure 5-12 in this thesis shows the mechanism of how a millimeter sized pellet breaks up into micrometer sized particles. This mechanism is speculated as the real mechanism for polymer blends processed in industrial mixers. This work is beneficial to create and control the morphology of polymer blends by knowing the effects of viscoelastic properties and different types of processing flow. The morphology development mechanism is more complex than proposed in previous studies [4-6]. There is still much to investigate to understand this mechanism. In addition, it is interesting to know how a relaxation flow can facilitate the breakup process.

6.2 Recommendations for future work

6.2.1 Critical drop size for drop breakup

It is discovered in Chapter 4 that there is a critical drop size below which viscoelastic drops cannot break up in the flow direction. Similar observation was found by De Bruijn who did not reach a vorticity direction breakup [3]. Below this size, this work found that the drop elongates in the vorticity direction and then breaks up. The breakup shear rate will be much higher for the vorticity direction breakup than the flow direction drop breakup. Therefore, it is important to know the critical drop size for a given viscoelastic system.

To avoid other complexity, fluid systems can be designed as Boger fluid drop suspended in Newtonian matrices under shear flow. There are two approaches to find the critical drop size. One is experimental and the other is mathematical modeling. In both approaches, the viscosity ratio and the drop phase relaxation time should be fixed as constant. A range of drop size is then tested under a quasi-steady increasing shear rate to find out the breakup modes and conditions. The critical drop size should be related to viscosity ratio and relaxation time. Results from both approaches should be compared with each other. Three-component correlations among the critical capillary number (z axis), viscosity ratio (x axis) and critical Deborah number (y axis) are possible to construct a framework to characterize the drop breakup conditions for viscoelastic drop/Newtonian matrix system. It should be noted that the critical drop size is incorporated in the critical capillary number and indirectly in the Deborah number.

6.2.2 Compatibilization during polymer blending

In Chapter 2, the effect of in-situ graft reactive compatibilization on the initial mixing stage of polymer blending is investigated. However, there are other kinds of compatibilization methods yet to be studied. The effect of different compatibilization methods on polymer drop breakup can be different [7, 8]. Compatibilization has multiple effects on drop deformation and breakup: 1) reducing the interfacial tension; 2) suppressing interfacial slip; 3) causing Marangoni effect; 4) forming a rigid interfacial layer. These effects either facilitate or resist drop breakup. The future work can study the comapitibilization effect of block copolymer, graft reaction and cross-linking. The coverage of compatibilizer, and the reaction rate of in-situ compatibilization should also be examined. To quantify the effect of different compatibilizations, the processing conditions may be designed so that the thickness of the films of dispersed phase can be measured.

6.2.3 Polymer blends under shear flow

The effect of viscoelasticity effect on polymer blend morphology development is qualitatively discussed in Chapter 5 using several model experiments. It can be further advanced by developing and using a simple shear device. The details of this work are given below:

1) constructing a transparent cone-plate device or a transparent Couette type device based on the internal batch mixer (Haake Rheomix 600) so that a simple shear flow can be generated. The basic design is shown in Figure 6-1.

2) using a high speed camera (5000frame/min) to investigate the morphology development under high rotation speed and high shear rate. The morphogical change is very rapid under high shear rate. A high speed camera can give clear pictures of the drop deformation and breakup process.

3) investigating polymer blends with a large range of viscosity ratio and elasticity ratio. Different combinations of viscosity ratio and elasticity ratio cause different morphology. The effect of viscoelasticity on the morphology development of polymer blends can be completed by a systematic investigation of polymer systems with different viscoelasticities. For example, polymer systems can be classified into four categories for the investigation: 1) high viscosity ratio and high elasticity ratio; 2) high viscosity ratio and low elasticity ratio; 3) low viscosity ratio and high elasticity ratio; 4) low viscosity ratio and low elasticity ratio.

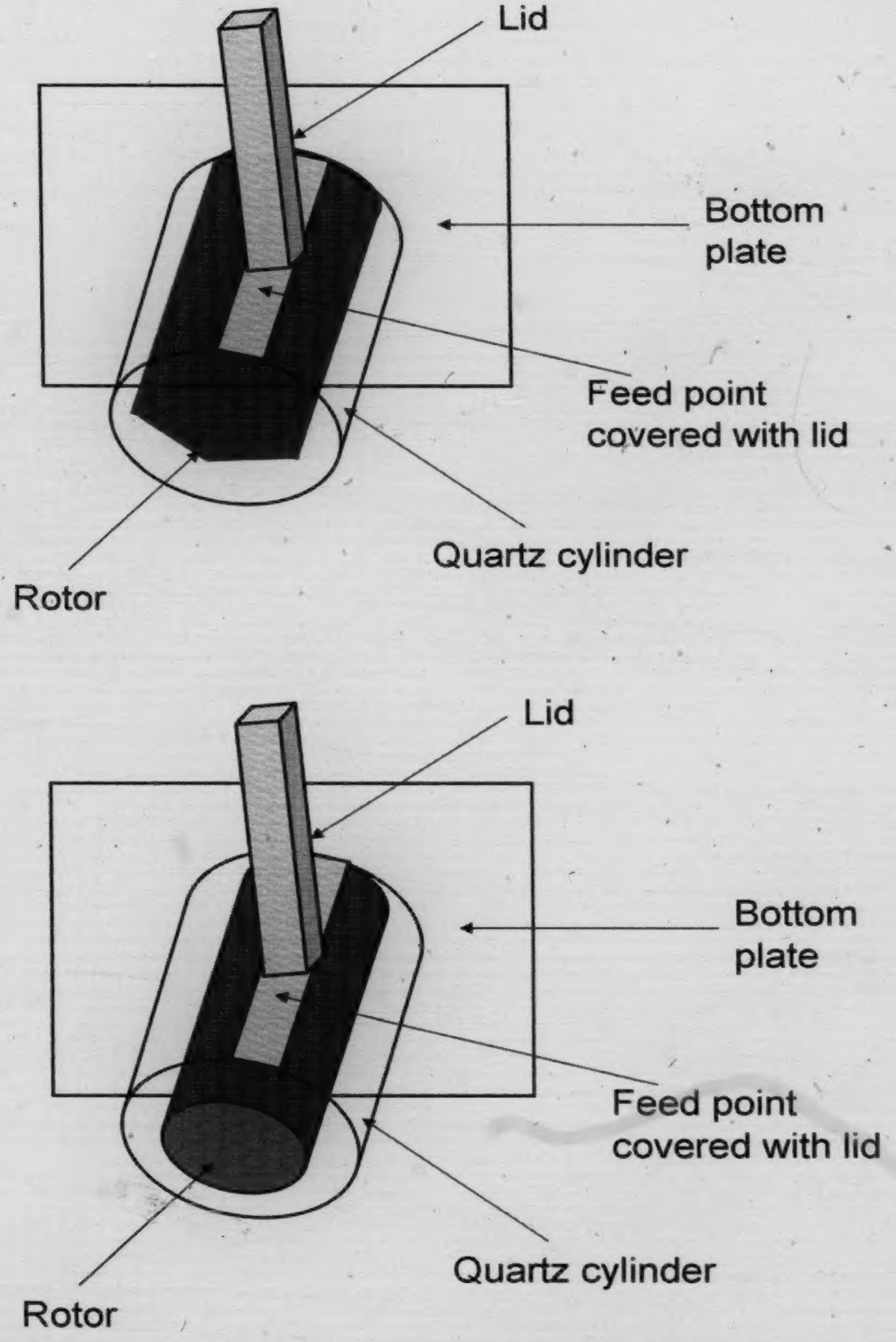

Figure 6-1 Basic design of cone-plate (top) and Couette device (bottom) for simple shear flow.

6.3 References

[1] U. Sundararaj and C. W. Macosko, "Drop breakup and coalescence in polymer blends - the effects of concentration and compatibilization," Macromolecules **28**, 2647 (1995).

[2] S. T. Milner and H. W. Xi, "How copolymers promote mixing of immiscible homopolymers," J. Rheol. **40**, 663 (1996).

[3] R. A. De Bruijn, PhD Thesis, "Deformation and breakup of drops in simple shear flows", Eindhoven University of Technology, Eindhoven (1989).

[4] C. E. Scott and C. W. Macosko, "Model experiments concerning morphology development during the initial stages of polymer blending," Polymer Bulletin **26**, 341 (1991).

[5] U. Sundararaj, C. W. Macosko, R. J. Rolando and H. T. Chan, "Morphology development in polymer blends," Polym. Eng. Sci. **32**, 1814 (1992).

[6] C. E. Scott and C. W. Macosko, "Morphology development during the initial stages of polymer-polymer blending," Polymer **36**, 461 (1995).

[7] B. Lin, PhD Thesis, "Visualization of polymer blending and drop breakup", University of Alberta, Edmonton (2005).

[8] B. Lin, F. Mighri, M. A. Huneault and U. Sundararaj, "Effect of premade compatibilizer and reactive polymers on polystyrene drop deformation and breakup in simple shear," Macromolecules **38**, 5609 (2005).

Appendix I
Flow in Couette Device

Consider the flow of a fluid confined in a Couette cell with the inner cylinder rotating at Ω_i and outer cylinder rotating at Ω_o. Here we assume:

(1) The fluid is incompressible and can be described by power law:

$$\eta = m\dot{\gamma}^{n-1} \text{ and } \tau = \eta\dot{\gamma} = m\dot{\gamma}^{n}$$

where η is the viscosity, $\dot{\gamma}$ is shear rate, τ is shear stress and m and n are constants.

(2) Steady, laminar, isothermal flow

(3) Velocity are $v_\theta = r\Omega$ only and $v_r=v_z=0$

(4) Negligible gravity and end effects and wall effects

(5) no-slip conditions

(6) Symmetry in θ, $\partial/\partial\theta = 0$

Then the equations of motion in cylindrical coordinates can be simplified as

$$r: -\rho\frac{v_\theta^{\,2}}{r} = -\frac{\partial P}{\partial r} \tag{I.1}$$

$$\theta: 0 = \frac{1}{r^2}\frac{\partial}{\partial r}(r^2\tau_{r\theta}) \tag{I.2}$$

$$z: 0 = -\frac{\partial P}{\partial z} + \rho g_z \tag{I.3}$$

where P is pressure, ρ is density, and g is gravity constant.

The boundary conditions are

$$v_\theta = \Omega_i r_i \text{ at } r=r_i$$

$$v_\theta = \Omega_o r_o \text{ at } r=r_o$$

where r_i and r_o are the inner and outer radii of the gap formed by the two cylinders of the Couette device.

From the above equations, we can get the velocity profile and the shear rate profile as:

$$v_\theta = \left[\frac{\Omega_o - \Omega_i}{r_i^{-2/n} - r_o^{-2/n}}\right]\left(r_i^{-2/n} - r^{-2/n}\right)r + \Omega_i r \tag{I.4}$$

and

$$\dot{\gamma} = r\frac{\partial}{\partial r}\left(\frac{v_\theta}{r}\right) = \frac{2}{n}\frac{\Omega_o - \Omega_i}{r_i^{-2/n} - r_o^{-2/n}} r^{-2/n}$$

(I.5)

which gives the shear rate at walls:

$$\dot{\gamma}_i = \frac{2}{n}\frac{\Omega_o - \Omega_i}{r_i^{-2/n} - r_o^{-2/n}} r_i^{-2/n} \text{ at } R=r_i \tag{I.6}$$

$$\dot{\gamma}_o = \frac{2}{n}\frac{\Omega_o - \Omega_i}{r_i^{-2/n} - r_o^{-2/n}} r_o^{-2/n} = \dot{\gamma}_i\left(\frac{r_o}{r_i}\right)^{-2/n} \text{ at } R=r_o \tag{I.7}$$

and the average shear rate is estimated as:

$$\dot{\gamma}_{ave} = \frac{\dot{\gamma}_i + \dot{\gamma}_o}{2}$$

For Newtonian fluids which are used in this thesis, n=1, and the average shear rate is

$$\dot{\gamma}_{ave} = \frac{\dot{\gamma}_i + \dot{\gamma}_o}{2} = (\Omega_o - \Omega_i)\frac{r_i^{-2} + r_o^{-2}}{r_i^{-2} - r_o^{-2}} \tag{I.8}$$

Appendix II

Magnification from the Side View of Couette Device

The Couette device acts as a cylindrical lens for the side view images. Figure II-1 shows the schematic of the cross-section of the Couette device. The gap is filled with silicon oil and the outer cylinder is made from quartz. The refraction indices of silicon oil, quartz and air are

$n_s = 1.4$

$n_q = 1.6$

$n_a = 1$

Consider a 1mm segment AA' in the middle of the gap. B is the middle point of AA'. Arrowed lines AP and ACDG are light paths. PQ is the image of AB.

The knowns based on the geometries of the Couette device are

AB = 0.5 mm

OC = 55 mm

OD = 61 mm

OA = 53 mm

BC ~ 2 mm

The angles can be calculated as:

$\angle AOB = \arcsin(AB/OA) = 0.54$ degree (II.1)

$\angle ACO = \arctan(AB/BC) = 14$ degree (II.2) and from $\frac{\sin(\angle ACO)}{\sin(\angle ECD)} = \frac{n_q}{n_s}$ (II.3)

we have

$\angle ECD = 12.2$ degree (II.4)

In Δ COD:

OC = 55 mm

OD = 61 mm

$\angle OCD = 180 - \angle ECD = 167.8$ degree (II.5)

Solving Δ COD we have

CD = 6.13 mm (II.6)

and $\angle COD = 1.24$ degree

$\angle CDO = \angle ECD - \angle COD = 10.96$ degree (II.7)

and from $\frac{\sin(\angle CDO)}{\sin(\angle FDG)} = \frac{n_q}{n_a}$ (II.8)

we have

$\angle FDG = 17.7$ degree (II.9)

In ΔPOD:

OD = 61 mm

$\angle PDO = \angle FDG = 17.7$ degree (II.10)

$\angle POD = \angle AOB + \angle COD = 1.78$ degree (II.11)

Solving ΔPOD we have

OP = 56.4mm (II.12)

The Magnification is

Magnification = AB/PQ = OA/OP = 1.06 (II.13)

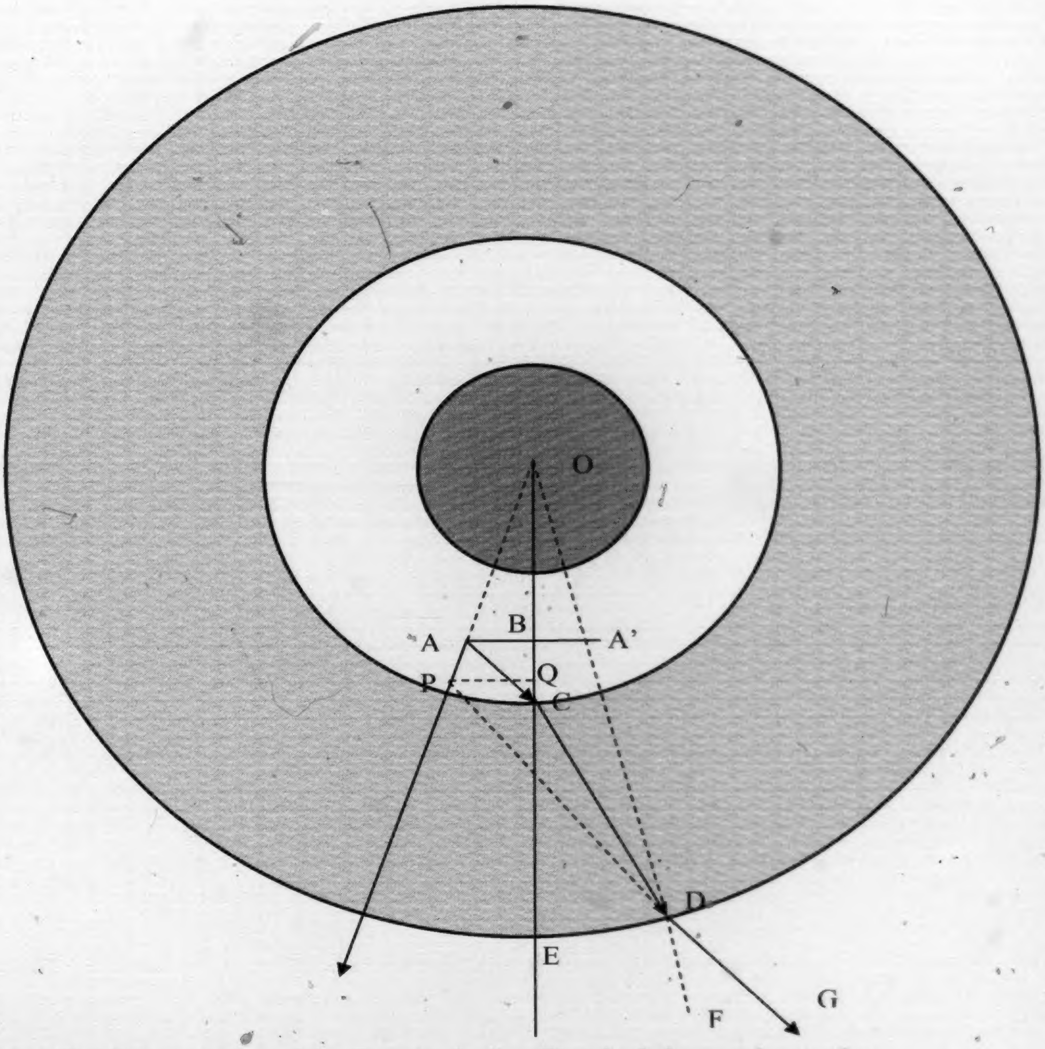

Figure II-1 Cross section of the Couette device. The shaded areas denote the inner cylinder and the outer cylinder respectively. Figure not drawn to scale.